

See discussions, stats, and author profiles for this publication at: <https://www.researchgate.net/publication/330271332>

# The Pathway to Intelligence: Using Stimuli-Responsive Materials as Building Blocks for Constructing Smart and Functional Systems

Article in *Advanced Materials* · January 2019

DOI: 10.1002/adma.201804540

---

CITATIONS

181

READS

1,188

13 authors, including:



Xuan Zhang

National University of Singapore

7 PUBLICATIONS 349 CITATIONS

[SEE PROFILE](#)



Linfeng Chen

China University of Geosciences

31 PUBLICATIONS 1,199 CITATIONS

[SEE PROFILE](#)



Spandhana Gonuguntla

National University of Singapore

8 PUBLICATIONS 428 CITATIONS

[SEE PROFILE](#)



Dicky Pranantyo

National University of Singapore

50 PUBLICATIONS 1,845 CITATIONS

[SEE PROFILE](#)

# The Pathway to Intelligence: Using Stimuli-Responsive Materials as Building Blocks for Constructing Smart and Functional Systems

Xuan Zhang, Linfeng Chen, Kang Hui Lim, Spandhana Gonuguntla, Kang Wen Lim, Dicky Pranantyo, Wai Pong Yong, Wei Jian Tyler Yam, Zhida Low, Wee Joon Teo, Hao Ping Nien, Qiao Wen Loh, and Siowling Soh\*

Systems that are intelligent have the ability to sense their surroundings, analyze, and respond accordingly. In nature, many biological systems are considered intelligent (e.g., humans, animals, and cells). For man-made systems, artificial intelligence is achieved by massively sophisticated electronic machines (e.g., computers and robots operated by advanced algorithms). On the other hand, freestanding materials (i.e., not tethered to a power supply) are usually passive and static. Hence, herein, the question is asked: can materials be fabricated so that they are intelligent? One promising approach is to use stimuli-responsive materials; these “smart” materials use the energy supplied by a stimulus available from the surrounding for performing a corresponding action. After decades of research, many interesting stimuli-responsive materials that can sense and perform smart functions have been developed. Classes of functions discussed include practical functions (e.g., targeting and motion), regulatory functions (e.g., self-regulation and amplification), and analytical processing functions (e.g., memory and computing). The pathway toward creating truly intelligent materials can involve incorporating a combination of these different types of functions into a single integrated system by using stimuli-responsive materials as the basic building blocks.

## 1. Introduction

Intelligence is commonly defined as the ability of a system to sense the environment, store and analyze information, and respond to its surrounding accordingly.<sup>[1]</sup> Many biological systems are considered intelligent (Figure 1a). Humans are highly intelligent species due to our ability to remember and analyze logically large amount of information. Many animals, such as dogs, dolphins, monkeys, and elephants, are regarded as intelligent because of their capability to communicate, understand

instructions, learn, analyze, and produce appropriate actions.<sup>[2]</sup> Some plants are also considered intelligent because of their ability to detect changes in their surroundings, analyze, and produce a response.<sup>[3]</sup> One well-known example is the Venus flytrap, which senses and captures insects by closing its trap. Logical analysis of information is involved in this process: the trap closes only when two action potentials are activated sequentially within 30 s apart by a sufficiently long signal. This analysis is important for the plant to save energy when there are false alarms caused by other types of short disturbances.<sup>[4]</sup>

A cell, the basic unit of complex biological organisms, can be considered to have a primitive form of intelligence. Despite being small (i.e., micrometers), it is a highly complex system that performs a wide range of advanced extracellular and intracellular functions (Figure 1b). These functions can generally be categorized into three groups: practical functions, regulatory functions, and analytical processing functions.

Practical functions include the changes in shape (e.g., mitotic rounding),<sup>[5]</sup> changes in size (e.g., expansion after cytokinesis),<sup>[6]</sup> self-assembly (e.g., the actin filaments and microtubules),<sup>[7]</sup> motion of the cell,<sup>[8]</sup> and communication by intracellular (e.g., signaling from the membrane to the nucleus) and extracellular signaling (e.g., signaling between cells).<sup>[9]</sup> The internal regulatory functions include self-regulation (e.g., the regulation of intracellular pH via the Na<sup>+</sup>/H<sup>+</sup> antiporters),<sup>[10]</sup> amplification (e.g., the enhancement of a shallow concentration gradient outside of the cell to a large gradient within the cell for polarization),<sup>[9]</sup> self-replication (e.g., DNA),<sup>[11]</sup> self-oscillation (e.g., waves of calcium ions within the cell),<sup>[9]</sup> and self-organization (e.g., the network of cytoskeleton).<sup>[7]</sup> In addition, cells are capable of performing basic logical analyses. For example, the lactose operon is activated only when lactose, but not glucose, is present for the production of monosaccharides (i.e., the carbon catabolite repression). However, when both glucose and lactose are present, the lactose operon is inactivated, thus allowing the cell to obtain energy from glucose rather than the less efficient lactose.<sup>[12]</sup>

X. Zhang, Dr. L. Chen, K. H. Lim, S. Gonuguntla, K. W. Lim, Dr. D. Pranantyo, W. P. Yong, W. J. T. Yam, Z. Low, W. J. Teo, H. P. Nien, Q. W. Loh, Prof. S. Soh  
Department of Chemical and Biomolecular Engineering  
National University of Singapore  
4 Engineering Drive 4, Singapore 117585, Singapore  
E-mail: chessl@nus.edu.sg

 The ORCID identification number(s) for the author(s) of this article can be found under <https://doi.org/10.1002/adma.201804540>.

DOI: 10.1002/adma.201804540

Intelligence has also been demonstrated in man-made electronic systems (Figure 1a). At the fundamental level, many smart basic electronic components have been fabricated, including logic gates and transistors. These electronic components are capable of controlling current flow,<sup>[13]</sup> amplifying current,<sup>[14]</sup> and performing logical operations.<sup>[13]</sup> The integration of these individual components has resulted in highly complex analytical machines, such as computers. Computers are able to collect and remember a large amount of information and process them logically. Building upon these electronic systems, humans have established the pathway to intelligence. First, highly advanced robots have been developed; they can sense their environment, collect and analyze information, and implement many functions. One example is the Curiosity Mars rover which is capable of sensing, motion, actuation (e.g., picking samples), self-regulation (e.g., temperature), communication (e.g., between the rover and earth), and complex logical analysis (e.g., autonomous navigation across treacherous terrain by 3D imaging of its surrounding and determining the safest route).<sup>[15]</sup> Second, artificial intelligence (AI) has also been achieved by humans. Based on complex electronic machines, advanced algorithms, and large data sets, AI machines are able to analyze situations autonomously and, at times, display superhuman performance.<sup>[16]</sup> One famous recent example is that an AI machine (i.e., the AlphaGo) has defeated the world champion in the game of Go.<sup>[17]</sup> However, these electronic machines are tethered: they require a constant power supply to operate. For many types of applications (e.g., biomedical), materials need to be freestanding and cannot be tethered to an external power supply.

The common impression of a piece of freestanding material (e.g., metallic, inorganic, or polymeric) is that it is static and passive; hence, it is generally not considered smart. One possible approach toward creating smartness in materials is to use stimuli-responsive materials. These materials are usually considered smart because of their ability to sense their surroundings and produce a simple and direct response. Stimuli-responsiveness is the ability to detect a signal that is applied remotely or sense a chemical species that is naturally occurring. Signals that can be applied remotely include possible changes in the surrounding such as temperature, pressure, electric field, and magnetic field. Naturally occurring chemicals include substances found in minerals (e.g., sodium and calcium) and those produced by biological organisms (e.g., proteins and enzymes). Hence, synthetic molecules that are not available naturally are not regarded as stimuli. Stimuli-responsive materials have been studied for many decades; a wide range of stimuli-responsive materials that respond to many different types of stimuli has been fabricated.

However, although stimuli-responsive materials are generally considered smart, they are not regarded as intelligent because they are not able to perform advanced types of functions (e.g., analytical, regulatory, or complex practical functions). Hence, we ask the question: can materials be fabricated so that they are intelligent? Herein, we briefly describe the fascinating systems that researchers have constructed in the pursuit of higher levels of smartness. We consider only stimuli-responsive materials that are



**Xuan Zhang** earned his B.Eng. degree and M.Eng. degree from the School of Science, Northwestern Polytechnical University (NPU) in 2011 and 2014, respectively. He is currently pursuing his Ph.D. degree from the Department of Chemical and Biomolecular Engineering at the National University of Singapore with Prof. Siewling Soh. His research interests focus on contact electrification and the design and fabrication of smart and functional systems using responsive hydrogels.



**Linfeng Chen** received his B.Eng. degree from the School of Chemistry and Chemical Engineering, Huazhong University of Science and Technology (HUST) in 2008 and obtained his Ph.D. degree from the Institute of Chemistry, Chinese Academy of Sciences (ICCAS) with Prof. Yanlin Song in 2014. Later, he worked as a postdoctoral researcher in the Department of Materials Science and Engineering, Technion-Israel Institute of Technology (2014–2016). He is currently a research fellow in the Department of Chemical and Biomolecular Engineering, National University of Singapore. His research interests include bioinspired functional materials, controlled-release systems, and contact electrification.



**Siewling Soh** received his Ph.D. degree from Northwestern University and studied under George Whitesides at Harvard University as a postdoctoral fellow. He is currently an Assistant Professor in the Department of Chemical and Biomolecular Engineering at the National University of Singapore. His research involves the design and fabrication of responsive, programmable, and functional polymeric systems via the combination of different types of advanced materials (e.g., particles and coatings), reactions, and transport. His research is highly interdisciplinary and includes other research fields such as the separation of charge at interfaces, electrostatics, magnetostatics, reaction-diffusion processes, chemical networks, self-assembly, and cell motility.

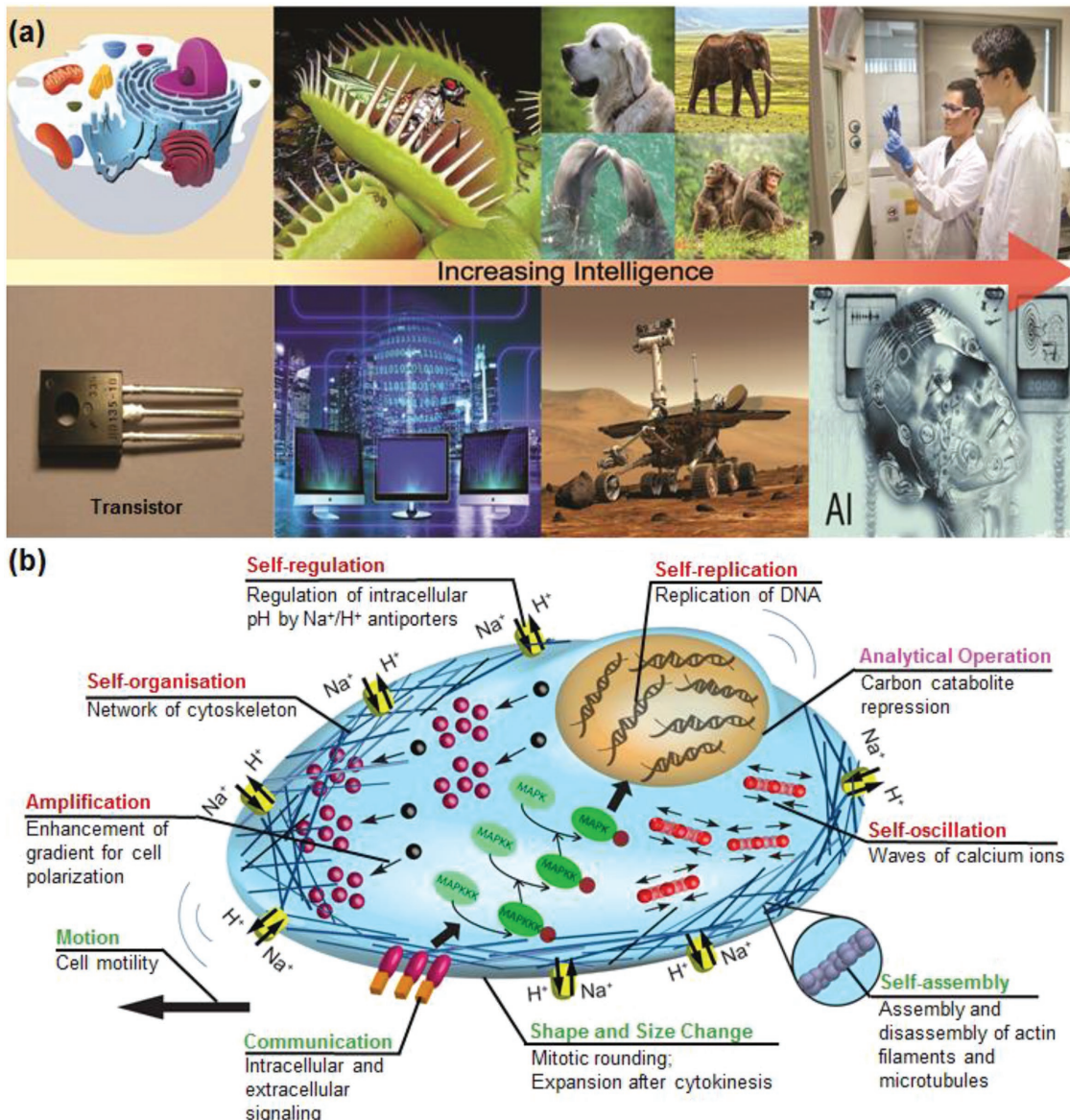


**Figure 1.** a) Intelligent biological and electronic systems. b) Various functions of a cell. Green headings represent practical functions; red headings represent regulatory functions; purple heading represents analytical processing function.

not tethered to any sources of energy. Energy is necessary for performing functions and analyses; for example, power is needed to drive electronic systems to accomplish complex tasks. When materials are not tethered, however, an alternative is needed to drive the operation: by using a (untethered) stimulus as the driving force for materials to perform their functions. Alternatively, the stimulus can be used to trigger the release of the internal energy stored in the system. By using stimuli-responsive materials as the building blocks for constructing complex systems, researchers around the world have created many interesting systems that are remarkably smart and functional. This review first discusses very briefly a few types of stimuli-responsive molecules that are commonly used in stimuli-responsive materials. We then review the many types of functions that have been achieved by

stimuli-responsive materials. We categorized these functions broadly into four classes: basic functions, practical functions, regulatory functions, and analytical processing functions (i.e., similar to a cell). **Figure 2** shows the tree diagram that illustrates the interconnectivity of the various functions and the level of complexity of each function. For each function, we first briefly define and describe its roles specifically for constructing intelligent systems. We will then discuss a few selected examples (out of the large number of systems that have been investigated) that describe the different types of capabilities of the functions and/or the synergistic combination of functions for creating smart systems. Through these few examples, we intend to showcase the functions developed by humans as an illustration of how we can establish the pathway to intelligence for materials.

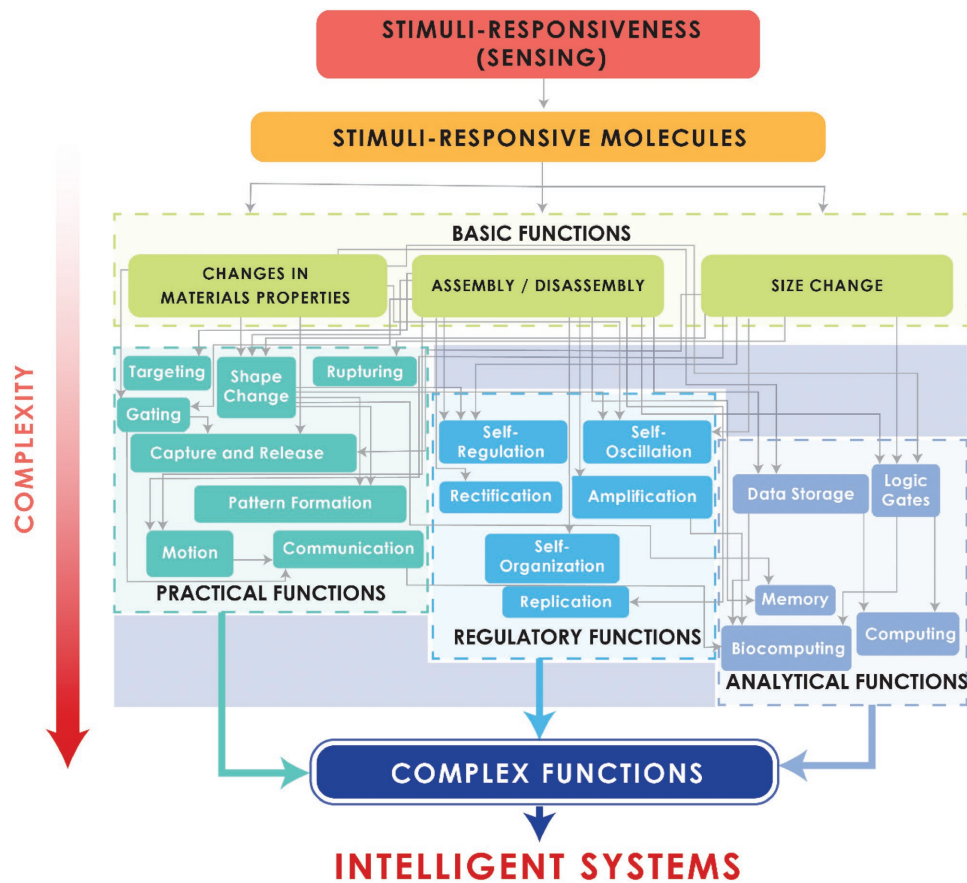


**Figure 2.** Pathway to intelligence of stimuli-responsive materials by creating different basic, practical, regulatory, and analytical processing functions with increasing complexity in the materials.

## 2. Molecular Function

For constructing advanced intelligent systems, the most basic elements are the molecules. A large number of molecules have been synthesized for responding to a wide variety of stimuli. Despite the many types of molecules that are available for selection, a majority of the smart devices fabricated by material scientists are usually based on a few common types of stimuli-responsive molecules. The responsiveness of these common types of molecules can broadly be grouped into three main categories: change in molecular structure, bond formation and/or cleavage, and response to external fields (Figure 3).

Many stimuli-responsive molecules undergo a change in molecular structure when they are exposed to an appropriate stimulus.<sup>[18–22]</sup> A common class of light-responsive molecules is based on azobenzene (AB) derivatives.<sup>[22]</sup> This type of molecule can undergo a *cis-trans* isomerization upon exposure to light (part (i) of Figure 3a). This transformation has been widely used for building smart systems because of the difference in the dipole moments of its *cis* or *trans* isomer. Specifically, for the *cis* isomer, the molecule has a dipole moment of around 3.1–4.4 D, while for the *trans* isomer, the dipole moment is a lot smaller (i.e., around 0–1.2 D).<sup>[23]</sup> This relatively large difference in dipole moment has allowed the molecule to be used in many applications (e.g., reversible assembly and disassembly) due to the switchable

interactions between the molecules. Another very common class of light-responsive molecules is the spiropyran derivatives.<sup>[19,21]</sup> Upon exposure to UV, this type of molecule undergoes a ring-opening process as illustrated in part (ii) of Figure 3a. Exposure to visible light allows the molecule to undergo the reverse (i.e., the ring-closing) process. Importantly, this transformation allows the molecule to have a relatively large change in polarity. When the ring opens, the molecule acquires a moiety with a positive charge and a moiety with a negative charge. The formation of charged groups increases the polarity of the molecule. In terms of temperature-responsive molecules, poly(*N*-isopropylacrylamide) (PNIPAM) is commonly used. Below its lower critical solution temperature (LCST), PNIPAM forms hydrogen bonds with the water molecules in the solution; hence, it adopts an extended chain conformation (part (iii) of Figure 3a). Increasing the temperature above the LCST dehydrates the polymer chains and allows the polymeric chains to form hydrogen bonds within and between themselves. These interactions result in a collapsed conformation of the polymeric chains.<sup>[24]</sup>

Stimulus can also be used for forming or breaking bonds between and/or within molecules. The type of bond formation and/or cleavage includes electrostatic attraction or repulsion, hydrophobic interaction, hydrogen bonding, host-guest interaction, and covalent bond (Figure 3b).<sup>[25–27]</sup> Part (i) of Figure 3b illustrates the case when two molecules undergo electrostatic

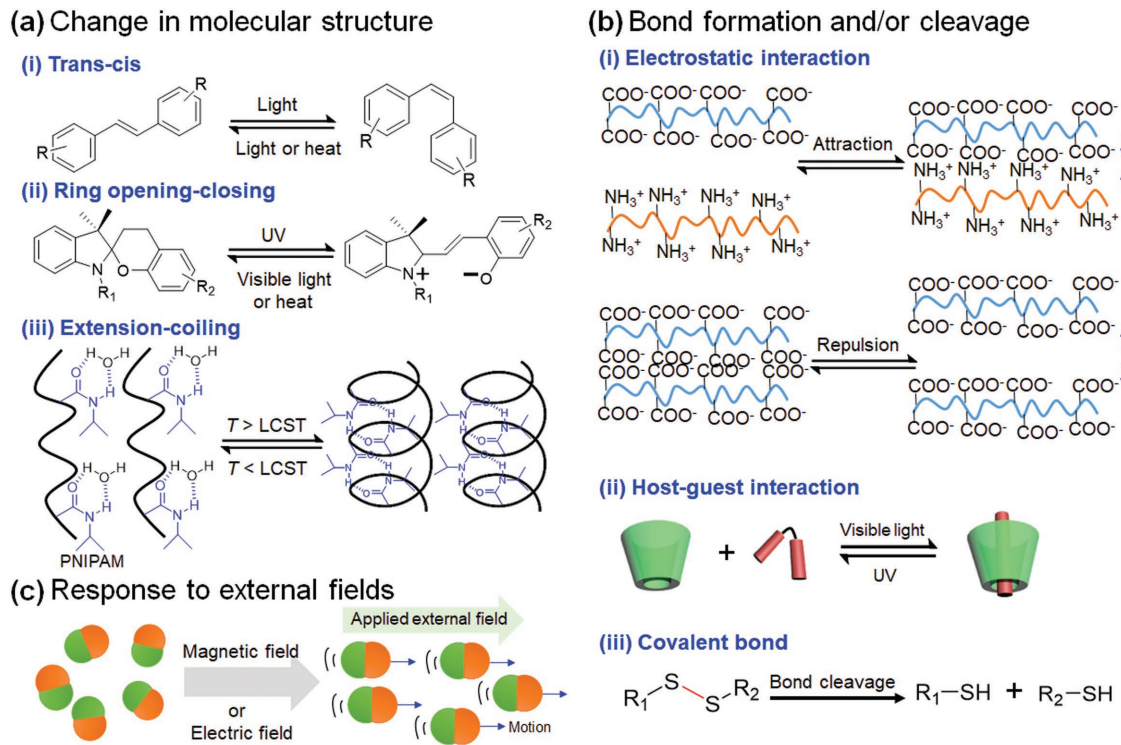


**Figure 3.** Stimuli-responsive molecules/particles. After detecting an external stimulus, the stimuli-responsive molecules may: a) undergo a change in molecular structure, or b) result in bond formation and/or cleavage. c) Particles produce a response to external fields.

attraction or repulsion. In order to achieve these interactions, the molecules need to have ionic or ionizable functional groups. Two widely used functional groups are the carboxylic acid ( $-COOH$ ) and the amine ( $-NH_2$ ) groups. When these functional groups are exposed to an appropriate pH, the  $-COOH$  group deprotonates to form the negatively charged  $-COO^-$  group, while the  $-NH_2$  group protonates to form the positively charged  $-NH_3^+$  group. For example, if one polymeric chain has the  $-COO^-$  groups and another polymeric chain has the  $-NH_3^+$  groups, the chains attract electrostatically. If the two polymeric chains have only one type of charged group, the chains repel. Another useful type of molecular interaction is the host-guest interaction. Commonly used molecules include the  $\beta$ -cyclodextrin ( $\beta$ -CD) and AB derivatives.  $\beta$ -CD has a high binding affinity with the *trans*-AB derivatives and a low binding affinity with the *cis*-AB derivatives.<sup>[28-30]</sup> Therefore, the host-guest interaction can be controlled reversibly by UV and visible light (part (ii) of Figure 3b). A stimulus can also be used to cleave covalent bonds. A common example is the cleavage of the disulfide bond by glutathione (GSH).<sup>[31,32]</sup>

Magnetic and electric fields are also commonly used as the stimuli for stimuli-responsive materials (Figure 3c). For example, if a material contains molecules that are magnetic or charged, it can orient and move with the externally applied field.

### 3. Basic Function

A vast range of functions and applications have been achieved by using these stimuli-responsive molecules for the fabrication

of stimuli-responsive materials. Some functions of these stimuli-responsive materials are basic: they usually form the basis for creating other types of functions. These functions include the change in material property, change in size, and self-assembly or disassembly. They are classified as basic because they are highly connected to other types of functions as shown in Figure 2 (although they may also serve as practical or regulatory functions). First, many types of stimuli-responsive materials detect a stimulus and produce a change in a property of the material. A wide range of changes in properties (e.g., color, wettability, magnetic, stiffness, electrical conductivity, solubility, and many others) have been demonstrated. The reader is referred to reviews elsewhere for functions that involve only changes in the property of a material under the influence of a stimulus.<sup>[33-37]</sup>

#### 3.1. Size Change

One of the most basic functions of stimuli-responsive materials is the change in size. Materials that change their sizes upon the influence of a stimulus have been developed and used for many decades. By now, stimuli-responsive materials can be fabricated to change their sizes based on a wide variety of stimuli, including temperature, pH, light, electric field, magnetic field, pressure, gases, ions, salts, alcohols, glucose, enzymes, and antigens.<sup>[38-41]</sup> In addition, stimuli-responsive materials can be fabricated to respond to more than one type of stimuli.<sup>[38,39,42]</sup> The ability of these stimuli-responsive materials to change their sizes allows them to be used in a wide range of applications,

such as drug delivery, diagnostic devices, detection, and microgel lenses.<sup>[40,43]</sup> Being the basic function of stimuli-responsive materials, many studies have used the change in the size of the materials to produce other types of functions, such as a change in the property of materials (e.g., wettability and color)<sup>[44,45]</sup> and many other functions that we will discuss in the subsequent sections. As a brief overview, we discuss the mechanisms of the change in size of stimuli-responsive materials under the influence of two of the most common stimuli: temperature and pH.

A widely used stimuli-responsive material that responds to temperature is the PNIPAM hydrogel. At temperatures below the LCST of PNIPAM, the hydrogel expands; at temperatures above the LCST, the hydrogel contracts. Similar to the mechanism at the molecular level, the expansion of the hydrogel at temperatures below the LCST is due to the formation of hydrogen bonds of the hydrophilic groups (i.e., amide groups) of PNIPAM with water molecules in the solution.<sup>[39,40,43,46,47]</sup> Due to the favorable interactions, the hydrogel absorbs water and expands. Above the LCST, however, PNIPAM becomes

more hydrophobic. It then expels water out of its polymeric matrix and contracts.

One commonly used pH-responsive material is poly(acrylic acid) (PAA). The PAA hydrogel expands at high pH and contracts at low pH. The change in size of the PAA hydrogel occurs due to the protonation or deprotonation of its carboxylic acid groups.<sup>[40,43,48]</sup> At high pH, the carboxylic acid groups deprotonate; thus, the electrostatic repulsion among the ionic groups allows the hydrogel to expand and absorb water. At low pH, the carboxylic acid groups protonate and the hydrogel contracts.

In many cases, this change in size allows the stimuli-responsive materials to be used for self-regulation of a system. An important application involves using stimuli-responsive hydrogels as smart valves for controlling the flow of fluid in microfluidic channels (i.e., blocking the channels by expanding or opening the channels by contracting the hydrogels).<sup>[49]</sup> One specific study involved two types of pH-responsive hydrogels placed in two sides of a T-shaped channel (Figure 4a).<sup>[50]</sup> The hydrogel on the right side of the T-shaped channel as shown in Figure 4a (i.e., poly(2-hydroxyethyl methylacrylate-co-acrylic),

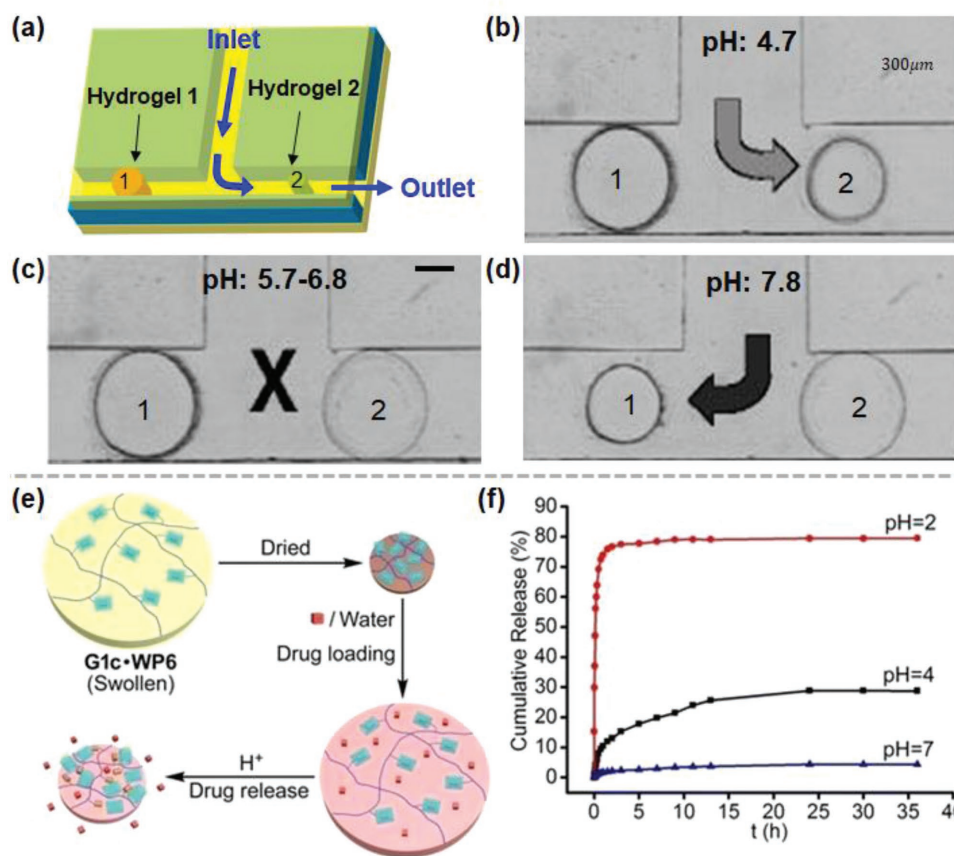


**Figure 4.** Change in size of stimuli-responsive materials. a–d) Using stimuli-responsive hydrogels as smart self-regulating valves for blocking channels in microfluidic channels when expanded, and opening channels when contracted under the influence of the stimulus. a) Scheme illustrating the T-shaped microfluidic channels for controlling the direction of flow by using pH-responsive hydrogels as self-regulating valves. b–d) The liquid flowed to the right at a low pH of 4.7 (b), stopped flowing at a moderate range of pH 5.7–6.8 (c), and flowed to the left at a high pH of 7.8 due to the changes in size of the stimuli-responsive hydrogels (d). b–d) Reproduced with permission.<sup>[50]</sup> Copyright 2000, Springer Nature. e,f) Using stimuli-responsive hydrogels for controlling the release of chemicals from the interior of the hydrogel under the influence of the stimulus for drug delivery. e) Scheme illustrating the loading and releasing of a drug from the change in size of a pH-responsive hydrogel. f) Release profiles of the drug from the hydrogel at different pH. e,f) Reproduced with permission.<sup>[51]</sup> Copyright 2016, American Chemical Society.

P(HEMA)-co-AA) contracted in low pH and expanded in high pH. On the other hand, the hydrogel on the left (i.e., poly(HEMA-co-(dimethylamino)ethyl methacrylate), P(HEMA-co-DMAEMA)) had an opposite behavior: it expanded in low pH and contracted in high pH. Therefore, at a low pH of 4.7, the hydrogel on the left expanded and the hydrogel on the right contracted; hence, the flow of fluid was directed to the right of the T-shaped channel (Figure 4b). At a high pH of 7.8, the hydrogel on the right expanded and the hydrogel on the left contracted; in this case, the flow of fluid was directed to the left (Figure 4d). At a moderate pH range of 5.7–6.8, both hydrogels expanded and completely blocked the flow of fluid across both the channels (Figure 4c). This system is thus self-regulating because it was able to control autonomously the flow of fluid in the T-shaped channel, depending on the pH of the fluid flowing in the channel (i.e., not due to an externally applied stimulus for controlling the flow).

The change in size of a stimuli-responsive hydrogel can also be used for controlling the amount of chemicals released from the interior of the hydrogel—a feature that is important for drug delivery. One study described a pH-responsive hydrogel with ferrocene side groups that were able to form host-guest inclusion complexes with the water-soluble pillar[6]arene (WP6).<sup>[51]</sup> By forming the WP6-ferrocene inclusion complex, the hydrophobic ferrocene subunits became hydrophilic complexes; this transformation allowed the hydrogel to absorb water and produced a large change in size (i.e., a 11-fold increase in size compared to when the hydrogel was immersed in pure water without WP6). Importantly, this change in size is pH-responsive. In an acidic medium, the protonation of WP6 led to the decomplexation of the hydrophilic complex; hence, the hydrogel shrank. In a basic medium, the hydrogel swelled. This large change in size due to the difference in pH of the medium was found to be effective in controlling the rate of release of a drug (e.g., doxorubicin) preloaded in the hydrogel. When the hydrogel shrank in an acidic medium, the drug molecules were squeezed out and released from the hydrogel (Figure 4e,f).

### 3.2. Self-Assembly

Self-assembly is the process in which separated discrete components come together to form a higher ordered structure.<sup>[52–54]</sup> Self-assembly is extensively observed in nature. At the molecular scale, polypeptides self-assemble into folded globular proteins; at the microscopic scale, a large number of amoebas (*dictyostelium discoideum*) can self-assemble into slime molds when there is a lack of food (i.e., bacteria).<sup>[55]</sup> For synthetic systems, many materials reported in previous studies require a stimulus to be applied before the self-assembly occurs spontaneously. Stimuli-responsive self-assembly usually consists of a few elements: the discrete components, stimulus needed for the self-assembly to occur, and forces for assembling the components. A diverse range of systems that self-assemble has been developed in previous studies. These systems include discrete components that range from nanoscale (i.e., nanoparticles, nanotubes, and nanorods) to microscale (i.e., particles). Stimuli that have been used include pH,<sup>[56]</sup> temperature,<sup>[57]</sup> ionic strength,<sup>[58]</sup> electric field,<sup>[58]</sup> magnetic field,<sup>[59]</sup> and light.<sup>[59]</sup>

Different types of forces are responsible for the assembly, such as van der Waals interactions,  $\pi$ - $\pi$  interactions, electrostatic forces, and hydrogen bonding. A few common self-assembled structures are micelles,<sup>[57,60,61]</sup> vesicles,<sup>[62]</sup> nanocrystal superlattices,<sup>[63]</sup> and nanofibers (e.g., from the assembly of nanoparticles or peptide amphiphiles).<sup>[58,64,65]</sup>

Self-assembly of small discrete components into a larger ordered structure is considered as an attractive approach for autonomous bottom-up fabrication of materials with the desired features. For example, metallic nanoparticles ( $\approx 5$  nm) coated with oppositely charged pH-responsive ligands were demonstrated to self-assemble into a larger diamond lattice structure ( $\approx 1$   $\mu$ m) via electrostatic interactions.<sup>[66]</sup> Specifically, two types of nanoparticles were used: gold nanoparticles functionalized with alkane thiols that contained carboxylic groups (i.e.,  $\text{HS}(\text{CH}_2)_{10}\text{COOH}$ ) and silver nanoparticles functionalized with alkane thiols that contained tertiary amine groups (i.e.,  $\text{HS}(\text{CH}_2)_{11}\text{NMe}_3^+\text{Cl}^-$ ; Figure 5a). At basic pH (i.e., pH 9.7), the carboxylic groups on the gold nanoparticles deprotonated; thus, the nanoparticles became negatively charged. Because the silver nanoparticles were positively charged due to the charged amine groups, the oppositely charged silver and gold nanoparticles attracted each other via electrostatic interactions. Different types of self-assembled structures were achieved using this method (i.e., amorphous aggregates or crystalline) depending on the distribution of the size of the nanoparticles used (Figure 5b).

Dynamic self-assembly is an important class of self-assembly.<sup>[67]</sup> It is a type of nonequilibrium assembly that is maintained in steady state by the balance of a constant influx of energy applied externally to the system and the dissipation of energy of the assemblies. In the absence of the external source of energy, the assembly falls apart. Dynamic self-assembly is commonly found in living systems, such as the formation of actin filaments (e.g., for cell motility and mitosis),<sup>[53]</sup> growth of bacterial colonies,<sup>[68]</sup> and swarming motion of a school of fish.<sup>[69]</sup> Many types of chemical fuels (or stimuli), such as the adenosine triphosphate (ATP)<sup>[62]</sup> and enzymes,<sup>[70]</sup> are often needed for these dynamic assemblies to occur.

For artificial systems, the complexity of dynamic self-assembly was demonstrated elegantly in one study in which magnetic disks fabricated by filling hollow polyethylene tubes with a magnetite-doped polymer (i.e., polydimethylsiloxane, PDMS) were placed at the surface of a liquid mixture (i.e., ethylene glycol and water).<sup>[71]</sup> A bar magnet was placed below the dish containing the liquid mixture as illustrated in Figure 5c. When the bar magnet rotated, the average magnetic field generated by the rotating magnet (i.e., the stimulus) drew the disks to the center of the dish; hence, the disks assembled at the center. At the same time, each disk spun around its own axis with the same angular frequency as the rotating bar magnet. The spinning disk generated convective currents around the disk that led to hydrodynamic repulsion between the disks. In general, the balance between the magnetic attraction and hydrodynamic repulsion resulted in the formation of patterns of the aggregated magnetic disks rotating at the liquid-air interface. Various interesting patterns (i.e., polygons and multishell structures) were observed depending on the number of magnetic disks used (Figure 5d).

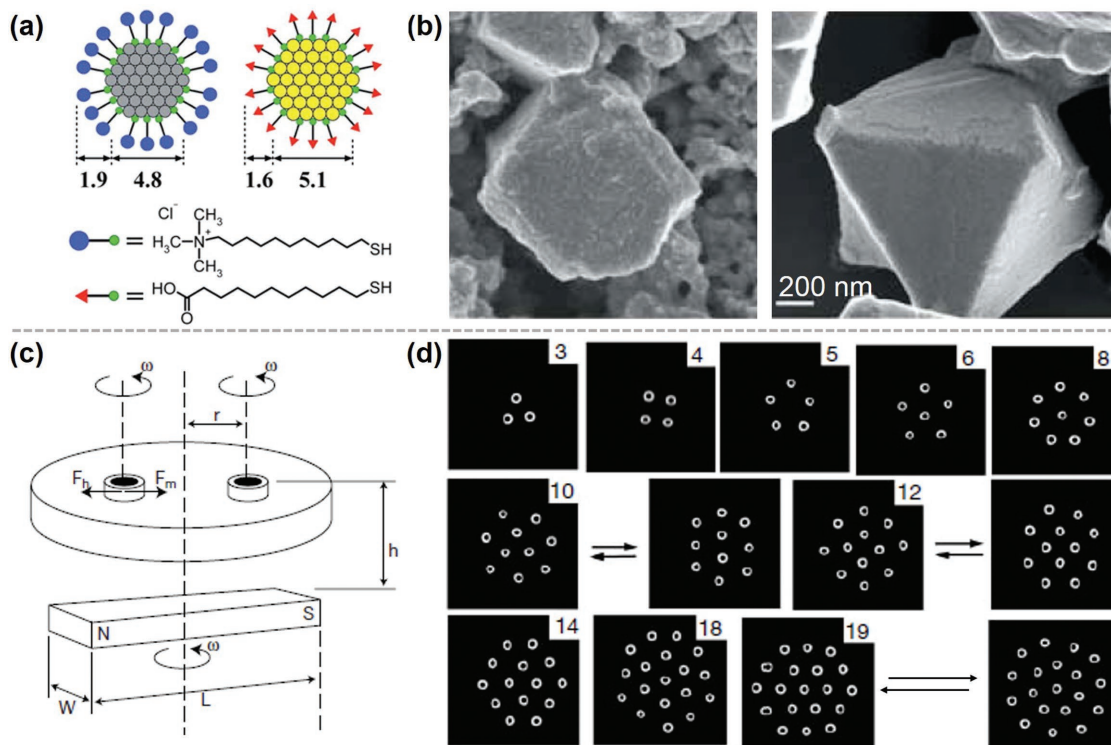


**Figure 5.** Self-assembly. a,b) Electrostatic self-assembly of oppositely charged nanoparticles. a) Silver (left) and gold (right) nanoparticles functionalized with alkane thiols containing tertiary amine groups and carboxylic groups, respectively. b) Different types of structures obtained by the self-assembly of the functionalized silver and gold nanoparticles at pH 9.7. a,b) Reproduced with permission.<sup>[66]</sup> Copyright 2006, The American Association for the Advancement of Science (AAAS). c,d) Dynamic self-assembly. c) Scheme illustrating the experimental setup for the dynamic self-assembly of magnetic disks under the influence of a rotating magnetic field. d) Patterns formed by the dynamic self-assembly of different numbers of the magnetic disks. c,d) Reproduced with permission.<sup>[71]</sup> Copyright 2000, Springer Nature.

## 4. Practical Function

### 4.1. Targeting

Targeting is a function that enables materials to recognize a specific microenvironment (e.g., via diffusible chemicals produced only at the localized region)<sup>[72]</sup> or selectively locate functionalized surfaces at target sites (e.g., receptors overexpressed on surfaces of cancer cells).<sup>[73,74]</sup> Many biological systems need the function of targeting for locating a specific site; examples include animals moving toward a source of food (e.g., by smell) or the chemotaxis of leukocytes toward sites of infection or injury. Targeting is important for many practical applications, especially for the delivery of drugs and other types of biomedical applications. An important example is the treatment of cancer. Many drug molecules that are used for treating cancer are also harmful to healthy cells; hence, they can cause undesired side effects to the human body.<sup>[75]</sup> Therefore, it is important to deliver the drug molecules only at the tumor sites. As the microenvironment around the tumor site usually has a lower pH and a slightly higher temperature than the surrounding healthy regions,<sup>[76–78]</sup> it is possible to target the tumor site by designing nanocarriers that are responsive to pH and/or temperature. In one study, for example, nanoparticles (i.e., P(NIPAM-*co*-AA)-*b*-polycaprolactone) that were responsive to both temperature and pH were specifically designed and fabricated for targeting

tumor sites.<sup>[79]</sup> Many other types of materials that are sensitive to pH between 4 and 6 have also been reported for the release of drugs at the targeted tumor sites.<sup>[80]</sup>

Another way to achieve targeting is by using a magnetic field to guide and accumulate drug-containing magnetic particles at a targeted site.<sup>[81,82]</sup> It was demonstrated that magnetic fluid-loaded liposomes (MFLs) could be used to target the tumor site in the striatum of mice. The MFLs were PEGylated phospholipids vesicles (~212 nm in diameter) with superparamagnetic nanocrystals entrapped in their aqueous cores. Results showed that when the tumor site was subjected to an external magnetic field, the concentration of particles at the tumor site was higher than that of the control experiment in which the magnetic field was not applied.<sup>[83]</sup>

### 4.2. Gating

Gating is the control of the opening of a material. By controlling the opening, this function is commonly used for regulating the passage of different types of substances through a material (e.g., the passage of ions through the ion channels on cell membranes).<sup>[84]</sup> A common example involves a porous particle that consists of stimuli-responsive polymers grafted on its surface and chemicals stored within its pores. The stimuli-responsive polymers control the opening of the pores and the release of

the chemicals. PNIPAM is usually used as the stimuli-responsive polymer.<sup>[85]</sup> At a low temperature (e.g., 32 °C or lower), the polymeric chains adopt an extended conformation, thus blocking the pores. When heat is applied to the particle (i.e., the stimulus), the polymeric chains undergo a change in conformation and collapse. Hence, the pores open and the chemicals are released from the pores.<sup>[86,87]</sup> Because of the importance of gating in the wide field of drug delivery, many different types of particles and membranes that can perform the function of gating have been developed.<sup>[26,88]</sup> These materials can be fabricated to respond to a wide range of stimuli, including light, temperature, magnetic field, ultrasound, pH, ions, biomolecules, and enzymes.<sup>[26]</sup>

Another typical example involves gating by the disassembly of a large molecule that blocks the release of chemicals from the pores. In one study, mesostructured silica nanoparticles loaded with rhodamine B (Rh B) were functionalized on their outer surfaces with a light-responsive molecule (i.e., a (*E*)-4-((4-(benzylcarbamoyl)phenyl)diazenyl)benzoic acid derivative).<sup>[89]</sup>

$\beta$ -CDs were allowed to form inclusion complexes with the *trans*-isomer of the grafted light-responsive molecules. The large  $\beta$ -CDs effectively blocked the release of the Rh B. Upon irradiation with light (i.e., 351 nm), the AB units of the light-responsive molecules isomerized from the *trans* to the *cis* isomer. Due to the low binding affinity between  $\beta$ -CD and the *cis*-AB derivatives,  $\beta$ -CD disassembled and was released from the nanoparticle. Subsequently, Rh B was released from the pores (Figure 6a,b). Hence, gating was achieved indirectly by the function of disassembly of the complexes.

#### 4.3. Rupture

Rupturing is useful for many purposes, such as the extraction or releasing of contents within an enclosure (e.g., the rupturing of fruits by animals and seed pods for spreading of seeds) and breaking objects. For drug delivery, stimuli-responsive rupturing is commonly used for releasing drugs from a particle.

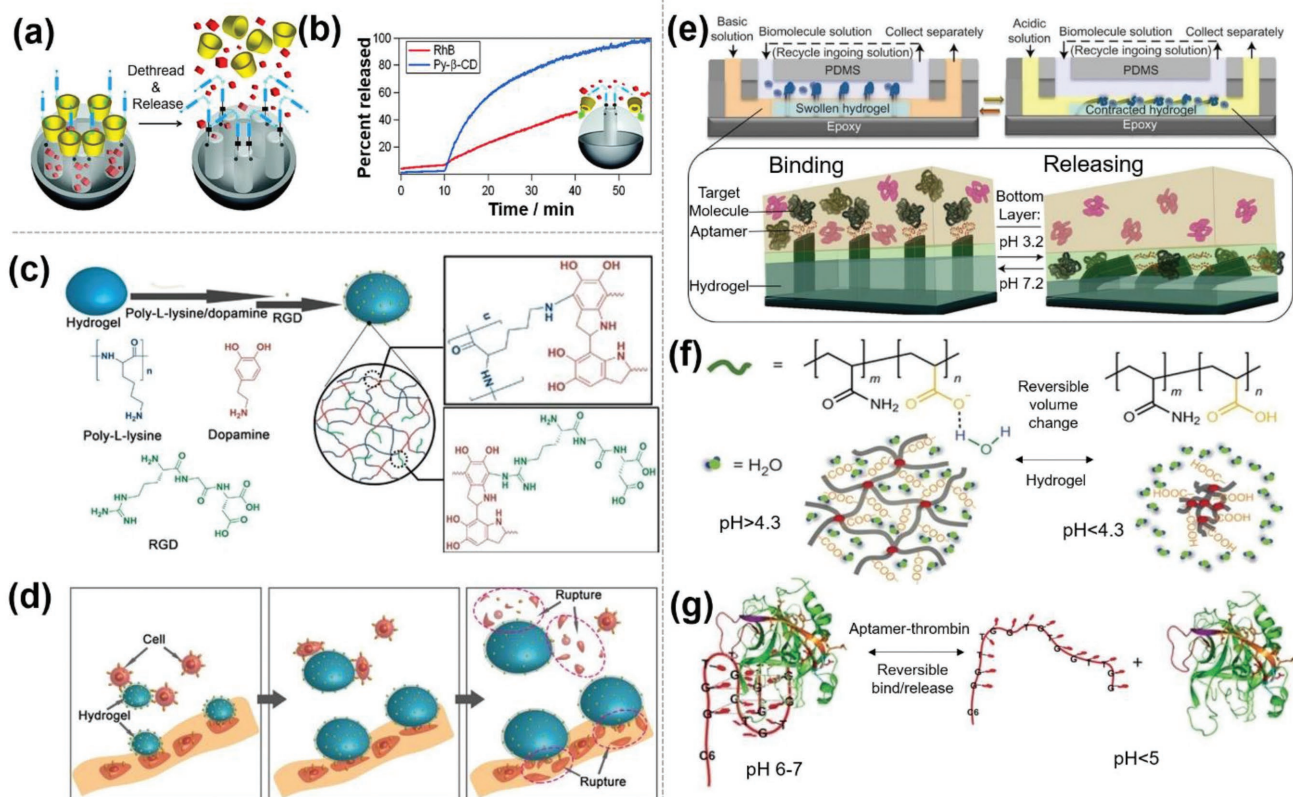


**Figure 6.** Gating, rupturing, and capture and release. a,b) Gating for controlling the release of chemicals from the pores. a) Scheme illustrating the process of gating of the pores of mesoporous silica nanoparticles controlled by the light-triggered host–guest disassembly of a large molecule (i.e.,  $\beta$ -cyclodextrin). b) Release profiles showed the rates of release of the large molecules that blocked the pores (blue line) and the molecules loaded in the mesostructured silica nanoparticles (red line) upon UV irradiation. a,b) Reproduced with permission.<sup>[89]</sup> Copyright 2009, American Chemical Society. c,d) Rupturing cancer cells using temperature-responsive hydrogels. c) Scheme illustrating the surface modification of the temperature-responsive hydrogel (PNIPAM) with RGD peptides. d) Scheme illustrating the rupturing of the cancer cells attached onto the surface of the hydrogel after the hydrogel expands by a decrease in temperature. c,d) Reproduced with permission.<sup>[46]</sup> Copyright 2018, Springer Nature. e–g) Reversible capture and release of proteins by changes in pH. e–g) Cross-sectional view of the two-channel microfluidic system with constant laminar flow. The polymeric micro-rod modified with DNA aptamers embedded in the hydrogel captured thrombin from the upper layer of liquid at pH 7.2 and release it to the lower layer of liquid when pH was changed to 3.2. f) Reversible change in volume of the hydrogel by changing pH. g) Reversible binding and releasing of thrombin by the DNA aptamer by changing pH. e–g) Reproduced with permission.<sup>[95]</sup> Copyright 2015, Springer Nature.

One example involved a microcapsule that consisted of a crosslinked temperature-responsive shell (i.e., PNIPAM) and a core containing a liquid mixed with nanoparticles.<sup>[90]</sup> The shell protected the liquid and encapsulated nanoparticles when the temperature was below the LCST of PNIPAM. When the temperature was higher than the LCST of PNIPAM, the PNIPAM shell contracted dramatically, thus leading to a sudden increase in pressure inside the microcapsule. When the internal pressure reached a critical amount, the PNIPAM shell ruptured; hence, the liquid together with the encapsulated nanoparticles were released from the microcapsule.

For destroying objects, we have previously demonstrated that the expansion of stimuli-responsive hydrogels could physically rupture cancer cells that were attached onto the surfaces of the hydrogels.<sup>[46]</sup> We used a temperature-responsive hydrogel (i.e., PNIPAM) coated with a layer of arginine–glycine–aspartate (RGD) peptides on its surface (Figure 6c). When the temperature-responsive hydrogel was allowed to come into contact with cancer cells, the cells attached onto the surface of the hydrogel by binding onto the RGD peptides (Figure 6d). Subsequently, the temperature was decreased (i.e., the stimulus) and the hydrogel expanded. Through observing the cells by scanning electron microscopy (SEM) after expanding the hydrogels, we observed that the cells ruptured into smaller fragments. Results from the MTT assay and analysis based on trypan blue showed that almost all the cancer cells attached were killed by the hydrogels. The lowering of temperature of the body is a common method used for the treatment of a variety of illness (e.g., via using packs, blankets, or vests filled with ice). This study thus demonstrated that cancer cells can be killed effectively by a physical force in contrast to other chemical (e.g., drug molecules) and biological methods (e.g., immunotherapy) currently used for the treatment of cancer.

#### 4.4. Capture and Release

Capture and release are the actions of catching a target onto a material and then releasing it. Biological systems often need this function for transporting materials. In the human body, for example, hemoglobin in the blood carries oxygen from the lungs to other parts of the body (e.g., tissues).<sup>[91]</sup> Stimuli-responsive capture and release can allow a highly specific target to be transported by capturing the target at one location, moving it, and then releasing it at a desired location. The material used usually involves a substrate functionalized with the stimuli-responsive molecules on its surface.<sup>[92–96]</sup> This function of capture and release has been used on many types of targets, including proteins, enzymes, DNA, and cells.<sup>[97–99]</sup> Different types of stimuli have been used, such as UV light, temperature, pH, and CO<sub>2</sub>.<sup>[92,94,96,100,101]</sup> Some applications of stimuli-responsive capture and release include diagnosis (e.g., through capturing and releasing of circulating tumor cells), separation, sensing, and regulation (e.g., caffeine).<sup>[93,95,96,100,102]</sup> A representative example involves Si(001) substrates coated with molecules (i.e., 4'-carboxy-4-(dimethylamino)azobenzene) that consisted of photoactive AB moieties and –N(CH<sub>3</sub>)<sub>2</sub> groups for the capture and release of ssDNA.<sup>[92]</sup> The –N(CH<sub>3</sub>)<sub>2</sub> groups protonated and charged positively in a medium that

had a pH of 6.8. When exposed to visible light (i.e., the stimulus), the AB moiety was in the *trans* configuration. This configuration had an extended molecular structure that allowed the protonated –N(CH<sub>3</sub>)<sub>2</sub> groups to be directed away from the underlying substrate and exposed the charged group to the surrounding medium. Any negatively charged ssDNA present in the medium then bound to the protonated –N(CH<sub>3</sub>)<sub>2</sub> groups through attractive electrostatic forces. In this way, the ssDNA was captured onto the substrate. Upon irradiation of UV, the AB moiety became a *cis* isomer. This configuration allowed the protonated –N(CH<sub>3</sub>)<sub>2</sub> groups to be directed toward the underlying substrate. Because these groups were no longer exposed to the surrounding solution, the ssDNA was released from the substrate.

One fascinating example of capture and release is a complex system that combined multiple other functions: the change in size of a stimuli-responsive hydrogel, the change in shape of microrods, and the change in configuration of an aptamer.<sup>[95]</sup> This system was used for the separation of a protein (i.e., thrombin) by capturing it from one stream of fluid and releasing it into another stream of fluid. The system consisted of two layers of microfluidic channels. The bottom channel was fed with a solution of a specific pH, and the top channel was fed with a solution that contained thrombin (Figure 6e). A pH-responsive hydrogel (i.e., poly(acrylamide-co-acrylic acid)) that expanded at high pH (i.e., > 4.3) and contracted at low pH (i.e., < 4.3) was placed in the bottom channel (Figure 6f). Polymeric microrods were embedded within and covalently conjugated to the pH-responsive hydrogel. Thrombin-specific aptamers were functionalized on the microrods. At pH 6–7, the thrombin aptamer remained in its folded configuration that could bind with thrombin as illustrated in Figure 6g. However, at pH < 5, the thrombin aptamer denatured and lost its ability to bind with thrombin; any bound thrombin was thus released (Figure 6g).

Operationally, a high pH solution was first fed into the bottom microfluidic channel. With this solution, the hydrogel expanded and caused the microrods to stand upright. By standing upright, the top portion of the microrods extended into the solution in the top channel, thus allowing the aptamer to interact with the thrombin present in the top channel (Figure 6e). Subsequently, a low pH solution was fed into the bottom microfluidic channel. This resulted in the contraction of the hydrogel. Because the microrods were covalently bound to the hydrogel, the contraction caused the microrods to bend sideways (Figure 6e); hence, the aptamers were immersed into the bottom microfluidic channel. The low pH denatured the aptamer and released the bound thrombin into the outflow of the bottom microfluidic channel. Therefore, thrombin was separated (or “captured”) from the solution in the top microfluidic channel and released into the bottom channel. The authors reported superior separation of thrombin at low levels of concentration (i.e., 20 × 10<sup>-9</sup> M) with a 95.5% efficiency.

#### 4.5. Shape Change

Systems that change their shapes due to the influence of a stimulus are commonly found in nature. A few examples include

the inflating of a pufferfish when they feel threatened, opening and closing of pinecones when there is a change in humidity, and folding of the *Mimosa pudica* when touched. The changes in shapes of these natural living systems have inspired many researchers to fabricate adaptive materials that change their shapes in the three-dimensional space upon the application of an external stimulus (e.g., temperature, light, electric field, magnetic field, chemicals, and biomolecules). Shape-changing materials are used in many applications, such as sensors,<sup>[103,104]</sup> actuators,<sup>[105,106]</sup> and drug-delivery systems.<sup>[90]</sup> There are two main approaches by which the stimuli-responsive materials can transform their shape: by applying: 1) a directional stimulus to a homogeneous material and 2) a uniform stimulus to an inhomogeneous material. For the second approach (2), we discuss three general ways used in previous studies for fabricating the inhomogeneous material: varying the property of a single piece of material spatially in 2D or 3D (e.g., via patterning techniques), fabricating a composite material, and 4D printing of active materials.

One of the easiest ways to obtain transformations of shapes is by selectively applying a stimulus in a specific direction to a desired region of a material. For example, light irradiation on one side of a UV-responsive hydrogel was able to induce the bending of the hydrogel due to the asymmetric expansion of the hydrogel.<sup>[107]</sup> In another common example, placing a droplet of water on one face of a water-absorbing material (e.g., polypyrrole film, PPy) induced an asymmetric swelling and a gradual deformation of the surface; the original shape could be recovered by allowing the water to evaporate.<sup>[108]</sup>

On the other hand, the stimulus are usually present uniformly throughout the environment (e.g., a uniform change in temperature or pH of the medium) in many circumstances. Nevertheless, complex changes in shape (e.g., bending, twisting, and rolling) can still be achieved by fabricating a material with spatially nonuniform properties. Through the use of advanced fabrication techniques (e.g., stereolithography, multiphoton lithography, interference lithography, photolithography, and 3D printing), precisely tailored 2D or 3D nonuniform properties can be fabricated in a material. These techniques can be used on a wide selection of stimuli-responsive materials with easily tunable physical and chemical properties for achieving complex changes in shapes.<sup>[109]</sup> Nonuniform properties in polymers can be achieved by introducing spatially different concentration of the monomers,<sup>[110,111]</sup> density of the crosslinkers,<sup>[111–113]</sup> and volume of the pores.<sup>[114,115]</sup>

One study demonstrated the possibility of fabricating a stimuli-responsive material with spatially nonuniform properties in 2D that changed its shape in 3D under the influence of a stimulus. The spatial inhomogeneity was introduced by varying the crosslinking density spatially across the material by a method called “halftone gel lithography.” This method was inspired by the traditional half-tone reprographic screen printing technique in which differently sized dots are printed on a background to create an illusion of continuous gradients. Using this concept, temperature-responsive hydrogels (i.e., P(NIPAM-co-AA)) containing photo-crosslinkable benzophenone units were patterned with a gradient of differently sized circular and highly crosslinked regions by photolithography (part (i) in Figure 7a).<sup>[112]</sup> When the temperature was decreased,

the temperature-responsive hydrogel swelled. Because of the gradient of crosslinking density throughout the hydrogel, it swelled to different extents spatially. These differences in the expansion caused nonuniform in-plane stresses to be built up. In order to relieve the stress, the hydrogel deformed out of the 2D plane; thus, it buckled and was able to form complex 3D shapes. Many interesting three-dimensional shapes (e.g., saddle, cone, spherical cap, and hybrid Enneper's surfaces) were achieved by swelling differently patterned flat 2D pieces of the hydrogel (part (ii) in Figure 7a). The transformation from 2D to 3D was reversible by changing the temperature.

Complex 3D changes in shape can also be achieved by fabricating a composite stimuli-responsive material that consists of multiple different types of materials assembled (or layered) together. Changes in shape can be obtained by harnessing the differential response of the different materials to the same stimulus.<sup>[116,117]</sup> The most commonly reported composite material is a bilayer that consists of a layer of stimuli-responsive polymer and a layer of non-responsive material. When the stimuli-responsive polymer expands (or contracts) under the influence of a stimulus, the composite material bends toward (or away from) the layer of the non-responsive material. Many different types of composite materials with a bilayer have been fabricated; examples include those that are responsive to stimuli such as pH,<sup>[118]</sup> temperature,<sup>[116,119,120]</sup> humidity,<sup>[121,122]</sup> electric field,<sup>[123]</sup> and biomolecules.<sup>[124]</sup> Many types of non-responsive materials have been used, including materials that are stiff (e.g., reduced graphene oxide)<sup>[119,125]</sup> or elastic (e.g., PDMS).<sup>[117]</sup> In some cases, the bilayer consists of two layers of stimuli-responsive polymers with different expansion ratios.<sup>[117,126,127]</sup>

One study demonstrated the possibility to program the self-folding origami of photo-crosslinkable polymers into complex 3D shapes.<sup>[128]</sup> The material was composed of three layers: two layers of polymer (i.e., poly(*p*-methylstyrene), PpMS) that sandwiched a temperature-responsive layer (i.e., PNIPAM) in the middle (part (i) in Figure 7b). The trilayer film was fabricated by first spin-coating the bottom PpMS layer on a substrate and then crosslinking the polymer to form a film. Importantly, a pattern was formed by crosslinking only selected regions of the layer using a patterned source of UV (i.e., via a digital micromirror array device). Most of the area of the layer was crosslinked except for a number of thin straight regions. After dissolving away these regions that were not crosslinked, thin straight gaps were formed between the crosslinked regions; these thin straight gaps served as the lines at which the polymeric film folded. A layer of temperature-responsive hydrogel was then coated and polymerized over the bottom layer of PpMS. Subsequently, a top layer of PpMS with a different pattern of crosslinked regions from the bottom layer of PpMS was crosslinked. In addition, pendant reactive groups at the interfaces between the layers crosslinked all the layers together; thus, the trilayer film was fabricated (part (i) in Figure 7b). This trilayer film self-folded under a change in temperature. At the region of the gap (either on the top or bottom layer), the remaining trilayer film consisted of only a bilayer: a layer of temperature-responsive hydrogel and a layer of PpMS. This bilayer bent in the same way as the stimuli-responsive bilayer discussed in the previous paragraph. Therefore, when the temperature-responsive hydrogel expanded due to a decrease

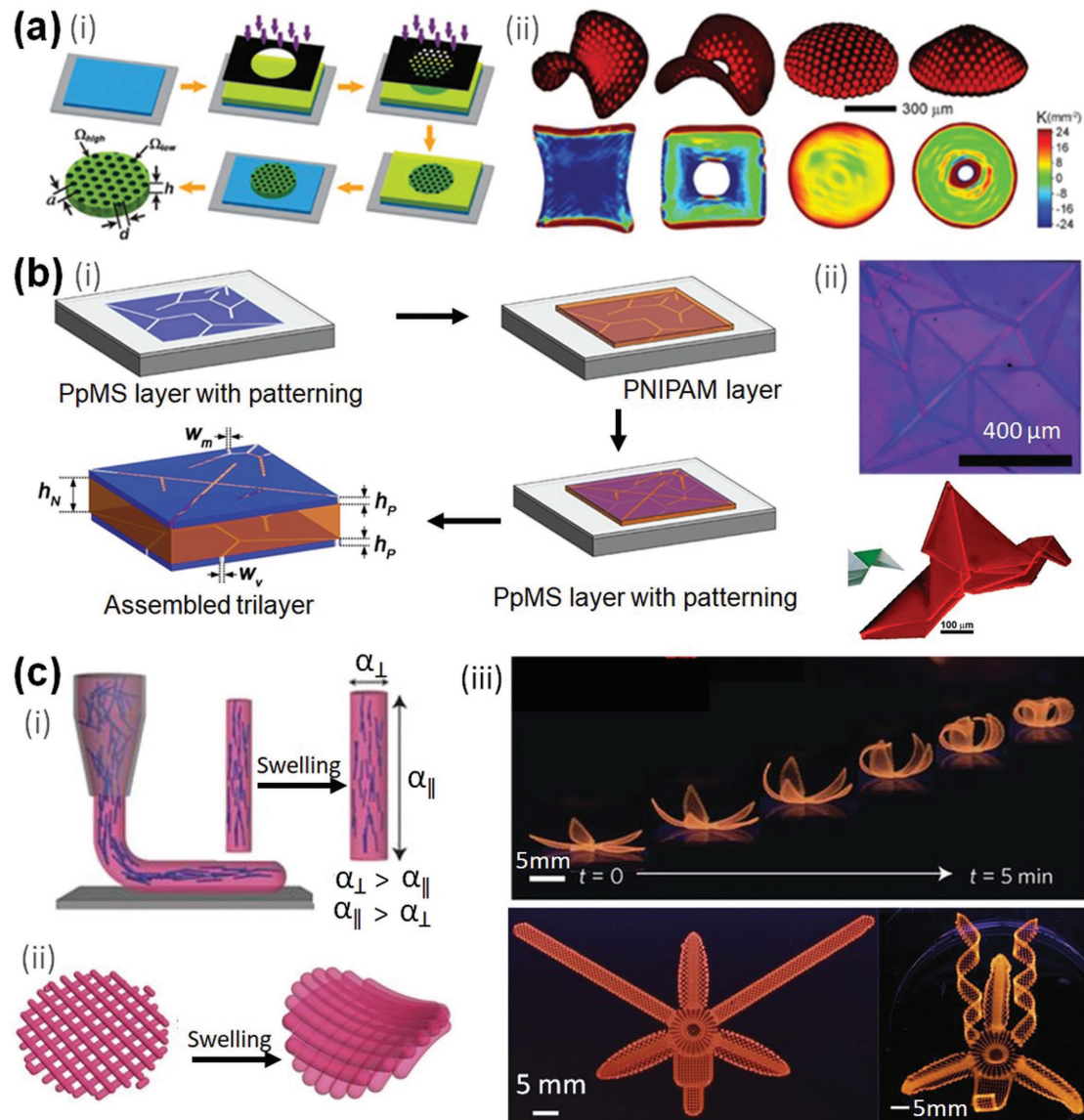


**Figure 7.** Shape change. a) Changing shape of a material with spatially inhomogeneous property under the influence of a stimulus. i) Scheme illustrating the method of patterning spatially different crosslinking density in a temperature-responsive hydrogel using the halftone gel lithography. ii) The patterned 2D disks of temperature-responsive hydrogel can generate surfaces with different 3D geometries (e.g., a saddle, spherical cap, and cone) after decreasing temperature. Reproduced with permission.<sup>[112]</sup> Copyright 2012, AAAS. b) Stimuli-responsive self-folding origami. i) Scheme illustrating the fabrication procedure of the PpMS-PNIPAM-PpMS trilayer film with patterned regions that are not crosslinked. ii) A trilayer film with a specific pattern self-folded into a flapping bird by a change in temperature. Top images show the lines at which the trilayer polymer self-folded. Bottom images show the flapping bird by folding the self-folding of the polymeric trilayer film (right). Reproduced with permission.<sup>[128]</sup> Copyright 2014, Wiley-VCH. c) Changing shape by 4D printing. i) Scheme illustrates the printing process. ii) Scheme illustrates the transformation of a 2D orthogonal bilayer to a 3D saddle when swollen. iii) Complex morphologies generated by 4D printing include shape-changing flowers (images on the top) and an orchid (images on the bottom). Reproduced with permission.<sup>[130]</sup> Copyright 2016, Springer Nature.

in temperature, any gaps at the top PpMS layer allowed the trilayer film to bend downward; on the other hand, any gaps at the bottom PpMS layer allowed the trilayer film to bend upward. In this way, self-folding origami of complex 3D geometries was achieved simply by changing the temperature (e.g., a flapping bird; see part (ii) in Figure 7b).

3D printing is a technique that allows 3D objects to be fabricated in a layer-by-layer manner. Recently, there has been a strong interest in 4D printing: the process of 3D printing

active materials such as shape memory polymers<sup>[129]</sup> and stimuli-responsive polymers.<sup>[130]</sup> This 3D-printed active material can change its shape under the influence of a stimulus (e.g., humidity or temperature) in a programmable manner. In particular, many fascinating shapes had been achieved in a previous study by 3D printing of a stimuli-responsive polymeric material in a one-step process.<sup>[130]</sup> A viscoelastic liquid that consisted of mainly a stimuli-responsive monomer (i.e., *N,N*-dimethylacrylamide or NIPAM), cellulose fibrils (aspect ratio  $\approx 100$ ),

and other additives were extruded through a nozzle (510  $\mu\text{m}$  in diameter). During the process of extrusion, shear-induced alignment allowed the long cellulose fibrils to align with the direction of flow. The subsequent polymerization of the material allowed the orientation of the aligned cellulose fibrils to be fixed. After the material was printed, it exhibited anisotropic swelling by immersing it in water (or changing the temperature) due to the alignment of the cellulose fibrils in the material (part (i) in Figure 7c). The swelling strain in the direction perpendicular to the printed path ( $\alpha_{\perp}$ ) was four times greater than the swelling strain in the parallel direction ( $\alpha_{\parallel}$ ). By printing different 3D shapes, different types of complex and programmable changes in shapes were achieved. In one example, only two layers were printed with crisscrossed lines as shown in part (ii) in Figure 7c (i.e., an orthogonal bilayer lattice). Importantly, because the lines of the two layers were printed to be perpendicular to each other at each intersecting joint, the direction of anisotropic swelling of the lines were also perpendicular. Based on our previous discussion of bending of a bilayer due to the different expansion ratios of the two layers, this perpendicular anisotropic swelling changed the shape from the original 2D plane to a 3D saddle after expanding the material in water (part (ii) in Figure 7c). This concept was used to print the shape of a flower. Upon immersion in water, this material was able to curl up in around five minutes (part (iii) in Figure 7c). Many other interesting shapes were produced, including nature-inspired architectures such as the orchid (*Dendrobium helix*) and calla lily flower (*Zantedeschia aethiopica*).

#### 4.6. Pattern Formation

Pattern formation is the generation of large-scale spatially ordered structure in a material. In many cases, the patterns are formed from the collective organization of many small features into a large ordered structure. Patterns are widely found in nature. A few examples include the spots on leopards, decorations on the feathers of peacocks,<sup>[131]</sup> periodic structures on the wings of butterflies,<sup>[132]</sup> and the hierarchical nano- to microsized features on leaves (e.g., lotus).<sup>[133]</sup> These patterns play an important role in nature, such as active camouflage, communication between the organisms, and self-cleaning of the surfaces.<sup>[134,135]</sup> Patterning, especially on surfaces, is important for the development of a wide range of technologies from controlling surface properties (e.g., friction, adhesion, and superhydrophobicity), to flexible displays,<sup>[136]</sup> and to guiding cell migration.<sup>[137]</sup> Surfaces can be patterned via many techniques, such as electron beam lithography, focused ion beam lithography, photolithography, and self-assembly of particles.<sup>[138–140]</sup> In most cases, the patterns on the surfaces were created by external means. For example, photolithography involves first printing a photomask with the specifically designed pattern and then using it for creating the same patterned features on a surface.<sup>[141]</sup> In recent years, patterns that are formed dynamically in response to an applied stimulus due to the intrinsic property of the material (i.e., not due to a pattern imposed by an external method) has drawn increasing attention in the materials community. Dynamic pattern formation has potential applications that

include dynamic light grating,<sup>[142]</sup> tunable friction and adhesion,<sup>[143]</sup> and display.<sup>[136]</sup>

Liquid crystal polymer network (LCN) is an interesting class of materials that has been used for dynamic pattern formation due to its ability to change its shape in solvent-free environments under the influence of a stimulus (e.g., light,<sup>[144,145]</sup> temperature,<sup>[146,147]</sup> electric field, and mechanical force<sup>[148,149]</sup>). One representative example involved a bilayer that consisted of a thin polystyrene (PS) film ( $\approx 30$  nm) coated on top of a thick liquid crystal elastomer (i.e., poly(methylhydrosiloxane) functionalized with liquid crystal molecules;  $\approx 0.36$  mm). The liquid crystal elastomer was composed of rod-like molecules that were fabricated to be aligned in a specific orientation (i.e., the director  $n$  as shown by the arrow in Figure 8a). When the temperature increased (e.g., from 30 to 40 °C), the order of the molecules along the aligned direction decreased. This decrease in the order resulted in the contraction of the liquid crystal elastomer in the direction of the director,  $n$  (and expansion in the direction perpendicular to  $n$ ). The in-plane compressive strain due to the contraction induced the wrinkling instability<sup>[150]</sup> and generated the wrinkle pattern as shown in Figure 8a. On the other hand, if the liquid crystal elastomer experienced a decrease in temperature (e.g., from 60 to 30 °C), the order of the molecules increased. This increase caused the liquid crystal elastomer to contract in the direction perpendicular to  $n$  (and expand in the direction parallel to  $n$ ); hence, the direction of the wrinkle pattern generated on the surface was perpendicular to the case when the temperature was increased (Figure 8b).<sup>[146]</sup>

Besides liquid crystal polymers, other types of materials can also generate patterns dynamically under the influence of a stimulus. Previous studies have investigated the reversible formation of patterns on the surface of elastomers under the influence of an electric field.<sup>[151,152]</sup> The whole system consisted of four layers (i.e., from top to bottom as illustrated in Figure 8c): a liquid electrode (e.g., a 20 wt% NaCl solution), a polymeric film (i.e., a silicone elastomer) that had the ability to form the pattern, a rigid polymeric substrate, and a metal electrode. When a high potential was applied onto the top liquid and bottom metal electrodes, the high electric field (up to  $10^8 \text{ V m}^{-1}$ ) caused the polymeric film to undergo an electromechanical instability as described in a previous study.<sup>[151–154]</sup> This electric field induced a horizontal compressive stress parallel to the plane of the film. This stress caused the initially flat surface of the polymer to form randomly oriented creases (Figure 8e). When a higher electric field was imposed onto the polymeric film, random craters were observed instead. In addition, prestretching the film before applying the potential could also change the type of pattern formed on the polymeric film (Figure 8c,d). Therefore, a variety of other patterns were formed by varying the amount of stress used for prestretching the film and the strength of the electric field (i.e., aligned creases, aligned craters, and aligned lines; Figure 8e).<sup>[155]</sup>

#### 4.7. Motion

Motion is essential for life. After millions of years, complex living organisms have evolved to acquire different mechanisms of motion for a wide range of purposes (e.g., the search

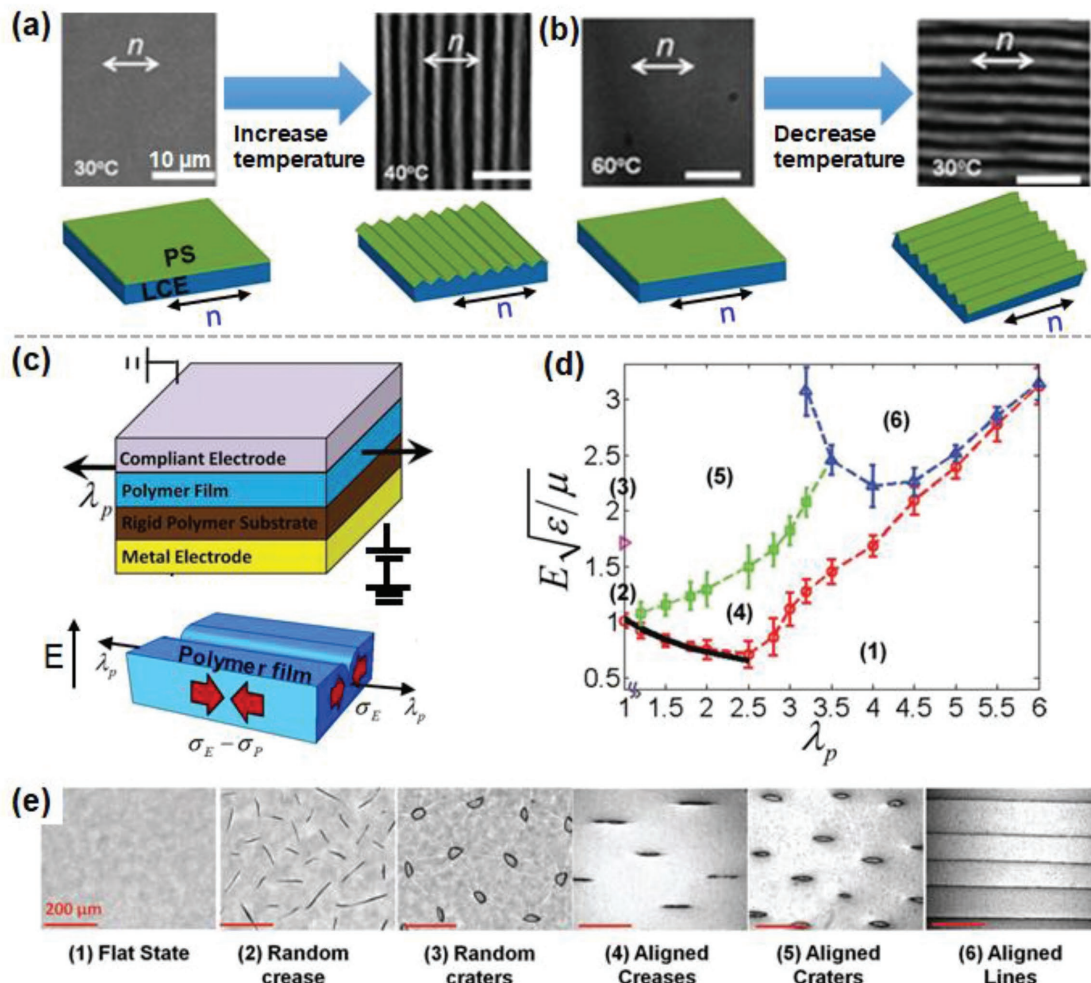


**Figure 8.** Pattern formation. a,b) Reversible formation of wrinkle patterns based on stimuli-responsive liquid crystal elastomers (LCEs). a) The polystyrene and LCE bilayer formed wrinkle pattern when temperature increased from 30 to 40 °C. b) The wrinkle pattern formed when temperature decreased from 60 to 30 °C. a,b) Reproduced with permission.<sup>[146]</sup> Copyright 2012, The Royal Society of Chemistry. c–e) Controlled pattern formation on a polymer film by an applied electric field. c) Schematic illustration of the experimental setup. A tensile stress was used to control the alignment of the pattern. d) A phase diagram showing the different patterns formed as a function of a quantity that is proportional to the electric field,  $E$  (y-axis) and the uniaxial prestretch ratio,  $\lambda_p$  (x-axis). e) Optical images of the different patterns formed on the polymer film. The numbers under each image correspond to those labeled in the phase diagram in (d). c–e) Reproduced with permission.<sup>[155]</sup> Copyright 2012, Wiley-VCH.

for food). Examples of biological motions include the migration of animals, cell migration, and the locomotion of motor proteins (e.g., kinesin and myosin) within a cell. Inspired by nature, a lot of progress has recently been made toward the fabrication of micro- or nanomotors (e.g., nanorods or Janus particles)<sup>[156–158]</sup> that can be propelled by different mechanisms, such as bubble propulsion,<sup>[159,160]</sup> self-electrophoresis,<sup>[161]</sup> diffusiophoresis,<sup>[162]</sup> and gradients of surface tension.<sup>[163,164]</sup> Hence, materials can be propelled to move by many different types of stimuli, including pH, light, ultrasound, magnetic field, electric field, and biomolecules.<sup>[165,166]</sup> These small motors have been proposed to be useful for applications such as targeted drug delivery, cell manipulation and isolation, bioimaging, biosensing, and environmental monitoring and remediation.<sup>[167]</sup> Within this rich field of fabricating motors for motion,<sup>[165,168–170]</sup> we describe four interesting examples that are driven by different types of stimuli:

magnetic field, generation of bubbles, gradient of surface tension, and gradient of water vapor.

A moving magnetic field is a conceptually straightforward way to induce motion of magnetic materials.<sup>[171]</sup> On the other hand, a moving magnetic field can also be used creatively to induce motion indirectly via a biomimicking component: the flagellum of a bacterium.<sup>[172]</sup> The microscopic artificial magnetic flagellum consisted of a linear chain of colloidal magnetic particles (i.e., superparamagnetic particles;  $\approx 1 \mu\text{m}$ ) covalently linked to each other by DNA as illustrated in Figure 9a. This artificial flexible flagellum was attached to a red blood cell. By applying the magnetic field in a specific direction,  $B_x$ , the flagellum aligned with the direction of the field. In addition, by changing the magnetic field in an oscillatory manner in the perpendicular direction,  $B_y$ , the flagellum was actuated to swing with a whiplike motion (Figure 9a). This oscillatory motion of the flagellum caused the fluid in the surrounding medium to flow;

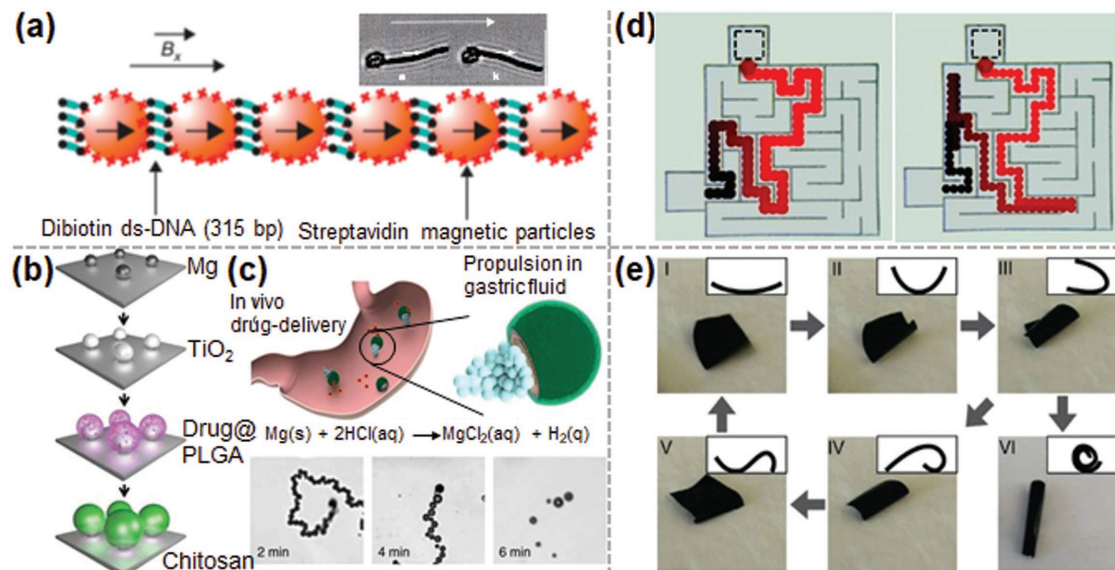


**Figure 9.** Motion. a) Motion of a microscopic artificial flagellum based on DNA-linked magnetic particles driven by a magnetic field. Reproduced with permission.<sup>[172]</sup> Copyright 2005, Springer Nature. b,c) Micromotors propelled by asymmetric generation of bubbles. b) Scheme illustrating the fabrication of the Mg-based multilayer micromotor on a substrate. c) Asymmetric generation of hydrogen bubbles propelled the micromotors to move in a gastric fluid. b,c) Reproduced with permission.<sup>[160]</sup> Copyright 2017, Nature Publishing Group. d) Self-propelled oil droplet solving a maze via the shortest path by sensing a source of low pH placed at the exit of the maze. Reproduced with permission.<sup>[164]</sup> Copyright 2010, American Chemical Society. e) The motion of a polymeric film driven by water gradients. Reproduced with permission.<sup>[173]</sup> Copyright 2013, AAAS.

this fluid then led to the motion of the whole material (i.e., the red blood cell and the flagellum) toward the direction indicated in Figure 9a. Therefore, the magnetic field was used to induce the motion of the artificial flagellum instead of directly using a moving magnetic field to induce the motion of the magnetic materials in the same direction.

The asymmetric generation of bubbles around a particle is another common way to induce motion as reported in many previous studies. Despite being widely studied, most of the systems investigated cannot be used in actual applications because the fuel needed for generating the bubbles (e.g., most commonly hydrogen peroxide) is usually not available in natural systems (e.g., in the environment or *in vivo*).<sup>[167]</sup> In one study, however, the authors designed an Mg-based micromotor that used the naturally available acidic medium as the fuel for treating gastric bacterial infection in the stomach of a mouse.<sup>[160]</sup> The micromotors (~20 μm) consisted of an Mg core, an outer layer of TiO<sub>2</sub>, an additional outer layer of poly(lactic-co-glycolic acid) (PLGA) that was loaded with the clarithromycin antibiotic, and an outermost layer of chitosan (Figure 9b). This multilayered particle was fabricated on a flat substrate; upon removing the particle from the substrate, the inner Mg core was exposed to its surrounding due to the truncated portion of the particle (when it formed on the surface). When the micromotors were exposed to low pH (i.e., the stimulus) in the gastric medium of the mouse, the reaction of the acid with Mg caused hydrogen gas to be generated (Figure 9c). This evolution of gas on one side of the micromotor (i.e., the side with the exposed Mg core) caused the micromotor to move unidirectionally. When the micromotor came into contact with the wall of the stomach, the positively charged chitosan adhered onto the wall. The subsequent release of the antibody from the

micromotor was thus localized in the vicinity of the wall of the stomach. Results showed that there was a significant reduction in the bacteria in the stomach of the mouse (without any apparent toxicity) compared to that of the control experiment in which drug carriers that did not move were used.

Surface tension driven flows of fluid can also be used to drive the motion of objects. In addition to motion, one study demonstrated that analytical operations could also be performed: an oil droplet containing a surfactant (i.e., 2-hexyldecanoic acid) was able to move and solve a maze via the shortest possible path.<sup>[164]</sup> The maze consisted of a complex geometry as shown in Figure 9d and was filled with an alkaline solution. A block of agarose gel filled with acid was placed at the exit of the maze (i.e., the stimulus applied for solving the maze). There was thus a concentration gradient of pH in the maze: more acidic at the exit and more alkaline at the starting point. Once the oil droplet was placed at the starting point, the surfactant diffused out of the droplet and was deprotonated in the alkaline environment. More surfactant, however, was protonated in the direction toward the source of the acid. This asymmetric concentration of surfactant around the droplet thus led to an asymmetric surface tension driven flow that propelled the droplet toward the exit. Since the gradient in pH was the steepest along the shortest route, the droplet experienced the greatest driving force along the same direction; hence, it was able to solve the maze via the shortest path (Figure 9d).

In a remarkable example, water vapor was shown to be able to drive the motion of a piece of polymer for harvesting energy and actuation. The motion was achieved by a water-responsive polymeric film that moved based on a gradient of water vapor present in the atmosphere.<sup>[173]</sup> The strong and flexible polymeric film consisted of an interpenetrating polymer network of

PPy and polyol-borate. When the polymeric film was exposed to water, the water hydrolyzed the crosslinking borate ester groups in the polyol-borate network, thus causing the polymer to swell. At the same time, the water also disrupted the intermolecular hydrogen bonding between the polyol-borate network and PPy, thus causing the polymer to swell further. In the absence of water, the process was reversed and the polymer contracted. When this polymeric film was placed on a moist piece of paper, the gradient of water vapor between the moist paper and air caused an asymmetric deformation of the polymeric film. Specifically, the portion of the polymeric film that was in contact with the moist paper absorbed water and swelled; at the same time, water evaporated at regions of the polymeric film that were farther away from the moist paper. This asymmetric swelling and evaporation caused the polymeric film to deform into a series of interesting shapes as shown in Figure 9e. At certain stages of the deformation, the bent polymeric film toppled under its own weight in one direction, thus causing the film to move laterally. The authors demonstrated that this motion allowed the polymeric film to lift objects, transport cargo, and harvest the energy from the gradient of water vapor in the surrounding.

#### 4.8. Communication

Communication is the process in which a signal (i.e., any transferrable form of information, such as molecules, sound, or gesture) is transferred from one entity to another, or the exchange of a signal between two entities. Communication is important in nature. Most living organisms (e.g., humans and animals) communicate with their external environments via different means (e.g., sight and sound).<sup>[174–177]</sup> Communication is also important within the organism; an important example is the rapid transfer of information via nerve impulses.<sup>[178]</sup> For smaller systems (e.g., millimeters and below), communication is commonly performed by the transport of small diffusible molecules. For example, cells communicate externally with their neighbors by exchanging chemicals<sup>[177,179]</sup> and internally via the numerous signaling molecules within the body of the cell.<sup>[180]</sup> Similarly, it is necessary for synthetic systems to be able to communicate effectively both externally with their environments and internally for coordinating the various operations functioning within the system. In many circumstances, the communication should only be established when needed. Hence, it is desirable for the system to be stimuli-responsive for triggering the communication only when required. In this section, we discuss three types of stimuli-activated communication demonstrated in synthetic systems: cascading communication, interactive communication, and targeted communication.

Cascading communication is the transport of a signal across multiple locations sequentially from one to another. One study demonstrated cascading communication by using three types of functional mesoporous silica nanoparticles (MSNs;  $\approx 100$  nm), labeled as S1, S2, and S3.<sup>[181]</sup> Each of these MSNs was loaded with a different type of chemical (i.e., the signal to be communicated) and capped with molecules that blocked the release of the chemicals. When a chemical (i.e., pancreatin) that served as the stimulus was added to the solution, it hydrolyzed and

cleaved the bonds (i.e., the glycosidic bond) of the molecules that capped S1 (i.e., a saccharide derivative; Glucidex). Once the capping molecules were cleaved, the signaling molecules (i.e., tris(2-carboxyethyl)phosphine, TCEP) that was loaded in S1 was released from its pores. These signaling molecules released from S1 then moved to S2 and cleaved the bonds (i.e., the disulfide bonds) of the molecules that capped S2 (i.e., polyethylene glycol, PEG). After cleaving the capping molecules of S2, the signaling molecules (i.e., dodecyl trimethylammonium bromide, DTAB) that was loaded in S2 was released. The process repeated by allowing the signaling molecules from S2 to move to S3 and cleave the bonds of the molecules that capped S3 (i.e., DOCP lipid bilayer). This process caused the fluorescent molecules loaded in S3 to be released; hence, a fluorescent output was detected. In this way, the signal was communicated from S1 to S2 and to S3 in a cascading manner.

Besides the unidirectional transfer of the signal, it has also been demonstrated that a signal can be exchanged interactively in both directions between two systems. In one study, two types of hybrid particles were fabricated, each of which consisted of a gold nanoparticle connected to a relatively larger MSN (Figure 10a).<sup>[182]</sup> For the first particle, S1<sub>gal</sub>, the MSN was loaded with signaling molecules ( $(Ru(bpy)_3)^{2+}$ ) in its mesochannels and the pores of the MSN were capped with  $\beta$ -CD attached via disulfide bonds. The MSN of the second particle, S2<sub>gox</sub>, was loaded with another type of signaling molecules (i.e., N-acetyl-L-cysteine) in its mesochannels; their pores were capped with a pH-responsive supramolecular nanovalve (i.e.,  $\beta$ -CD:benzimidazole). The surface of the gold nanoparticle of S1<sub>gal</sub> was modified with the enzyme  $\beta$ -galactosidase ( $\beta$ -Gal). For S2<sub>gox</sub>, on the other hand, the surface of the gold nanoparticle was modified with glucose oxidase (GOx). When lactose (i.e., the stimulus) was added to the solution containing both types of hybrid particles, the hydrolysis of lactose by  $\beta$ -Gal that was present on S1<sub>gal</sub> produced glucose. These glucose molecules generated was the signal that moved over to S2<sub>gox</sub>; it was then hydrolyzed into gluconic acid ( $pK_a = 3.6$ ) by the GOx of S2<sub>gox</sub>. The reduction in pH by the gluconic acid subsequently deprotonated the benzimidazole groups ( $pK_a = 5.55$ ) on S2<sub>gox</sub>. After being deprotonated, the supramolecular nanovalve disassembled and released the signaling molecule N-acetyl-L-cysteine. This signaling molecule then moved to S1<sub>gal</sub> and cleaved the disulfide linkage; hence, the  $(Ru(bpy)_3)^{2+}$  was released and a fluorescent signal was detected (Figure 10b). This system thus demonstrated the capability of exchanging information interactively between the two types of hybrid particles. This interactive communication was proven experimentally. When certain elements of the particles were not included (e.g., the surface of the gold nanoparticle was not functionalized with the enzymes), the  $(Ru(bpy)_3)^{2+}$  ions were not released (Figure 10b).

Targeted communication involved the guiding of the motion of one particle via a magnetic field to another targeted particle, and then allowing the two particles to communicate.<sup>[183]</sup> The particle to be guided was made of polystyrene ( $\approx 2 \mu m$ ) that was half coated with Ni (i.e., the magnetic component), Au and Ag. The targeted particle was made of SiO<sub>2</sub> ( $\approx 1.2 \mu m$ ) that was half coated with Pt. These particles were immersed in a solution that contained H<sub>2</sub>O<sub>2</sub> (1.5 wt%). In this solution, the Ag coated on

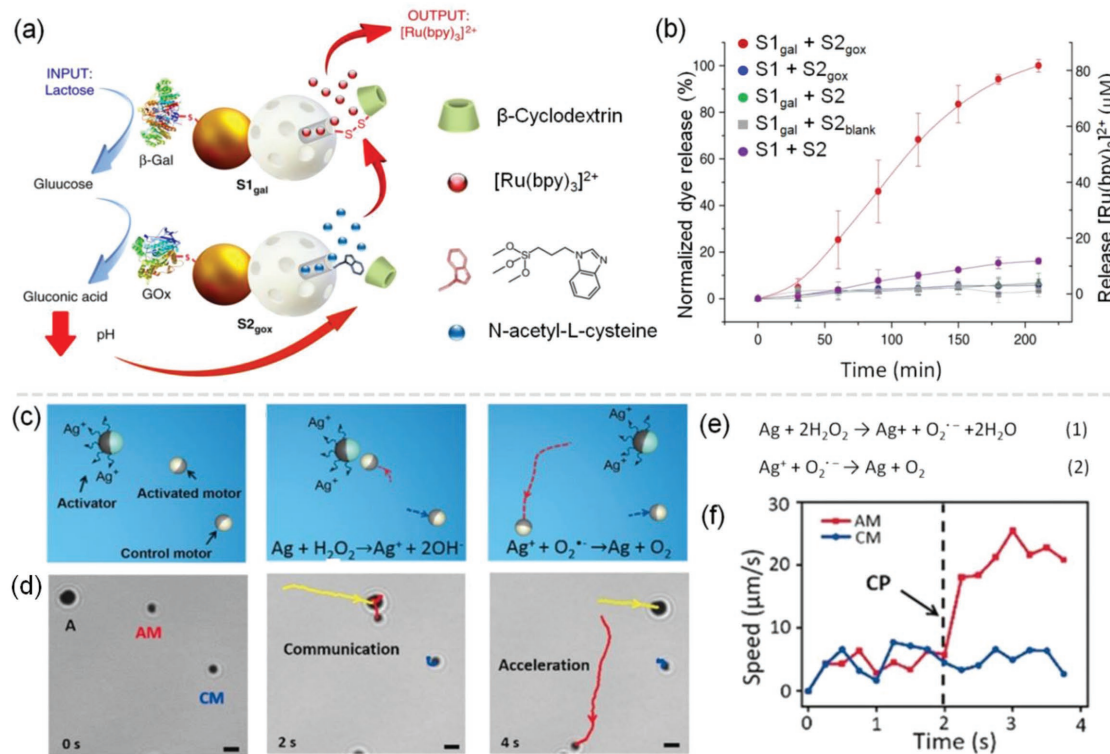


**Figure 10.** Communication. a,b) Exchanging communication between two particles. a) Scheme illustrating the communication from the hybrid gold/silica particle, S1<sub>gal</sub>, to a second hybrid gold/silica particle, S2<sub>gox</sub>, and then back to S1<sub>gal</sub> again. b) Experimental verification of the interactive communication between the particles (red line indicated the successful release of dye after the communication). Without any of the required component in the particles, only a small amount of dye was released. a,b) Reproduced with permission.<sup>[182]</sup> Copyright 2017, Nature Publishing Group. c–f) Magnetic field-targeted communication. c) Scheme illustrating the communication between two Janus particles (i.e., the activator, “A” and activated motor, “AM”) by Ag<sup>+</sup> under the guidance of a magnetic field. d) Time-lapse microscopy images of the communication between the particles. Particle A was guided to approach and communicate with particle AM, resulting in a dramatic increase in the speed of particle AM. e) Reactions for Ag dissolution and deposition. f) Moving speed of particle AM greatly increased after communication with particle A (red curve). c–f) Reproduced with permission.<sup>[183]</sup> Copyright 2018, Wiley-VCH.

the PS particle reacted with the H<sub>2</sub>O<sub>2</sub> according to reaction (1) illustrated in Figure 10e; this reaction produced Ag<sup>+</sup> and superoxide radicals (O<sub>2</sub><sup>·-</sup>).<sup>[184]</sup> The process involved first using a magnetic field to move the PS particle (i.e., the activator or “A” as indicated in Figure 10c,d) toward the targeted SiO<sub>2</sub> particle (i.e., the activated motor or “AM” as indicated in Figure 10c,d). When the distance between the two particles was less than one body length of the PS particle, the Ag<sup>+</sup> and O<sub>2</sub><sup>·-</sup> reacted on the Pt surface of the targeted SiO<sub>2</sub> particle according to reaction (2) (Figure 10e).<sup>[184]</sup> This reaction allowed Ag metal to be deposited rapidly onto the SiO<sub>2</sub> particle because of the good match between the crystal lattices of Ag and Pt.<sup>[185,186]</sup> In short, the communication between the two types of particles was accomplished by the transfer of Ag from the PS particle to the targeted SiO<sub>2</sub> particle. Transmission electron microscopy (TEM) and X-ray photoelectron spectroscopy (XPS) confirmed the deposition of Ag on the SiO<sub>2</sub> particle and the formation of the bimetallic Ag/Pt surface. This bimetallic material and the increase in surface area (due to the increase in surface roughness) after the deposition of Ag resulted in the greatly enhanced catalytic decomposition of H<sub>2</sub>O<sub>2</sub>.<sup>[187,188]</sup> This increased rate of decomposition of H<sub>2</sub>O<sub>2</sub> allowed more O<sub>2</sub> gas to be evolved; hence, the speed of the SiO<sub>2</sub> particle increased greatly from 4.1 to 24.3 μm s<sup>-1</sup>

(Figure 10f). Therefore, by moving the PS particle and allowing it to communicate with its targeted SiO<sub>2</sub> particles, it was possible to propel the motion of the SiO<sub>2</sub> particles.

## 5. Regulatory Function

### 5.1. Self-Regulation

Self-regulation (or homeostasis) is the ability of a system to control the amount of a process variable (e.g., temperature, pH, glucose, and pressure) at a desired level when the system is perturbed. Many systems found in nature are self-regulating. An important example involves the regulation of the body temperature at 37 °C. Upon sensing a change in the temperature of the body, the thermoregulatory neuronal signaling pathways in the brain can produce a response (e.g., the secretion of sweat when temperature increased and shivering when temperature decreased) to counter the change.<sup>[189]</sup>

In fact, many systems discussed previously herein can be considered as self-regulating because of the ability of stimuli-responsive materials to detect a stimulus and respond accordingly. For example, the change in pH of the fluid flowing

in a microfluidic channel allowed the stimuli-responsive valves to respond and deviate the flow of the fluid into a specific channel (Figure 4a). Because the direction of flow was determined by the property of the fluid within the microfluidic channel rather than an externally applied stimulus, the system is self-regulating. On the other hand, the stimuli-responsive materials sensed pH but produced a response (i.e., the control of the direction of flow) that did not affect the pH of the fluid.

A more advanced form of self-regulation is the closed-loop self-regulation. Stimuli-responsive closed-loop self-regulation is the ability to sense a stimulus and produce a response that influence the stimulus by a feedback mechanism. In many cases, the system contains a cargo that can be released to counteract the change in the environment due to the applied stimulus. For example, when the concentration of a chemical decreases, the stimuli-responsive system detects the change in concentration and releases the same chemical into its surrounding. In general, this approach of regulating the stimulus has many important applications, especially in the field of drug delivery. Many types of systems have been developed, including the delivery of antibiotics to treat bacterial infections,<sup>[190]</sup> drugs to treat obesity,<sup>[191]</sup> and heparin to control the rate of blood coagulation.<sup>[192,193]</sup>

A classic and important example of closed-loop self-regulation is the class of glucose-responsive systems that release insulin for the management of diabetes. Reported as early as the 1980s,<sup>[194–196]</sup> many types of materials have been developed for closed-loop drug delivery of insulin, including microgels,<sup>[197,198]</sup> membranes,<sup>[196]</sup> capsules,<sup>[194,199–201]</sup> nanovesicles,<sup>[202]</sup> nanoparticles,<sup>[203]</sup> and microneedles.<sup>[204]</sup> As a specific example, one recent study investigated a closed-loop transdermal patch for the delivery of insulin.<sup>[204]</sup> Most of the previous studies reported systems that operated under *in vitro* conditions; on the other hand, this study showed the efficacy of the transdermal patch on diabetic mice. The transdermal patch consisted of glucose-responsive microneedles loaded with insulin, glucose oxidase, and catalase as shown in Figure 11a. The microneedles were fabricated using a degradable polymer (i.e., poly(vinyl alcohol), PVA) that was crosslinked using H<sub>2</sub>O<sub>2</sub>-labile crosslinkers. Chemically modified insulin was covalently bound to the matrix of the polymer using the same H<sub>2</sub>O<sub>2</sub>-labile crosslinkers. When the concentration of glucose increased, the glucose molecules diffused into the microneedles, thus allowing the glucose oxidase to catalyze the glucose into gluconic acid and H<sub>2</sub>O<sub>2</sub>. The H<sub>2</sub>O<sub>2</sub> then cleaved the crosslinkers to release insulin into the bloodstream. This release of insulin triggered biological pathways for cells to absorb the glucose for metabolism and decreased the blood-glucose concentration as shown in Figure 11b, thus completing the feedback loop. Subsequently, the enzyme catalase removed the harmful H<sub>2</sub>O<sub>2</sub> from the body by converting it into H<sub>2</sub>O; hence, the system was compatible for *in vivo* conditions.

Creative designs of systems that consisted of many components and a combination of functions (e.g., size change and shape change) have been used for the self-regulation of temperature via a complex chemo-thermo-mechanical feedback loop.<sup>[205]</sup> The system consisted of two layers of immiscible liquids: the bottom layer was an aqueous solution and the top layer was organic and filled with a reactant for the exothermic reaction (i.e., 1-hexene). A temperature-responsive hydrogel

(i.e., PNIPAM) was immersed in the bottom layer. Microfins were partially embedded and covalently bonded to the temperature-responsive hydrogel as illustrated in Figure 11c. The tips of the microfins were coated with a catalyst (i.e., H<sub>2</sub>PtCl<sub>6</sub>). Interaction between the catalyst and the reactant allowed an exothermic reaction to occur. This self-regulating system operated by allowing the temperature-responsive hydrogel to be in its expanded state at low temperature. In this state, the microfins were in an upright position; thus, the tips of the microfins extended into the top organic phase. The reactant then interacted with the catalyst. Because of the exothermic reaction, the temperature of the system increased. Subsequently, the temperature-responsive hydrogel contracted and caused the covalently bounded microfins to bend. The catalyst at the tips of the microfins thus no longer exposed to the reactant and the exothermic reaction stopped. A subsequent decrease in temperature by dissipation of heat into the surrounding allowed the temperature-responsive hydrogel to expand and the microfins to return to their initial upright position. The cycle then repeated for regulating the temperature.

## 5.2. Self-Oscillation

Self-oscillation is the generation of sustained periodic cycles of a signal (e.g., a measurable quantity such as size or concentration) over a period of time.<sup>[203]</sup> Self-oscillating processes are commonly found in living systems, such as the beating of a heart, pulsatile secretion of hormones, and peristaltic motions in the digestive tract.<sup>[206]</sup> Inspired by these autonomous oscillatory phenomena in living systems, a number of synthetic self-oscillating systems have been developed. Applications of these systems include the oscillating biomimetic actuators<sup>[207,208]</sup> and the periodic waves of expansion and contraction of a material for the transport of particles across surfaces.<sup>[209–211]</sup>

The most common way of constructing stimuli-responsive self-oscillating systems is to use the self-oscillating Belousov–Zhabotinsky (BZ) reaction. A temperature-responsive hydrogel (PNIPAM; ≈600 μm) that contained covalently bound ruthenium tris(2,2'-bipyridine) (Ru(bpy)<sub>3</sub>). Ru(bpy)<sub>3</sub> was used as the catalyst for the BZ reaction.<sup>[212]</sup> This temperature-responsive hydrogel was immersed in an aqueous solution that contained the complex mixture of chemicals for driving the BZ reaction (e.g., nitric acid, malonic acid, and sodium bromate). When stress was not applied (or an insufficient amount of stress was applied) onto the hydrogel, the authors did not observe any oscillation at steady state (i.e., parts (i) to (iii) of the plot shown in Figure 11d). However, when the hydrogel was compressed with a sufficient amount of stress, the concentration of Ru(bpy)<sub>3</sub> within the hydrogel increased (Figure 11d). This increase in concentration of the catalyst caused the BZ reaction to occur inside the hydrogel. This self-oscillating BZ reaction produced the periodic cycles of oxidation of Ru(bpy)<sub>3</sub><sup>2+</sup> and reduction of Ru(bpy)<sub>3</sub><sup>3+</sup> in the hydrogel. Because the different oxidation states of the catalyst (i.e., Ru(bpy)<sub>3</sub><sup>2+</sup> and Ru(bpy)<sub>3</sub><sup>3+</sup>) had different colors, the color (or hue) of the hydrogel exhibited corresponding oscillatory changes according to the periodic cycles of the BZ reaction (i.e., parts (iv) and (v) of the plot shown in Figure 11d).

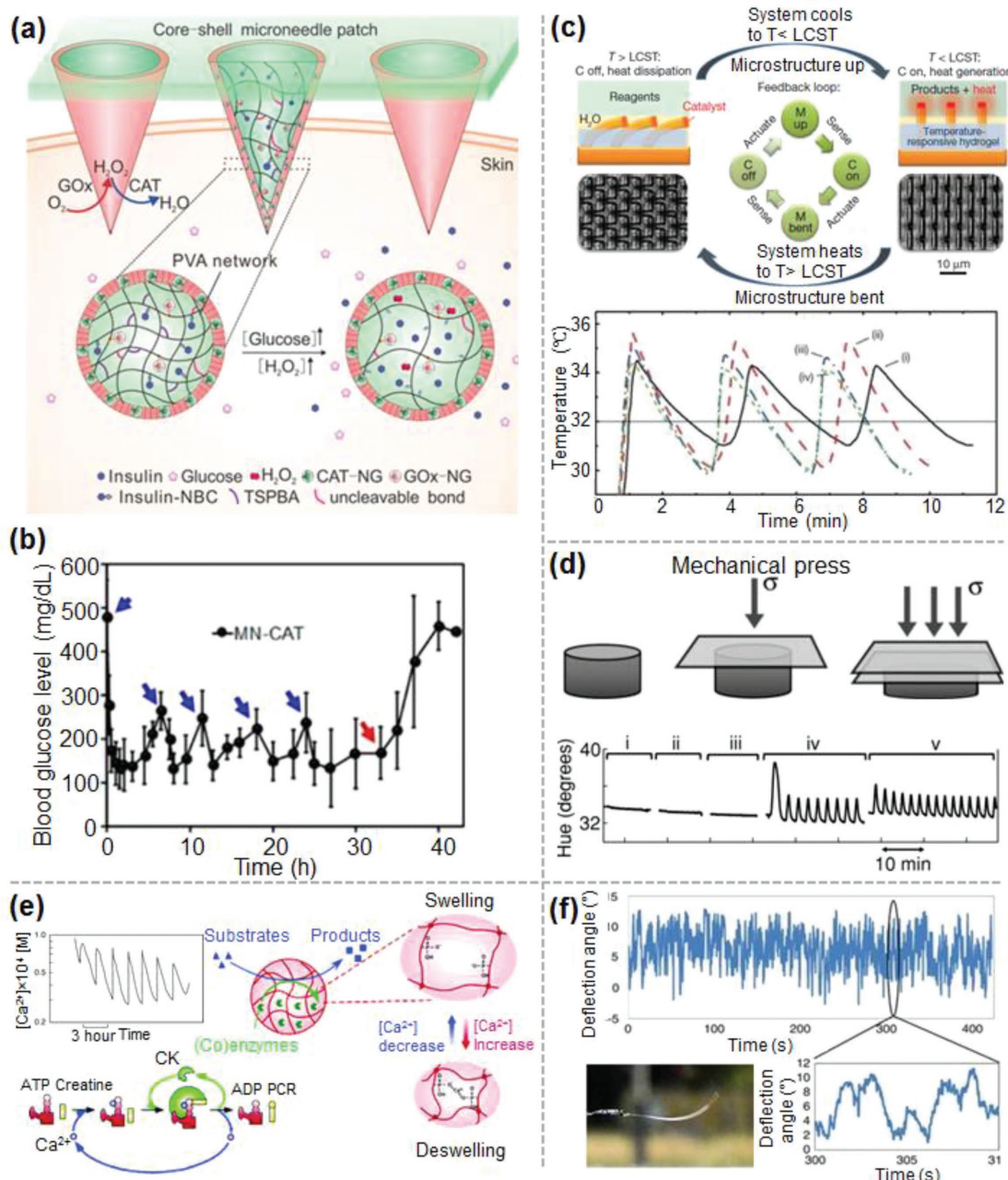


**Figure 11.** Self-regulation and self-oscillation. a,b) A closed-loop self-regulating system for controlling the level of glucose. a) Schematic representation of the glucose-responsive insulin delivery system that consisted of the core–shell microneedle patch. b) Self-regulating changes in blood-glucose levels of mice treated with the microneedle patch. a,b) Reproduced with permission.<sup>[204]</sup> Copyright 2018, American Chemical Society. c) Self-regulation of temperature via a complex chemo–thermo–mechanical feedback loop. Scheme illustrating the process of self-regulation (top). Temperature was measured experimentally to be maintained by the self-regulating process (bottom). Reproduced with permission.<sup>[205]</sup> Copyright 2012, Springer Nature. d) Stress-responsive self-oscillation. The color (or hue) of the NIPAAm-*co*-Ru(bpy)<sub>3</sub> hydrogel oscillated after a mechanical stress was applied on the hydrogel containing the chemicals for performing the Belousov–Zhabotinsky reaction. Reproduced with permission.<sup>[212]</sup> Copyright 2012, Wiley-VCH. e) Self-oscillation of Ca<sup>2+</sup> by an oscillating enzymatic reaction. The poly(NIPAAm-*co*-MEP) hydrogel underwent repeated cycles of expansion and contraction in the presence of ATP and creatine (i.e., the stimuli). Reproduced with permission.<sup>[213]</sup> Copyright 2005, American Chemical Society. f) A self-oscillating polymeric actuator driven by sunlight. Plot shows the deflection angle of the self-oscillating polymeric film. Reproduced with permission.<sup>[214]</sup> Copyright 2016, Nature Publishing Group.

Very few examples demonstrated self-oscillation without the use of BZ reactions. One study reported a biomimetic gel that exhibited autonomous and repeated cycles of expansion and

contraction, similar to the beating motion of the heart driven by a self-oscillating enzymatic reaction.<sup>[213]</sup> The reaction consisted of the adenosine triphosphate and creatine as the reactants,

and creatine kinase and  $\text{Ca}^{2+}$  ion as the catalysts. In this reaction, the catalysts converted the ATP to adenosine diphosphate (ADP) and creatine to phosphocreatine (PCr) according to the reaction mechanism illustrated in the bottom left scheme of Figure 11e. Importantly, the  $\text{Ca}^{2+}$  ions first bound with ATP during the course of the reaction, thus causing the concentration of the free  $\text{Ca}^{2+}$  ions in the solution to decrease. Subsequently, the generation of ADP allowed the bound  $\text{Ca}^{2+}$  ion to be released into the solution. This release increased the free  $\text{Ca}^{2+}$  ions in the solution. The repeated cycles of increasing and decreasing the concentration of the free  $\text{Ca}^{2+}$  ions in the solution caused the concentration of  $\text{Ca}^{2+}$  ions to self-oscillate. This self-oscillating enzymatic reaction was used together with a hydrogel (i.e., poly(NIPAAm-co-2-(methacryloyloxy) ethyl phosphate)). The hydrogel consisted of phosphoric groups in the polymeric chains and was filled with creatine kinase and calcium chloride. The phosphoric groups in the hydrogel chelated with the divalent calcium ion; thus, the polymer crosslinked and contracted (Figure 11e). When ATP and creatine (i.e., the stimuli) were added to the solution containing this hydrogel, the self-oscillating concentration of  $\text{Ca}^{2+}$  allowed the hydrogel to undergo repeated cycles of expansion (i.e., by removing the crosslinks of the polymer due to a decrease in  $\text{Ca}^{2+}$  ions) and contraction (i.e., the crosslinking of the polymer by an increase in  $\text{Ca}^{2+}$  ions) accordingly. Through using the chemical energy of this self-oscillating biological reaction, an artificial ATP-fueled biomachine that mimicked the heart muscle was achieved.

A light-responsive self-oscillating polymeric actuator has been proposed to be used in many applications, such as a coating that self-cleans (i.e., by shaking foreign objects off the surface), self-propelling soft actuators, and a system for converting solar to mechanical energy. The material consisted of a light-responsive molecule (i.e., *ortho*-fluoroazobenzene) embedded in a liquid crystalline polymeric network.<sup>[214]</sup> Although the mechanism that underlays the self-oscillation was not completely understood, the material underwent repeated cycles of bending and straightening when exposed to sunlight (i.e., the angles of deflection ranged from  $-2^\circ$  and  $12^\circ$ ; Figure 11f).

### 5.3. Rectification

Rectification (or asymmetric conduction) is the selective transport of a chemical species in a specific direction (but not in the opposite direction) through a channel (e.g., a nanopore). Rectification occurs commonly in ion channels (e.g.,  $\text{Na}^+$  or  $\text{K}^+$  ion channels) on cellular membranes (e.g., in cardiac and neuronal cells) when ions are pumped unidirectionally across the membrane.<sup>[215–217]</sup> This function is important for cells to communicate with the extracellular environment and maintain cellular ion homeostasis. Rectification can potentially be useful in many applications, such as information transfer, sensors,<sup>[218]</sup> molecular filtration,<sup>[219,220]</sup> or highly efficient devices for energy conversion.<sup>[221,222]</sup>

Rectification has been achieved in synthetic nanochannels with an asymmetric structure: a tapered channel with a large opening on one side (i.e., the “base”) and a small opening on the opposite side (i.e., the “tip”).<sup>[223–226]</sup> This effect allows ions to

flow from the tip to the base but not in the opposite direction. In one illustrative example, asymmetric nanochannels were fabricated through a polymeric film (i.e., poly(ethylene terephthalate), PET).<sup>[227]</sup> The walls of the nanochannels were functionalized with carboxylate groups ( $\approx 1.5$  groups  $\text{nm}^{-2}$ ) by chemical etching. The overall system consisted of an electrolyte solution that was separated into two compartments by the polymeric film with the nanochannels. An electrode with a positive potential was applied to the compartment on the left and an electrode with a negative potential was applied to the compartment on the right as illustrated in Figure 12a. At basic or neutral pH, the carboxylate groups were deprotonated; hence, the walls of the nanochannels were negatively charged. A negatively charged channel allowed only positively charged ions in the solution to flow through. However, due to the asymmetric geometry of the nanochannel, the flow of positively charged ions from the base to the tip of the nanochannel was limited (i.e., the small amount of current that flowed in the range of positive voltages as shown in Figure 12b). On the other hand, if the potentials of the electrodes were switched (i.e., the potential of the electrode on the left compartment was negative and the potential of the electrode on the right compartment was positive), the positively charged ions flowed readily across the tip to the base of the channel (i.e., the large amount of current that flowed in the range of negative voltage as shown in Figure 12b). The asymmetric current–voltage ( $I$ – $V$ ) curve indicated the presence of the rectifying effect. There are a few possible explanations for this rectification of ions through the asymmetric nanochannel. One of them is based on the ratchet model. Briefly, when the positively charged ions attempt to flow from the base to the tip of the channel, their movement is restricted by an “electrostatic potential trap” at the tip. Because of the small diameter of the tip, the negatively charged wall produces a highly negative potential in the channel near the tip. This highly negative potential interacts favorably with the positively charged ions and traps the movement of the ions at the tip. On the other hand, when the positively charged ions flow from the tip to the base, the widening diameter of the channel results in lesser interaction with the ions (than the flow in the opposite direction); hence, the ions are not trapped and can move across the channel.<sup>[223]</sup> As a control experiment, the  $I$ – $V$  curve was found to be linear when the wall of the channel was not charged (e.g., at pH 3); hence, there was no rectification (Figure 12b).<sup>[227]</sup>

Alternatively, the wall of the channel can be functionalized with a light-responsive molecule for controlling the rectifying effect by light. For example, a light-responsive spirobifluorene derivative was functionalized on the inner surface of the conical channel through a PET membrane (Figure 12c).<sup>[228]</sup> Without irradiation with UV light, the molecule was neutral and hydrophobic; in this case, negligible amount of ions flowed through the channel. With UV light and at pH 7, the molecule acquired a negative charge (see molecular structure in Figure 12c). Under these conditions, rectification of positively charged ions in the solution was observed (Figure 12d). The rectification of the type of ions could be controlled by changing the pH of the electrolyte solution. At pH 3, the light-responsive molecule acquired a positive charge with UV irradiation (Figure 12c). In this case, the rectification of negatively charged ions was observed (Figure 12d).

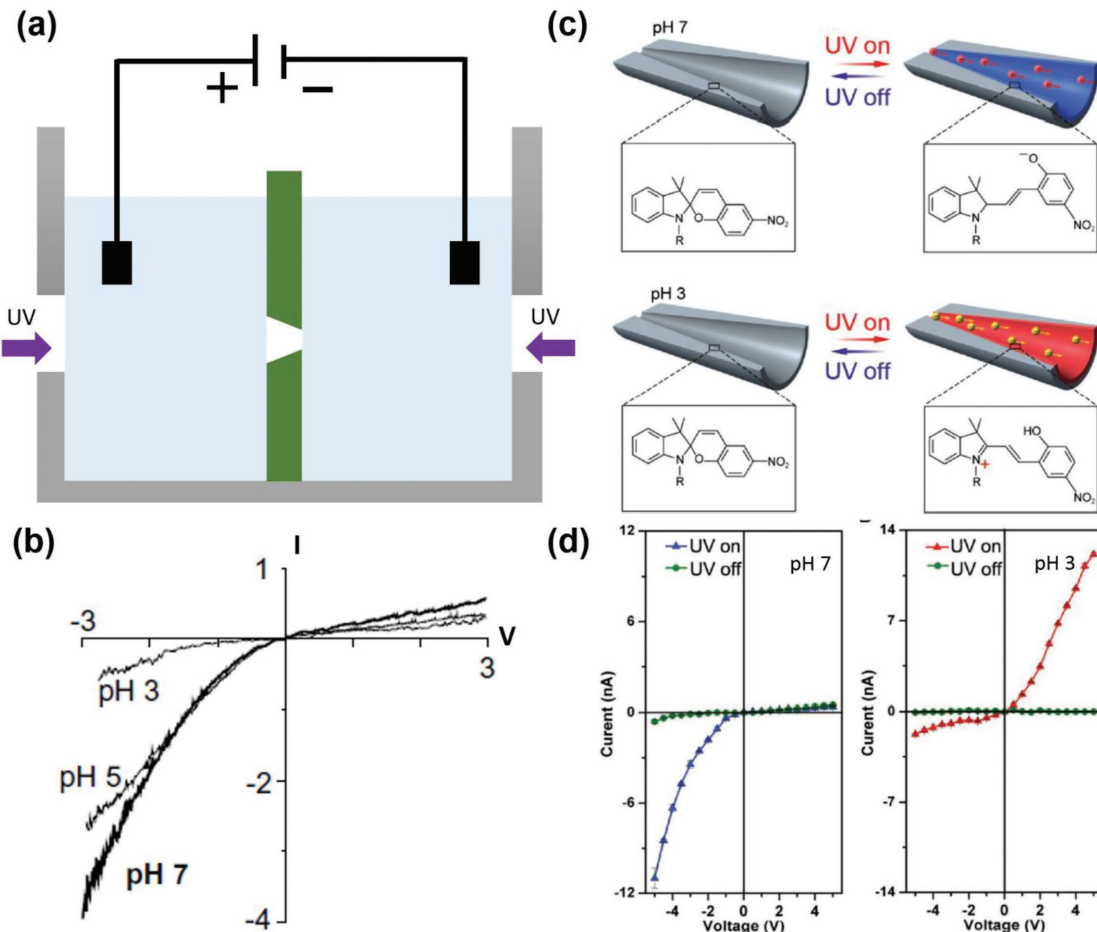


**Figure 12.** Rectification. a) Experimental setup for observing the rectification of current by an asymmetric nanochannel. b) Plot of potential (V) against current (I) showing the rectification at different pH. Reproduced with permission.<sup>[227]</sup> Copyright 2003, Elsevier. c) Light-responsive rectification. The inner surface of the asymmetric channel was modified with a spirobifluorene derivative that changed its surface polarity by UV light. Changing pH changed the characteristic of the rectification. d)  $I$ - $V$  curves for the spirobifluorene-modified nanochannel under different conditions (i.e., UV and pH). c,d) Reproduced with permission.<sup>[228]</sup> Copyright 2012, Wiley-VCH.

#### 5.4. Amplification

Amplification is the process in which a small amount of input can produce a dramatically enhanced output.<sup>[229–231]</sup> Amplification is commonly used in living systems; two examples include the amplification of molecules that we smell in olfactory processes<sup>[232–234]</sup> or the sensing of chemical gradients in cells.<sup>[9,235]</sup> Amplification is widely used for detection. By amplifying the small input into a large output, there is no need for sensitive and expensive equipment for the detection. Applications of amplification include the diagnosis of diseases,<sup>[236–240]</sup> detection of chemicals (e.g., ions<sup>[241]</sup> and explosive compounds<sup>[242–244]</sup>), and drug delivery.<sup>[245]</sup> Amplification can be triggered by many types of stimuli, including organic molecules,<sup>[238]</sup> biomolecules,<sup>[236,238–240,246–248]</sup> and DNA.<sup>[237,249,250]</sup> Strategies of stimuli-responsive amplification can broadly be classified into five types: 1) catalysis, 2) polymerization, 3) disassembly, 4) assembly and disassembly, and 5) self-accelerating cycles of expansion and diffusion.

The first strategy uses stimuli-responsive catalysts (or enzymes) as the amplifying agent. Upon the influence of the

stimulus, the catalyst activates and allows reactants in the surrounding medium to interact with the catalyst. When a large amount of reactant is available in the medium, the catalytic reaction can produce a large amount of a chemical product that is readily detectable. Therefore, the input is amplified: by using a small amount of stimulus to activate the catalyst, a large output can be produced and detected. Previous studies have demonstrated the viability of this approach for detection of substances, such as antigens,<sup>[251]</sup> antibodies,<sup>[251]</sup> ions,<sup>[252]</sup> and DNA.<sup>[253]</sup> One specific example involved a system that consisted of a synthetic supramolecular allosteric catalyst (that was activated by  $\text{Cl}^-$  or CO), reactants in the solution (i.e., acetic anhydride and pyridyl carbinol), and a fluorophore (i.e., diethylaminomethylanthracene) that produced fluorescence in acidic conditions.<sup>[252]</sup> In the presence of  $\text{Cl}^-$  or CO, the catalyst activated; thus, the reactants interacted with the catalyst to produce a large amount of acetic acid. The production of acetic acid reduced the pH of the solution and allowed the fluorophore to produce fluorescence that was detected at a wavelength of 365 nm.

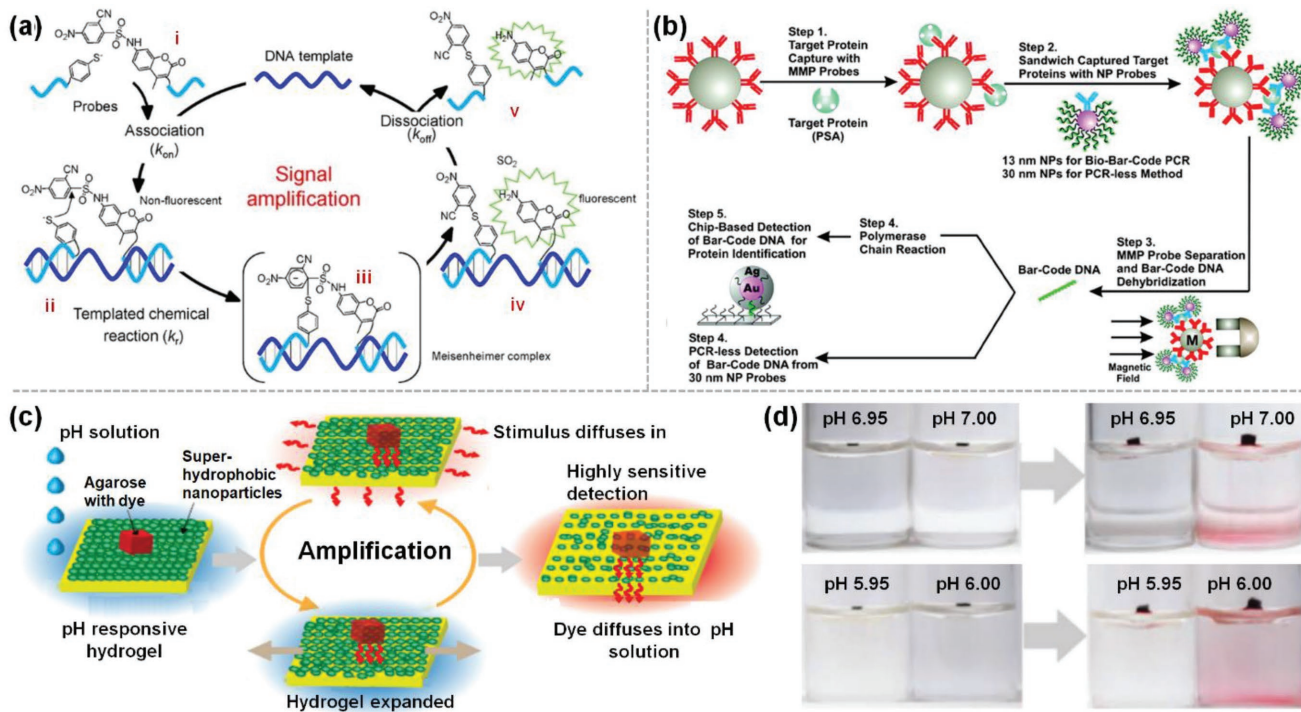


**Figure 13.** Amplification. a) Using DNA as the catalyst (and the stimulus) for producing an amplified output signal (i.e., fluorescence). Scheme illustrating the cycle of reactions for amplifying the signal. Reproduced with permission.<sup>[250]</sup> Copyright 2013, American Chemical Society. b) Highly sensitive detection of proteins by assembling a large amount of DNA onto a particle, and then disassembling the DNA after detecting the targeted protein for amplification of the output signal. Reproduced with permission.<sup>[267]</sup> Copyright 2003, AAAS. c,d) Highly sensitive detection of small changes of a stimulus using stimuli-responsive hydrogel coated with a layer of superhydrophobic nanoparticles. c) Scheme illustrating the process of amplification using self-accelerating repeated cycles of expansion of the hydrogel and diffusion of chemicals through the hydrogel. d) Photographs showing the changes in color caused by a small change in pH. c,d) Reproduced with permission.<sup>[231]</sup> Copyright 2018, Wiley-VCH.

DNA is a common type of material used as a catalyst for amplification. For this general class of systems, the DNA acts both as the stimulus and the catalyst.<sup>[250,254–258]</sup> In one specific example, the system consisted of two probes and a DNA template (i.e., the stimulus).<sup>[250]</sup> One of the two probes was a prefluorophore (i.e., 2-cyano-4-nitrobenzenesulfonyl-protected aminocoumarin), which was a molecule that could become fluorescent after a specific reaction. The other probe was a nucleophilic molecule (i.e., 4-mercaptopbenzoic acid (MBA)). Both these probes were functionalized with strands of DNA that were complementary to the DNA template (part (i) of Figure 13a). When the DNA template (i.e., the stimulus) was present in the solution, the two probes hybridized with the DNA template (part (ii) of Figure 13a). Hybridization of the probes with the DNA template reduced the activation energy required for the reaction between the two probes (i.e., the fluorogenic nucleophilic aromatic substitution reactions). After the reaction, one of the probes became fluorescent (part (iv) of Figure 13a). Subsequently, the probes disassembled from the DNA template and allowed the DNA template to be reused as the catalyst (part (v) of Figure 13a). This cycle then repeated for producing a significant amount of fluorescent molecules. It was estimated that the fluorescence output was amplified by 1500 times from the concentration of the stimulus (i.e., the DNA template).

The second strategy of amplification uses stimuli-responsive materials and polymerization to produce a detectable output (e.g., a macroscopically visible polymer)<sup>[238,240]</sup> or

fluorescence<sup>[236]</sup>). Many types of biomolecules (i.e., the stimuli) can be detected by this mechanism, including biotin,<sup>[236,238,240]</sup> antigens,<sup>[259,260]</sup> and DNA.<sup>[261]</sup> The system usually consists of two main components: biomolecules (e.g., protein,<sup>[236,238,240]</sup> or DNA<sup>[261]</sup>) coated on a surface that can detect the stimulus and a solution containing the initiators (e.g., photoinitiated free radicals,<sup>[236,238,240]</sup> peroxy radicals<sup>[260]</sup>) and the monomers for polymerization. When the stimulus is added to the system, the interaction between the biomolecules, stimulus, and initiator allows the free-radical polymerization to occur. The amplification thus involves the production of the macroscopically visible piece of polymer from the small amount of stimulus added to the system.

The third strategy of amplification involves the disassembly of a large probing material upon the influence of a stimulus. This type of amplification is usually performed in two ways: the release of chemicals from a particle and self-immolation of materials (e.g., dendrimers). The first method usually consists of a stimuli-responsive material (e.g., liposomes<sup>[237]</sup> or micelles<sup>[239]</sup>) filled with a large amount of reporter molecules that can be detected easily (e.g., fluorophores).<sup>[237,239]</sup> When exposed to the specific stimulus, the material releases the reporter molecules, thus producing the detectable output. For example, long-chain polymeric molecules (i.e., benzyl-benzene boronic acid pinacol ester-decorated block polycarbonates; PMPC-Bpe) that contained both hydrophobic and hydrophilic groups were allowed to self-assemble into micelles that contained amylose.<sup>[239]</sup> Upon

addition of hydrogen peroxide (i.e., the stimulus), the boronate pinacol ester group of the polymer (i.e., the hydrophobic group) was cleaved. Without the hydrophobic groups, the micelle disassembled and released the amylose. Amylose was detected readily by reacting it with  $\text{KI}/\text{I}_2$  to produce a visible blue color.

For self-immolation, the material involved is usually a stimuli-responsive dendrimer. The dendrimer consists of a trigger group (i.e., a moiety that can be cleaved by a stimulus), reagent groups (i.e., a moiety that can serve as the stimulus for cleaving the trigger group), and reporter groups for producing the detectable output (e.g., fluorescence).<sup>[247,248,262–264]</sup> Upon the addition of a stimulus, the trigger group is cleaved. Without the trigger group, the dendrimer undergoes a cascading reaction that leads to its disassembly and the release of the reagent and reporter groups. The released reagent molecules then serve as the stimulus for cleaving the trigger groups of other dendrimers, thus leading to the release of more reagent and reporter groups. Therefore, a small amount of stimulus can produce a large amount of reporter molecules that can be detected easily. Self-immolative dendrimers have been demonstrated to detect different types of stimuli, such as hydrogen peroxide,<sup>[247,248,262,264]</sup> thiol,<sup>[263]</sup> and antibodies.<sup>[245]</sup>

The fourth strategy involves an interesting but complex mechanism: the assembly of a multiple-particle complex for concentrating a large amount of DNA onto the particles, isolation, and disassembly of the particles for producing a large amount of dehybridized DNA as the output.<sup>[265–268]</sup> This approach has been demonstrated to detect stimuli such as DNA,<sup>[265]</sup> antigens,<sup>[266,267]</sup> and ligands.<sup>[268]</sup> One specific example involves the detection of prostate-specific antigen (PSA) using two types of particles of different sizes.<sup>[267]</sup> The larger magnetic microparticles (MMPs) were functionalized with PSA monoclonal antibodies (Figure 13b). The smaller gold nanoparticles were functionalized with PSA polyclonal antibodies and hybridized oligonucleotides that served as the reporter molecules (i.e., the “Bar-Code DNA”). In the presence of PSA (i.e., the stimulus), the particles assembled into a complex that consisted of the MMPs, gold nanoparticles, and PSA (steps 1–2 in Figure 13b). Subsequently, the complex was isolated magnetically and suspended in water to allow the Bar-Code DNA to dehybridize from the complexes (step 3 in Figure 13b). The Bar-Code DNA were then separated from the particles by using a magnetic field again. The two steps of separation using the magnetic field allowed the dehybridized Bar-Code DNA to be isolated with extremely high purity for detection. Using a scannometric method of detection—a method that did not involve the polymerase chain reaction (PCR)—a relatively high sensitivity was achieved ( $\approx 30 \times 10^{-18} \text{ M}$  of PSA; steps 4–5 in Figure 13b).

We previously demonstrated the fifth strategy by using a piece of stimuli-responsive hydrogel for sensing a small amount of stimulus and controlling the outflow of a large amount of visible dye. Specifically, we coated a piece of pH-responsive hydrogel with superhydrophobic nanoparticles on one of the surfaces.<sup>[231]</sup> A piece of agarose gel presoaked in a solution that had a high pH (i.e., pH 13) and a red dye was placed on top of the surface of the pH-responsive hydrogel coated with the superhydrophobic nanoparticles (Figure 13c). The material was initially fabricated such that the layer of superhydrophobic coating was able to effectively block any diffusion of chemicals

from the agarose gel into the stimuli-responsive hydrogel at a pH of 6.95. When the material was partially submerged in a pH solution of 7.00, the pH-responsive hydrogel expanded. This slight expansion created gaps between the superhydrophobic nanoparticles and allowed the solution from the agarose gel to diffuse through the layer of superhydrophobic coating into the hydrogel. The diffusion of the pH 13 solution then caused the hydrogel to further expand and created larger gaps between the nanoparticles. The cycle of expansion and diffusion repeated until the stimuli-responsive hydrogel fully expanded (Figure 13c). At the same time, the red dye diffused through the hydrogel and into the surrounding solution, thus producing a visible red output (Figure 13d). Importantly, this process of amplification allowed a small change in pH from 6.95 to 7.00—or the equivalent of a small change of  $10 \times 10^{-9} \text{ M}$  of  $\text{H}^+$  ions—to be detected by the large outflow of the dye without the use of external power supply or equipment. In addition, we demonstrated that this technique worked for different ranges of pH (e.g., from pH 5.95 to 6.00; Figure 13d).

## 5.5. Self-Organization

Self-organization is the process in which a system reconfigures from an initial structure to another ordered structure. Self-organization is important in nature; examples include the self-organization of cytoskeleton in a cell during migration<sup>[7]</sup> and collective behaviors of insects (e.g., while foraging for food).<sup>[269]</sup> In many synthetic systems, the self-organization of individual components within a self-assembled structure is activated by a stimulus (e.g.,  $\text{CO}_2$ , temperature, and pressure). One example involved the  $\text{CO}_2$ -responsive self-organization of micelles into complex morphologies.<sup>[270]</sup> A triblock copolymer with a hydrophilic block (i.e., poly(ethylene oxide) or “O”) and two hydrophobic blocks (i.e., poly(2,2,3,4,4,4-hexafluorobutyl methacrylate) or “F” and poly-(2-(diethylamino)ethyl methacrylate) or “E”) was synthesized (Figure 14a). The spontaneous self-assembly of the triblock copolymer formed spherical micelles with hydrophilic coronas O and hydrophobic cores. These cores were composed of a homogeneous assembly of E and F. E was  $\text{CO}_2$ -responsive: its tertiary amine protonated in the presence of  $\text{CO}_2$ . After protonation, block E became hydrophilic; thus, it segregated from the core and reorganized into the corona. F remained as the hydrophobic core. Because of the self-organization of block E in the presence of  $\text{CO}_2$ , a mixture of different types of complex assemblies (i.e., “hamburger,” “reverse hamburger,” “clover” or “footballs” structures) was obtained (Figure 14b). The process was reversible. By adding  $\text{N}_2$  to remove  $\text{CO}_2$ , the tertiary amine on E became deprotonated; thus, the complex assemblies reorganized back into the spherical micelles.

Although self-organization usually involves a change in the surrounding condition by a stimulus (e.g., by introducing  $\text{CO}_2$ ), it can also involve the reconfiguration of a self-assembled structure from one state to another under the same conditions.<sup>[271]</sup> One study used a diblock copolymer that consisted of a hydrophobic block (i.e., copolymerized NIPAM and *tert*-butyl acrylamide; P(NIPAM-*st-t*BAM)) and a hydrophilic block (i.e., poly(*N,N*-dimethyl-acrylamide), PDMAM). After synthesizing the molecules, they initially self-assembled spontaneously into

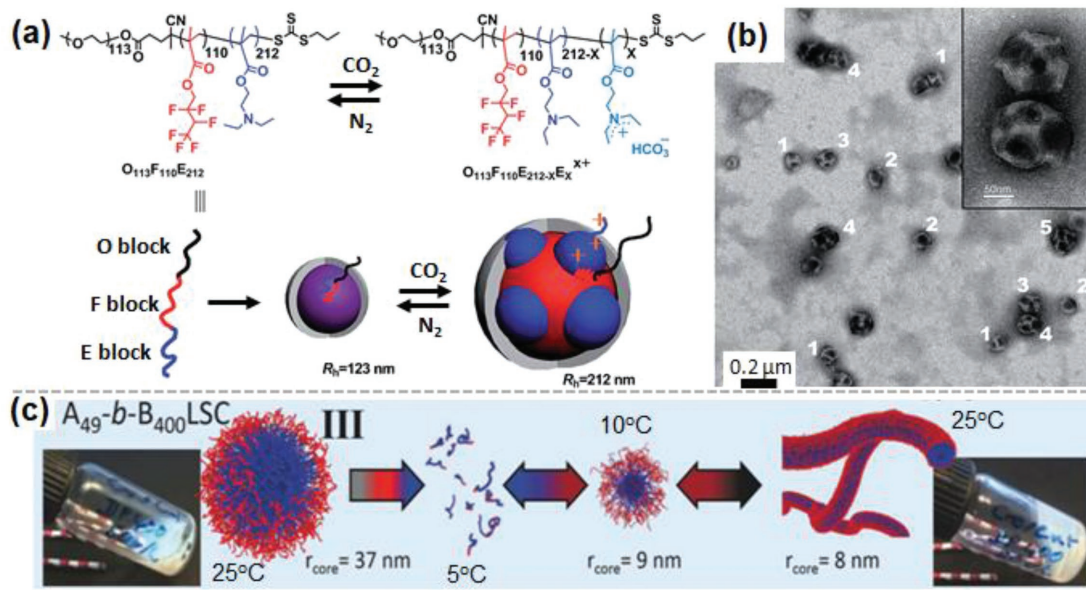


**Figure 14.** Self-organization. a,b) Morphology change due to the self-organization of the gas-responsive assembly of triblock copolymers. a) Scheme illustrating the reversible self-organization of the triblock copolymer ( $O_{113}F_{110}E_{212}$ ) in the presence of  $CO_2$  or  $N_2$ . b) TEM images of the assemblies of the triblock copolymers in water after bubbling  $CO_2$ . The different numbers indicated the different types of morphologies: 1) "hamburger," 2) "reverse hamburger," 3) "clovers," 4) "football," and 5) other more complex structures. a,b) Reproduced with permission.<sup>[270]</sup> Copyright 2014, The Royal Society of Chemistry. c) Self-organization of a self-assembled structure from one state to another at the same condition. Schematic representation of the changes in the morphology of micelles after experiencing a decrease in temperature, followed by an increase back to its initial temperature. Experimental image on the left shows the initial free-flowing liquid and image on the right shows the final gel phase. Reproduced with permission.<sup>[271]</sup> Copyright 2017, Wiley-VCH.

either spherical micelles or vesicles (depending on the concentration and degree of polymerization of the copolymer) in the solution at 25 °C. Importantly, the hydrophobic block was responsive to temperature. When the temperature was lowered to 5 °C (i.e., the stimulus), the assembled structure dissociated into free monomers. Upon heating back to 25 °C, the monomers self-assembled again; however, they did not assemble back to their initial structures. Instead, they self-assembled into worm-like micelles and the solution became a gel phase (Figure 14c). Therefore, the initial and final states were vastly different even though they had the same conditions (i.e., 25 °C). The authors suggested that this difference was because the initial state was only a metastable state. Hence, the self-organization allowed the structure to be reconfigured from a metastable to a more energetically favorable state.

## 5.6. Self-Replication

Self-replication is perhaps the most important function of living systems (e.g., cells). It is the process by which a material is used as a template for constructing an identical copy of itself (e.g., the replication of DNA).<sup>[272]</sup> Self-replication is believed to be critical for the survival of living organisms. According to Darwin's theory of evolution, only the species that can effectively repeat the cycle of self-replication and adaptation to its environment can evolve and survive in the competitive ecosystem. Research on self-replication may potentially allow us to understand living systems better<sup>[273,274]</sup> and construct synthetic machines that can duplicate a large amount of materials from

a template.<sup>[275]</sup> Due to its complexity, however, it has been very challenging for researchers to construct systems that mimic this advanced biological function. Many studies have used autocatalytic reactions that involve nucleic acid-based templates (e.g., DNA and RNA), peptide-based templates, or small synthetic molecules for achieving self-replication;<sup>[276–280]</sup> however, these systems have only been moderately successful.

One example of a stimuli-responsive self-replicating system consisted of three main components: the peptide (T), and the nucleophilic (N) and electrophilic (E) fragments as shown in Figure 15a,b.<sup>[281]</sup> The peptide was modified with a photocleavable moiety (i.e., 6-nitroveratryloxycarbonyl, Nvoc) on its Lys residue ( $T^{Nv}$ ); this moiety inhibited the peptide from performing its self-replicating function. Upon exposure to UV light, the Nvoc group was removed from  $T^{Nv}$ . This light-activated T then self-assembled to form dimers; these dimers were the template that allowed the E and N fragments to assemble onto the peptide. Importantly, the template was needed to bring the two fragments into close proximity for them to join together via a ligation reaction. By joining the two fragments together, the template was able to reproduce an identical copy of the peptide. The light-activated growth of T was much faster than that when T and light were not present (Figure 15c).

Another study reported the possibility of self-replicating polymeric microparticles.<sup>[282]</sup> The self-replicating system consisted of two main components: free microparticles in the solution and a template (Figure 15d). The microparticles (PS;  $\approx 1.05 \mu m$ ) were coated with a layer of DNA molecules; these DNA molecules were functionalized at their 5' terminal ends with a psoralen molecule, which served as a UV-responsive

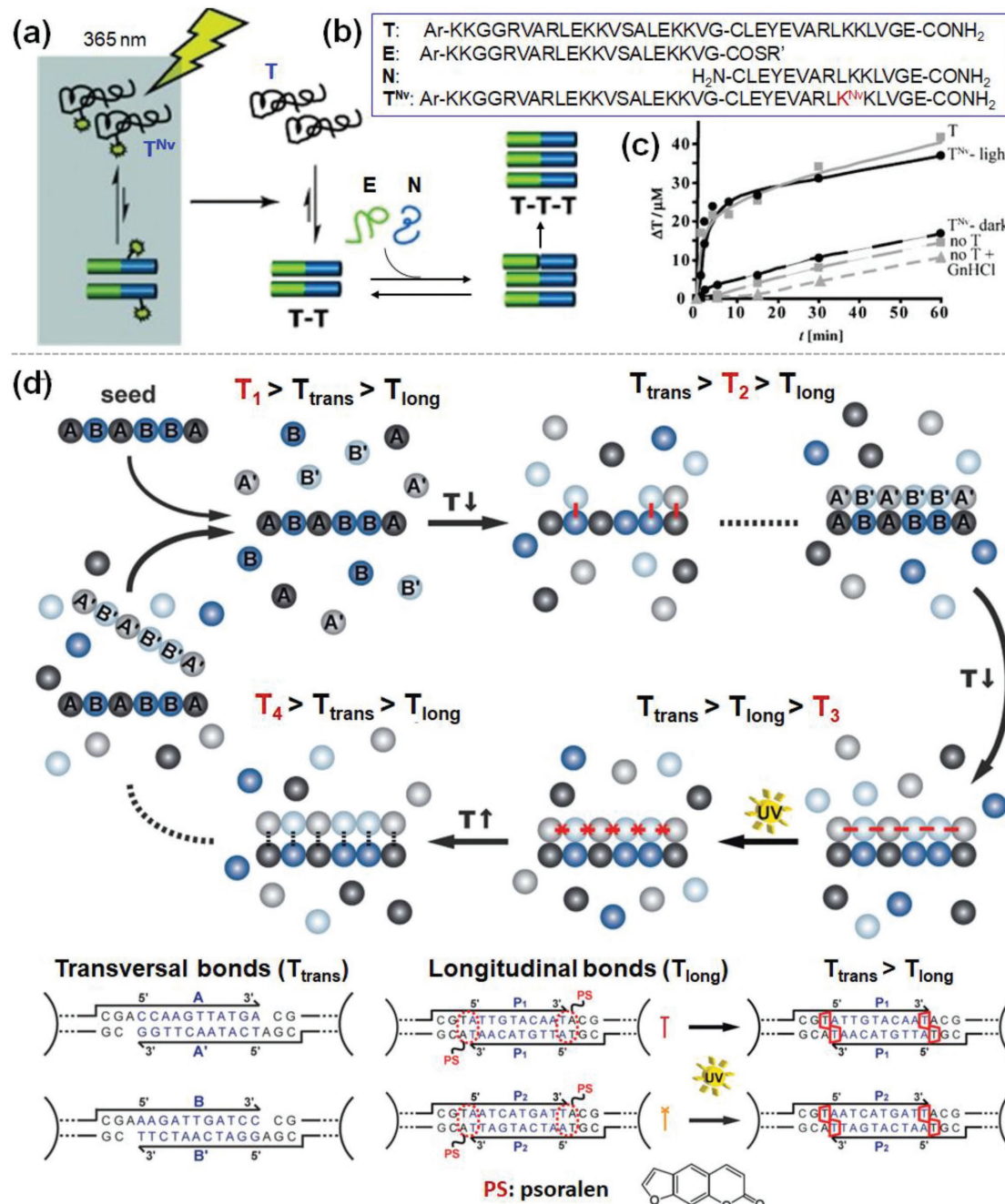


**Figure 15.** Self-replication. a–c) Light-responsive self-replication of peptides. a) After exposure to light, the activated peptide T served as the template for interacting with the fragments E and N; thus, the self-replicating process produced more T. b) Amino sequences of the peptide T, fragments E and N, and the light-responsive T<sup>Nv</sup> (as shown in the blue box). c) The process of self-replication was confirmed by the increase of T with time. a–c) Reproduced with permission.<sup>[281]</sup> Copyright 2010, Wiley-VCH. d) Scheme illustrating the self-replication by assembling the individual particles onto a template and then joining them together. Reproduced with permission.<sup>[282]</sup> Copyright 2009, The Royal Society of Chemistry.

crosslinker.<sup>[283]</sup> The template was composed of a linear chain of the same type of microparticles, except that they were modified with DNA molecules that were complementary to the DNA molecules coated on the free PS microparticles in the solution. After immersing the linear template into the solution that contained the free PS microparticles, the free microparticles were able to assemble onto the template via

the interaction between the complementary strands of DNA (Figure 15d). When the temperature of the system was lowered to below the melting temperature of DNA, the particles were connected by the DNA bonds. Subsequently, the microparticles were exposed to UV light for forming the covalent bonds between the particles via the crosslinking of the UV-responsive crosslinker. This permanent bonding between the particles

resulted in a linear chain of microparticles that was replicated from the template. The authors proposed that by increasing the temperature, the replicated chain of microparticles could be detached from the template, thus completing the process of self-replication. However, imperfections in the experiments had led to an incomplete self-replicating process.<sup>[282]</sup>

## 6. Analytical Processing Function

Besides practical and regulatory functions, intelligence can only be achieved by having an analytical processing unit that performs at least these two main functions: storage and analysis of information. Information is essential for intelligent systems. By having information, systems can acquire a vast range of abilities; a few examples include gathering knowledge for the operations of different tasks, learning from mistakes, and making better decisions. An advanced biological system (or a person) that has a larger memory for storing more information is usually considered more intelligent. Equally importantly, intelligent systems need to have the capability to perform logical analysis of the information collected to achieve their objectives. Therefore, intelligence of materials can formally be achieved by having the ability to remember a sufficiently large amount of information and perform complex analysis of the information. For example, artificial intelligence has been achieved in electronic systems by advanced algorithms that analyze large data sets effectively.

In this section, we will discuss how materials can store and analyze information. We describe the strategies for storing information via the functions of memory and data storage. With regard to analyzing information, we will describe the ways of performing logical analysis with increasing complexity. We will first discuss the ways by which materials can perform basic logical operations by the concept of logic gates. We will then examine how multiple logic gates can be integrated together—in a single material—for more complex analysis of information. Subsequently, we will discuss how materials can be used for performing more advanced computational tasks. In particular, many fascinating advanced analytical capabilities have been demonstrated using DNA as the means of biocomputing.

### 6.1. Memory and Data Storage

Memory and data storage are the processes of storing information in a medium. The ability to store information is one of the most important features in defining intelligence of an advanced biological system (e.g., a human being). At the fundamental level, information is coded in the specific sequence of base pairs in the DNA of a cell; this stored information is commonly regarded as the basis for the existence of life. In our human society, the storing of information has evolved through time, from the inscription of stones to optical drives, with the purpose of preserving knowledge. With the explosion of information in the world, research in memory and data storage has gained a lot of attention in the scientific community in the past few decades.

Although the terms memory and data storage are usually used in different contexts, we will discuss these functions together in this section because they play very similar roles in the construction of intelligent materials for storing information. We will first discuss two interesting properties of materials that are regarded as having the function of memory: hysteresis and shape memory. We will also discuss two types of data storage: optical data storage and write-erase pattern storage.

#### 6.1.1. Memory due to Hysteresis

Hysteresis of a stimuli-responsive material is the property that allows the material to be in different states at the same condition depending on the stimulus that was previously applied. This ability is commonly used for memory: information can be written by a stimulus and retrieved as one of the different states at a specific condition.<sup>[284]</sup> The most widely known type of hysteresis is based on the magnetization of ferromagnetic materials. Briefly, when an external magnetic field (i.e., the stimulus) is applied to the material, the material is magnetized in the same direction as the applied field (part (i) of the illustrative scheme shown in Figure 16a). Once magnetized, the material has the tendency to remain magnetized (part (ii) of Figure 16a). It can only be demagnetized when a sufficiently large magnetic field is applied in the opposite direction (part (iii) of Figure 16a). Because of the hysteresis, two states of magnetization are possible when no field is applied; these states serve as the memory by which information can be retrieved. The magnetic field is used to write the memory. A wide range of commercially available memory devices is based on this magnetic hysteresis, including hard disk, recording tape, and magnetic stripe card.<sup>[285,286]</sup>

Besides ferromagnetic materials, stimuli-responsive polymers can also exhibit hysteretic properties. Many types of stimuli-responsive polymers that show hysteretic properties have been fabricated. They can respond to different types of stimuli, such as temperature,<sup>[287–290]</sup> pH,<sup>[291,292]</sup> humidity,<sup>[293]</sup> light,<sup>[294]</sup> and electric field.<sup>[295]</sup> Importantly, information can be written in memory and retrieved in many different ways due to the different types and functions of the stimuli-responsive polymers. In one illustrative example, the walls of the nanoscale pores of a membrane (polyisoprene-*b*-polystyrene) was grafted with PAA.<sup>[292]</sup> At high pH (i.e., pH 13), the carboxylic acid groups of PAA deprotonated, thus causing the charged polymeric chains to repel one another electrostatically (Figure 16b). Hence, the polymeric chains extended and closed the pores of the membrane. At low pH (i.e., pH 1), the carboxylic acid groups of PAA protonated. They were then able to form hydrogen bonds with one another; hence, the polymeric chains collapsed and the pores of the membrane opened. Through varying the pH, the permeability of the membrane was observed to have a hysteresis (plot on the left of Figure 16b). This hysteretic effect was possibly due to the high density of hydrogen bonding within the network of the polymers in the confined nanopores. Because of the hysteresis, the permeability could be different at a specific pH. For example, if the solution was initially at pH 1 and the pH was increased, the permeability was at the point “2” at pH 5.5 as indicated in the plot in Figure 16b. On the

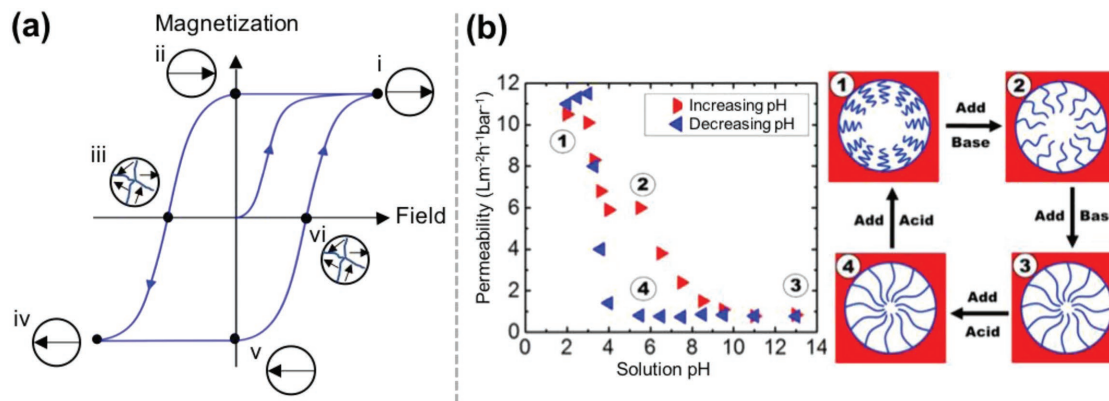


**Figure 16.** Hysteresis as a memory function. a) Scheme illustrating the hysteresis loop of the magnetization of a ferromagnetic material under the influence of an external magnetic field. b) Hysteresis of the permeability of a pH-dependent membrane (left). Schemes illustrating the changes in the opening of a pore at different pH. These numbers of the four states corresponded to the four points indicated in the plot on the left. Reproduced with permission.<sup>[292]</sup> Copyright 2016, American Chemical Society.

other hand, if the solution was initially at pH 13 and the pH was decreased, the permeability was at the lower point “4” at pH 5.5. Therefore, the information was recorded in memory by a sufficiently large change in pH (e.g., to either pH 1 or 13) and retrieved by pumping water through the membrane and measuring its permeability at a specific pH (e.g., pH 5.5). Other methods of retrieving the memory from the stimuli-responsive polymers with hysteretic properties include a change in color,<sup>[289,291,295]</sup> size, and shape;<sup>[287,288,293,294]</sup> hence, many ways of recording and retrieving memory are available for different types of applications.

### 6.1.2. Shape Memory

Shape memory materials (SMMs) refer to the general class of stimuli-responsive materials that can remember their shapes after being deformed to a temporary shape.<sup>[296]</sup> SMMs can be classified into two distinct groups based on the reversibility of the memory: one-way shape memory effect (SME) is irreversible, and two-way SME is reversible. Both these groups are further classified into subgroups based on the number of shapes that they can “memorize”; that is, they can have dual or multiple SMEs including the original permanent shape. Common stimuli include temperature,<sup>[297–303]</sup> pH,<sup>[304]</sup> light,<sup>[305,306]</sup> magnetic field,<sup>[307]</sup> humidity,<sup>[308]</sup> chemicals,<sup>[309]</sup> and radiofrequency.<sup>[310]</sup> Some materials respond to multiple stimuli (e.g., crosslinked metallo-supramolecular polymers respond to temperature, UV light, and methanol).<sup>[311]</sup> SMMs can be polymers, alloys, ceramics, or composites of more than one type of materials. SME has different types of applications, such as controlled wettability (e.g., the straightening of shape memory micro/nanostructured pillars) and the embolization of arteries (e.g., by the coiling of micrometer-sized shape memory strips).<sup>[298–302]</sup>

The most common type of SME is the one-way dual SME.<sup>[297–302]</sup> Part (i) of Figure 17a is a scheme that illustrates the one-way dual SME using the commonly studied thermo-responsive shape memory polymer as an example. The polymer with its original permanent shape as illustrated on the extreme left is

first heated above its transition temperature (i.e., typically the glass transition or melting temperature). At this heated state, stress is applied to deform the material to a desired temporary shape. By maintaining the applied stress and cooling the polymer, the desired temporary shape is retained even after the stress is removed. Different types of temporary shapes can thus be obtained by deforming the material to different shapes at high temperature and then cooling it down while maintaining the stress. The original permanent shape can be recovered by simply heating the material above its transition temperature again without applying any stress. The mechanism that underlies the SME is due to the two segments of the thermo-responsive shape memory polymer. The first segment consists of a stable network that has a tendency to recover its original shape when the applied stress is removed. The second segment exhibits a reversible change in stiffness depending on the temperature: soft at high temperature and rigid at low temperature. Due to this property, the material can be easily deformed when it is soft at high temperature. At low temperature, however, the material becomes rigid and its shape is fixed.<sup>[296]</sup> For this one-way dual SME, the memory is recorded by fabricating the SMM with the desired original permanent shape. After the SMM is deformed to its temporary shape, the memory can be retrieved by applying the stimulus (e.g., heat) to transform it back to its original permanent shape.

This one-way dual SME has been demonstrated in a previous study<sup>[297]</sup> for an organohydrogel that exhibited superior materials property. The organohydrogel consisted of micro-organogels that contained molten paraffin (melting point of 54–57 °C) and an elastic hydrogel framework. The organohydrogel was deformed into a temporary shape (i.e., extreme left image of part (ii) of Figure 17a) by first heating it above the melting point of the paraffin, softening the paraffin, deforming the material, and cooling the material down. By heating the organohydrogel again above the melting point, the original permanent shape was obtained after around 40 s (i.e., extreme right image of part (ii) of Figure 17a). This organohydrogel was highly elastic: it was able to fully recover its original shape after stretching up to 2600% (part (iii) of Figure 17a) or compressing up to 85% (part (iv) of Figure 17a).

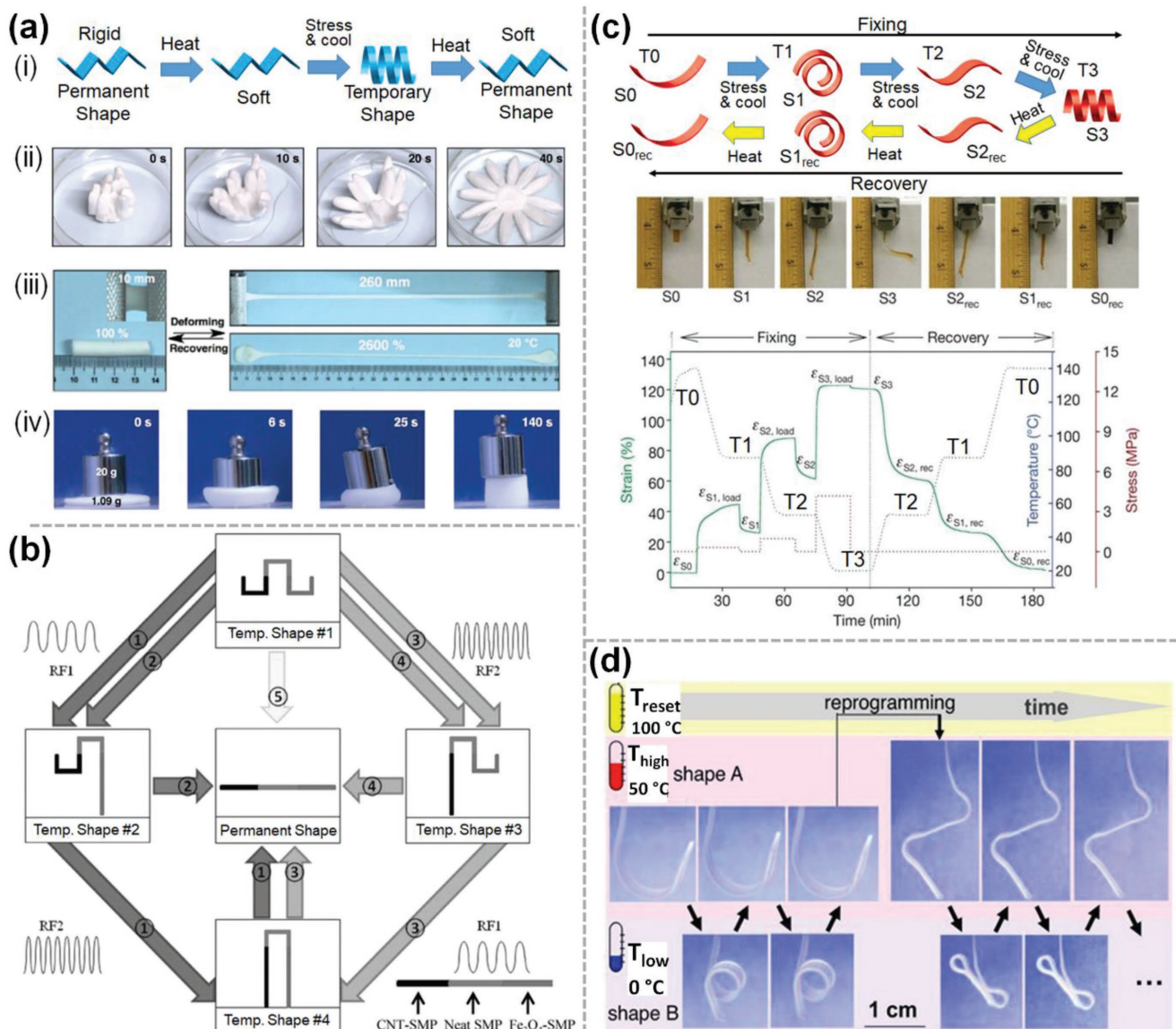


**Figure 17.** Shape memory. a) The thermo-responsive one-way dual shape memory organohydrogel. The gel presented high strain capacity. Reproduced with permission.<sup>[297]</sup> Copyright 2017, Wiley-VCH. b) Combining multiple one-way dual shape memory materials into a single polymer for achieving multiple memory states. The polymer consisted of three segments, each of which was a one-way dual shape memory materials. Reproduced with permission.<sup>[310]</sup> Copyright 2011, Wiley-VCH. c) Scheme on top illustrates the one-way multiple shape memory effect (MSME). The experimental images in the middle show the actual shapes and sizes of the Nafion ionomer at different states. The plot at the bottom shows the profiles of strain, temperature, and stress with respect to time for demonstrating the operation of the MSME. Reproduced with permission.<sup>[313]</sup> Copyright 2010, Springer Nature. d) Two-way shape memory effect. Demonstration of two temporary shapes (i.e., shapes A and B) that were reversible under different temperatures. The temporary shapes were reprogrammable for generating different shapes. Reproduced with permission.<sup>[317]</sup> Copyright 2013, Wiley-VCH.

In addition, by using a combination of multiple pieces of SMM with one-way dual SME, multiple memory states can be achieved. In one demonstration, the material consisted of three long segments joined together as shown in Figure 17b: a shape memory polymer that contained carbon nanotubes (CNTs) on the left, the same shape memory polymer which did not contain any fillers in the middle, and the same shape memory polymer that contained Fe<sub>3</sub>O<sub>4</sub> on the right.<sup>[310]</sup> All these three segments were originally straight. From this original shape, all the three segments of the material were deformed into the temporary shapes as illustrated as “Temp. Shape #1” in

Figure 17b. From this temporary shape, different memory states (i.e., different shapes of the polymer) can be accessed by selectively heating each segment above its transition temperature to return it to its original shape. Selective heating was achieved using different radiofrequencies. Specifically, the segment on the left that contained CNT dissipated heat at 13.56 MHz (indicated as “RF2” in Figure 17b) and the segment on the right that contained Fe<sub>3</sub>O<sub>4</sub>, dissipated heat at 296 kHz (“RF1”). Hence, the specific radiofrequency caused the corresponding segment to recover its original shape. Alternatively, by applying heat directly on the whole polymer, it returned to its original straight

geometry (i.e., illustrated as “Permanent Shape” in the center of Figure 17b). In this way, different sequences of the applied stimulus (i.e., a radiofrequency or heat) resulted in different sequences of shape recovery. In general, this shape memory polymer was capable of remembering four different states (or shapes) via the stimuli applied as shown in Figure 17b.

Besides combining multiple SMMs together, a single piece of SMM can exhibit one-way multiple shape memory effect (MSME). This material can be deformed into, and memorize, more than one temporary shape under varying extents of the stimulus.<sup>[296,312]</sup> In one study, both the MSME and temperature-memory effect (TME) were demonstrated by a Nafion ionomer.<sup>[313]</sup> This ionomer had a broad range of transition temperatures; hence, it could potentially remember multiple temporary shapes and their corresponding temperatures within this broad range of transition temperatures. As illustrated in a representative scheme in Figure 17c, the material had an original permanent shape S0. The ionomer was then deformed at a temperature T0 to a shape S1. It was subsequently cooled to a lower temperature T1 (i.e., T1 < T0) while maintaining the applied stress. When the external stress was removed, the ionomer retained its shape S1; hence, S1 was the first temporary shape of the material. To obtain the second temporary shape, the process was repeated at T1. Specifically, the ionomer was deformed to S2 at T1, followed by cooling to T2 (i.e., T2 < T1) while maintaining the stress. The third temporary shape S3 was obtained by repeating the process. Subsequently, the shapes stored in memory were accessed by heating the material. For example, heating the ionomer with the temporary shape S3 to T2 allowed the shape S2 to be recovered (i.e., S2<sub>rec</sub>). Further heating to T1 yielded the recovered S1 (i.e., S1<sub>rec</sub>). Subsequent heating to T0 or above allowed its permanent shape (i.e., S0<sub>rec</sub>) to be retrieved. In this way, the material (with its original shape S0) was able to record two memory states (i.e., S1 and S2) and their corresponding temperatures (T1 and T2). Therefore, the broad range of transition temperatures associated with the ionomer allowed many shapes and temperatures within the range to be memorized.<sup>[314]</sup> The images in Figure 17c showed the actual shapes investigated experimentally. The plot in Figure 17c showed the strain, stress, and temperature profiles of the fixing and recovery of the temporary shapes of the SMM with the MSME.

For one-way SME, the temporary shape of the SMM is lost irreversibly after it recovers its original shape. For example, for the common one-way dual SME, the only memory that can be recorded and retrieved is the fabrication of the SMM of the specific original shape. Once fabricated, the original shape is usually fixed; hence, the memory cannot be modified flexibly. On the other hand, two-way SME refers to the ability of the SMM to change reversibly between two shapes upon the influence of a stimulus.<sup>[296,315,316]</sup> Hence, the two shapes, including the temporary shape, can serve as the memory states that can be recorded and retrieved. Importantly, because the temporary shape can be changed flexibly to any desired shape (e.g., by an external stress), different types of memory can be recorded.

One example that demonstrated the reversible change between two shapes is the multiphase copolyester urethane network that consisted of poly( $\omega$ -pentadecalactone) (PPD) and 75 wt% poly( $\epsilon$ -caprolactone) (PCL).<sup>[317]</sup> The original shape of the polymer was a straight strip. It was coiled up into a shape

as shown as “shape B” in Figure 17d by first deforming it at 100 °C (i.e., T<sub>reset</sub>, a temperature that was above the transition temperature) and then maintaining the shape under stress at 0 °C (i.e., T<sub>low</sub> < transition temperature). This shape remained unchanged even after removing the stress due to the increased stiffness of the PPD at low temperature. When the temperature was increased to 50 °C, the PCL within the SMM expanded. After expansion, another temporary “shape A” formed. When the temperature was decreased to 0 °C, the PCL contracted and the SMM returned to “shape B.” Therefore, by switching the temperature repeatedly between 0 and 50 °C, the shape changed reversibly from shape A to B and vice versa. The stored memory of the temporary shape was erased by subjecting the SMM to T<sub>reset</sub>; at this temperature, the SMM recovered its original shape (i.e., the straight strip). After erasing the memory, a new memory could be recorded by deforming the SMM to another temporary shape at 100 °C and cooling to 0 °C. A limitation of this work is that the temporary “shape A” was obtained by the natural expansion of the SMM from “shape B” by increasing the temperature; thus, “shape A” was not programmable and a specifically desired memory could not be recorded in this state.

#### 6.1.3. Optical Data Storage

Optical data storage is one of the most common ways to store data among other methods (e.g., electrical and magnetic data storage).<sup>[318–320]</sup> Phase-change materials (PCMs) that respond to light are usually used due to their two distinct states: crystalline and amorphous states. Binary information can thus be written into the material by using light to switch between these two states of the material. Specifically, by irradiating a localized spot on the PCM with a high-intensity laser, the temperature of the material increases above its melting point. After moving the laser away from the spot, rapid quenching at room temperature leads to the formation of the amorphous state (Figure 18a). On the other hand, irradiating the PCM with a low-intensity laser heats the amorphous state above the glass-transition temperature but below the melting point; thus, the PCM crystallizes.<sup>[321]</sup> The information can be read by the difference in reflectivity of the crystalline and amorphous states of the PCM. Reflectivity is determined by irradiating another low-intensity laser emitted from a light emitting diode onto the PCM and measuring the reflected light received by the photodetector. Common PCMs used for optical data storage include Ge<sub>2</sub>Sb<sub>2</sub>Te<sub>5</sub>, Ge<sub>8</sub>Sb<sub>2</sub>Te<sub>11</sub>, and AgInSbTe.<sup>[318,322,323]</sup> This type of data storage is widely used in optical discs such as CDs, DVDs, and Blu-Rays. Besides binary information, a relatively recent study demonstrated the capability of multilevel storage using PCM (i.e., Ge<sub>2</sub>Sb<sub>2</sub>Te<sub>5</sub>) by having different proportions of the mixture of crystalline and amorphous states (Figure 18b).<sup>[324]</sup> This feature provides the PCM with a greater capacity to store information.

#### 6.1.4. Write-Erase Pattern Storage

Write-erase pattern storage involves using illustrations (or patterns) as the information to be stored.<sup>[325]</sup> Write-erase pattern storage is usually achieved by changing the color of a localized spot on a material under the influence of an external stimulus.

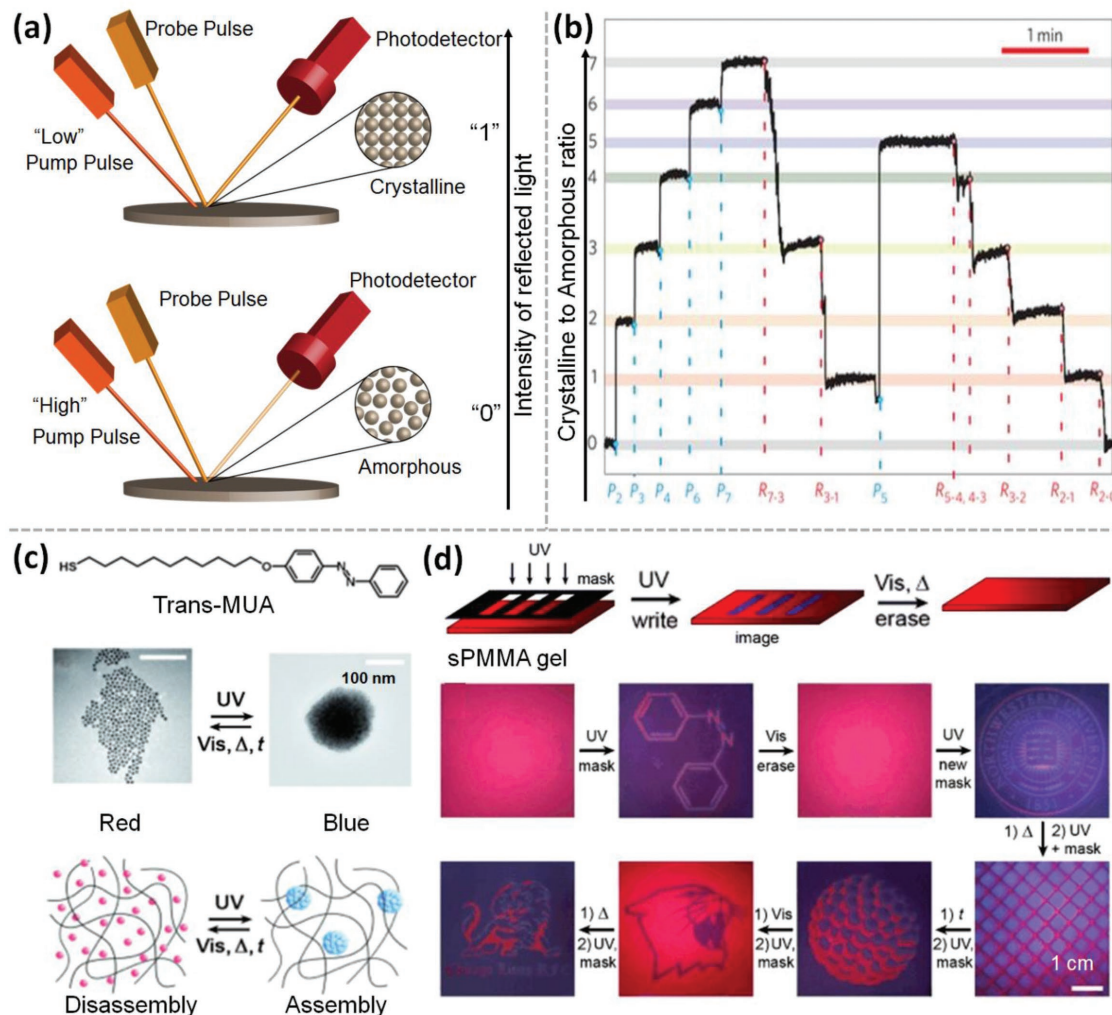


**Figure 18.** Data storage. a,b) Data storage based on light-responsive phase-change materials. a) Scheme illustrating the writing of binary information by switching between the amorphous and crystalline states of the PCM using different intensities of light. b) Eight different states were obtained by varying the proportion of the mixture of the crystalline and amorphous states. a,b) Reproduced with permission.<sup>[324]</sup> Copyright 2015, Springer Nature. c,d) Write–erase pattern storage. c) Light-induced reversible assembly and disassembly of gold nanoparticles modified with light-responsive molecules. d) Patterns being repeatedly drawn and erased by using different types of stimuli. c,d) Reproduced with permission.<sup>[328]</sup> Copyright 2009, Wiley-VCH.

Common mechanisms that can induce the change in color of materials include reversible isomerization,<sup>[326–332]</sup> self-assembly,<sup>[328,333,334]</sup> bond formation/cleavage,<sup>[335]</sup> metal–ligand coordination,<sup>[336–338]</sup> host–guest interaction,<sup>[339]</sup> and phase change.<sup>[340,341]</sup> Many different types of materials have been fabricated, including those that are photochromic,<sup>[327–329,335,336,338]</sup> hydrochromic,<sup>[330,333]</sup> mechanochromic,<sup>[331,332,339–342]</sup> thermochromic,<sup>[326,334,337]</sup> and halochromic;<sup>[343]</sup> these materials respond to light, water, mechanical stress, heat and pH, respectively. Importantly, the change in color is usually reversible depending on the type of stimulus. Because of their ability to change color reversibly, these materials are capable of writing, storing, and erasing information. Common applications include printing and display. In addition, the data stored in the materials can be protected for security purposes. For example, encryption of data can be achieved by storing the writing that is initially not visible; it can only be

visualized under certain conditions (e.g., UV for decoding the information).<sup>[344–346]</sup>

One study reports achieving the function of writing and erasing of patterned information by another function: the reversible self-assembly and disassembly of nanoparticles under the influence of light.<sup>[328]</sup> The rewritable medium consisted of an organogel (i.e., syndiotactic poly (methyl methacrylate)) embedded with nanoparticles that were coated with light-responsive molecules (i.e., *trans*-4-(11-mercaptoundecanoyl) azobenzene; Figure 18c). Under the influence of UV light, the light-responsive molecule isomerized from the *trans* to the *cis* isomer. This change in configuration led to an increase in the dipole moment of the molecule and allowed the molecules to interact more favorably via stronger van der Waals interactions. This stronger interaction caused the nanoparticles coated with the light-responsive molecules to self-assemble into supraspherical assemblies. When gold nanoparticles were used, the

self-assembly of the nanoparticles turned the organogel from red to blue; when silver nanoparticles were used, the organogel turned from yellow to violet. Multicolored illustrations on the material were obtained by using different times of UV irradiation for achieving different extents of change in the color of the organogel. The illustrations were erased by disintegrating the supraspherical assemblies via exposing the material to daylight for at least 9 h, intense visible light (i.e.,  $0.3 \text{ mW cm}^{-2}$ ) for about 60 s, or heat (i.e.,  $50^\circ\text{C}$ ) for 20 s. After erasing, information could be written again onto the material. The cycle of writing and erasing was repeated many times as shown in Figure 18d.

## 6.2. Logic Gates

Logic gates are the elementary building blocks for constructing complex electronic devices (e.g., computers). Since the pioneering work by de Silva et al.,<sup>[347]</sup> researchers have fabricated many types of molecules and materials that are not based on electronics as logic gates;<sup>[41,347–354]</sup> a few examples include hydrogels,<sup>[41,351,355]</sup> nanoparticles,<sup>[349]</sup> and photochromic molecules.<sup>[348,354]</sup> These logic gates can be responsive to many types of stimuli, including pH,<sup>[349–352,354]</sup> light,<sup>[349,351,353,354,356]</sup> temperature,<sup>[351]</sup> and ions.<sup>[350]</sup> These stimuli-responsive logic gates usually operate by a change in material properties (i.e., fluorescence),<sup>[350]</sup> self-assembly,<sup>[351]</sup> or a change in size.<sup>[41]</sup>

Logic gates have been used for complex analysis of multiple stimuli for applications such as sensing<sup>[357]</sup> and controlled drug delivery.<sup>[351]</sup>

The basic types of logic gates include NOT, AND, OR, NAND, NOR, XOR, and XNOR. Logical operations are usually performed by analyzing a combination of various stimuli. An AND gate, for example, gives an output “1” only when two unique stimuli (or inputs) are present; in all other cases, the outputs are “0.” In one study, the authors fabricated mesoporous silica nanoparticles that were responsive to both light and pH (Figure 19a).<sup>[349]</sup> Specifically, the walls of the pores of the silica nanoparticles were functionalized with light-responsive molecules (i.e., 4-phenylazoaniline; or the “nanoimpellers”) that underwent *cis-trans* isomerization under the exposure to light with a wavelength of 448 nm. Importantly, both the *cis* and *trans* states absorbed energy from this wavelength of light; hence, the molecules were capable of undergoing an oscillatory motion due to the repeated cycles of *cis-trans* isomerization under the influence of a single source of light. In addition, the opening of the nanopores was covered by pH-responsive molecules that consisted of mobile cucurbit[6]uril (CB[6]) rings and bisalkylammonium[2]pseudorotaxanes stalks tethered to the surface of the pores. At neutral pH, the CB[6] rings had strong ion-dipole attraction with the stalks; hence, the combination of the rings and the stalks blocked the opening of the pores. When  $\text{OH}^-$  was added, the deprotonation of the stalks disrupted the

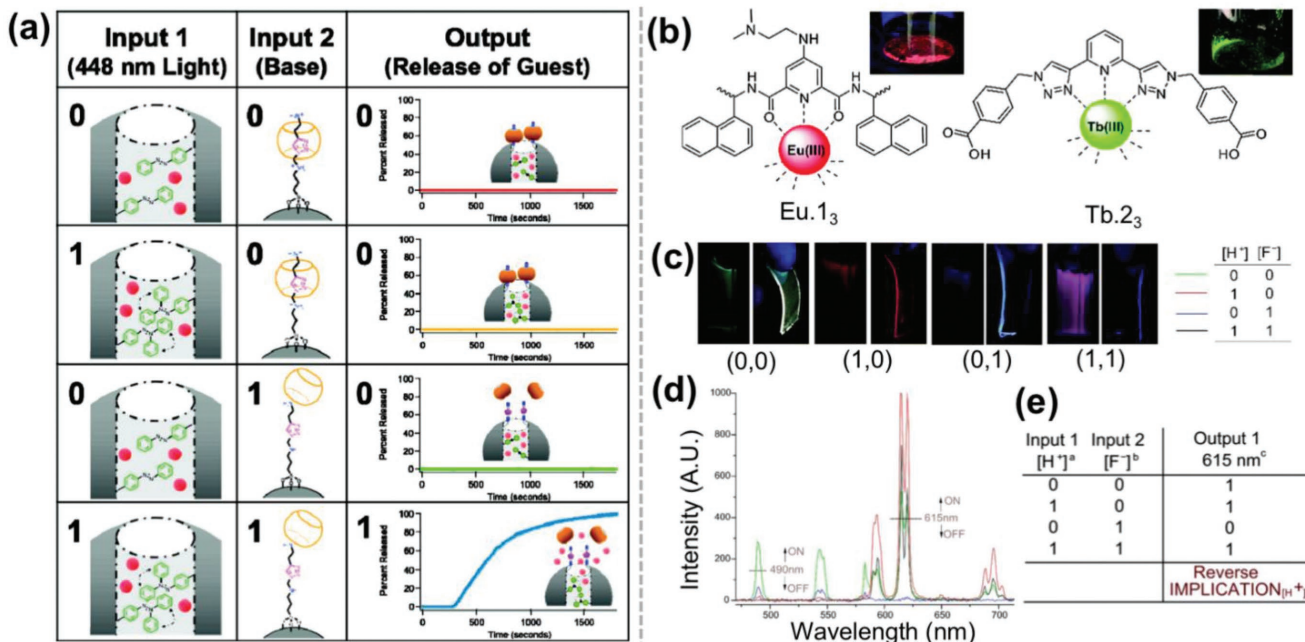


**Figure 19.** Logic gates. a) Truth table for an AND gate based on the controlled release of a guest from the pores of mesoporous silica nanoparticles. When light was present, the nanoimpellers (green molecules) drove the guest (red particles) out; when  $\text{OH}^-$  was present, the nanovalves opened (i.e., the yellow molecules disassembled). The guest was released from the nanoparticles only in the presence of both light and  $\text{OH}^-$ . Reproduced with permission.<sup>[349]</sup> Copyright 2009, American Chemical Society. b–e) Stimuli-responsive polymer that operated as a reverse-IMPLICATION gate. b) Molecular structures of **Eu.1<sub>3</sub>** that produced red emission and **Tb.2<sub>3</sub>** that produced green emission when excited by light. c) Photographs of the stimuli-responsive polymer that showed different colors depending on the inputs (i.e., the presence of  $\text{H}^+$  and/or  $\text{F}^-$  ions) as shown in the table. For each pair of images, the image on the left shows the solution and image on the right shows the gel. d) Phosphorescence spectra of the four possible input states as represented by the four differently colored lines. The legend of these colored lines is indicated in the table shown in (c). The output was defined at different wavelength and intensity (e.g., at a threshold intensity of 400 at 615 nm). e) Truth table for the reverse-IMPLICATION gate. b–e) Reproduced with permission.<sup>[350]</sup> Copyright 2015, The Royal Society of Chemistry.

strong attractions, thus allowing the CB[6] rings to dissociate from the stalks. After the rings dissociated, the pores opened. Therefore, these pH-responsive molecules acted as nanovalves for controlling the opening and closing of the pores (i.e., the function of gating). The nanoimpellers and nanovalves were used simultaneously to control the release of a chemical (e.g., drug) that was filled in the pores of the mesoporous silica nanoparticles. When the particles were exposed to light and a higher pH, the nanovalves opened and the nanoimpellers were able to drive the chemical out of the pores. When either the light and/or the higher pH was not present, the chemical was not found to release—hence, the AND gate was achieved (Figure 19a). In another study, the authors synthesized a fascinating molecule (i.e.,  $(HO)_2P(O)O-(CH_2)_8-Fum-Glu-(O-cyclohexyl)_2$ ) that was responsive to four different types of stimuli:  $Ca^{2+}$ ,  $OH^-$ , temperature, and light.<sup>[351]</sup> Depending on the pairs of stimuli applied to the molecule, it exhibited the function of either of the four types of basic logic gates: AND, OR, NAND, or NOR. The stimuli were able to cause a sol-gel transition of the molecule. The output was “0” when the material was in a solution phase and “1” when the material was in a gel phase.

Besides the basic logic gates, more advanced logic gates can also be achieved using stimuli-responsive materials. Some examples include the reverse-IMPLICATION,<sup>[350]</sup> TRANSFER,<sup>[350]</sup> and INHIBIT.<sup>[352]</sup> These more advanced types of logic gates usually need to be constructed out of a combination of a few basic logic gates. For example, the reverse-IMPLICATION can be constructed based on an OR gate with a NOT gate connected to one of the inputs. In one study, the reverse-IMPLICATION gate and TRANSFER gate were successfully constructed by a stimuli-responsive material that consisted of two ligands embedded in a polymer (i.e., poly(HEMA-co-MMA));<sup>[350]</sup> each of these ligands coordinated with either Eu(III) or Tb(III) to form Eu.1<sub>3</sub> and Tb.2<sub>3</sub> complexes, respectively as illustrated in Figure 19b. Upon excitation with light (i.e., 254 nm), the Eu.1<sub>3</sub> complex was red and the Tb.2<sub>3</sub> complex was green. This polymer was responsive to  $H^+$  and  $F^-$  ions, which interacted with the complexes to produce different colors. Interestingly, the four possible combinations of inputs based on whether  $H^+$  and/or  $F^-$  ions were added gave four distinctly different colors (Figure 19c). Specifically, without any added ions, the polymer was initially green because of the strong Tb(III) emission and the very weak Eu(III) emission. When only  $H^+$  was added, the polymer was red; when only  $F^-$  was added, the polymer was blue; when both  $H^+$  and  $F^-$  ions were added, the polymer was purple. To represent the reverse-IMPLICATION gate, the authors designated the intensity of phosphorescence at 615 nm with more than 400 units as output “1” and less than 400 units as output “0” (Figure 19d). Therefore, the output was “0” when  $H^+$  was not added (input “0”) and  $F^-$  was added (input “1”; the blue line shown in Figure 19d). The outputs were “1” for all the other combinations of inputs (i.e., the green, red, and black lines shown in Figure 19d); hence, the reverse-IMPLICATION gate was established according to its definition (Figure 19e). The TRANSFER gate was constructed based on the same material, except that the output was measured by fluorescence (instead of phosphorescence) at 338 nm and another designated intensity as the threshold for defining the outputs “1” and “0.”

### 6.3. Computing

More advanced analytical tasks can be performed by integrating a network of logic gates.<sup>[358–360]</sup> Previous studies have demonstrated that some types of stimuli-responsive materials (e.g., hydrogels<sup>[41,351]</sup> and phase-change alloys<sup>[360]</sup>) have the ability to perform the tasks of multiple logic gates. Stimuli that are commonly used to drive the operations of these advanced analytical functions include pH,<sup>[41,359,361]</sup> light,<sup>[360,362,363]</sup> heat,<sup>[41]</sup> and ions.<sup>[351]</sup>

Reasonably advanced analysis can be performed by combining just a few basic logic gates. For example, basic arithmetic calculations such as binary addition or subtraction can be performed using a half adder or half subtractor; each of these operations can be performed by combining two or three logic gates. Many interesting types of molecular logic gates<sup>[358,359,363]</sup> and stimuli-responsive materials<sup>[350,351]</sup> have been synthesized for performing the function of a combination of a few logic gates. One such system consisted of two hydrogels. The first hydrogel 1 (i.e.,  $(HO)_2P(O)O-(CH_2)_8-Fum-Glu-(O-cyclohexyl)_2$ ) was responsive to three inputs: UV light, EDTA, and  $OH^-$ . The second hydrogel 2 (i.e., GalNAc-suc-glu(O-cyc-hexyl)<sub>2</sub>) was responsive to UV light.<sup>[351]</sup> These two hydrogels were used to construct a logic circuit that consisted of three different gates (i.e., AND, OR, and YES) by sensing the three inputs (UV light, EDTA, and  $OH^-$ ) as illustrated in Figure 20a. This system produced two sets of binary outputs, O<sub>1</sub> and O<sub>2</sub>. Under the influence of the stimuli, the hydrogels could undergo sol-gel transitions; the solution was designated as an output “1,” whereas the gel was designated as an output “0.” We first consider the case when UV light was not present. When both EDTA and  $OH^-$  were present in the solution, hydrogel 1 turned into the solution state and hydrogel 2 remained in the gel state ( $O_1 = 1$ ,  $O_2 = 0$ ; see the truth table shown in Figure 20b). In all other cases (i.e., without EDTA and/or  $OH^-$ ), both the hydrogels remained as gel state ( $O_1 = O_2 = 0$ ). On the other hand, when UV light was present, both the hydrogels were in the solution state ( $O_1 = O_2 = 1$ ) regardless of whether EDTA and/or  $OH^-$  were added. This logic circuit was demonstrated to be capable of controlling the rate of release of vitamin B<sub>12</sub> with three different rates of release due to the two sets of binary outputs produced.

In the previous example, the specially synthesized material can only perform the tasks of the specific type and combination of logic gates by using the specific types of stimuli. Another type of material usually needs to be designed and fabricated for another specific combination of logic gates and stimuli. On the other hand, it is technically challenging to synthesize stimuli-responsive materials that can perform the tasks of multiple logic gates; in addition, there is probably a limit to the level of complexity that a single material can perform. In order to overcome these challenges, we proposed a technically simple approach that allows any desired type and combination of logic gates to be integrated. This simple approach involves integrating stimuli-responsive hydrogels that respond to only a single type of stimulus.<sup>[41]</sup> After decades of research, a wide variety of stimuli-responsive hydrogels that respond to only one type of stimulus have been fabricated. They can now be fabricated to respond to many different types of stimuli. By

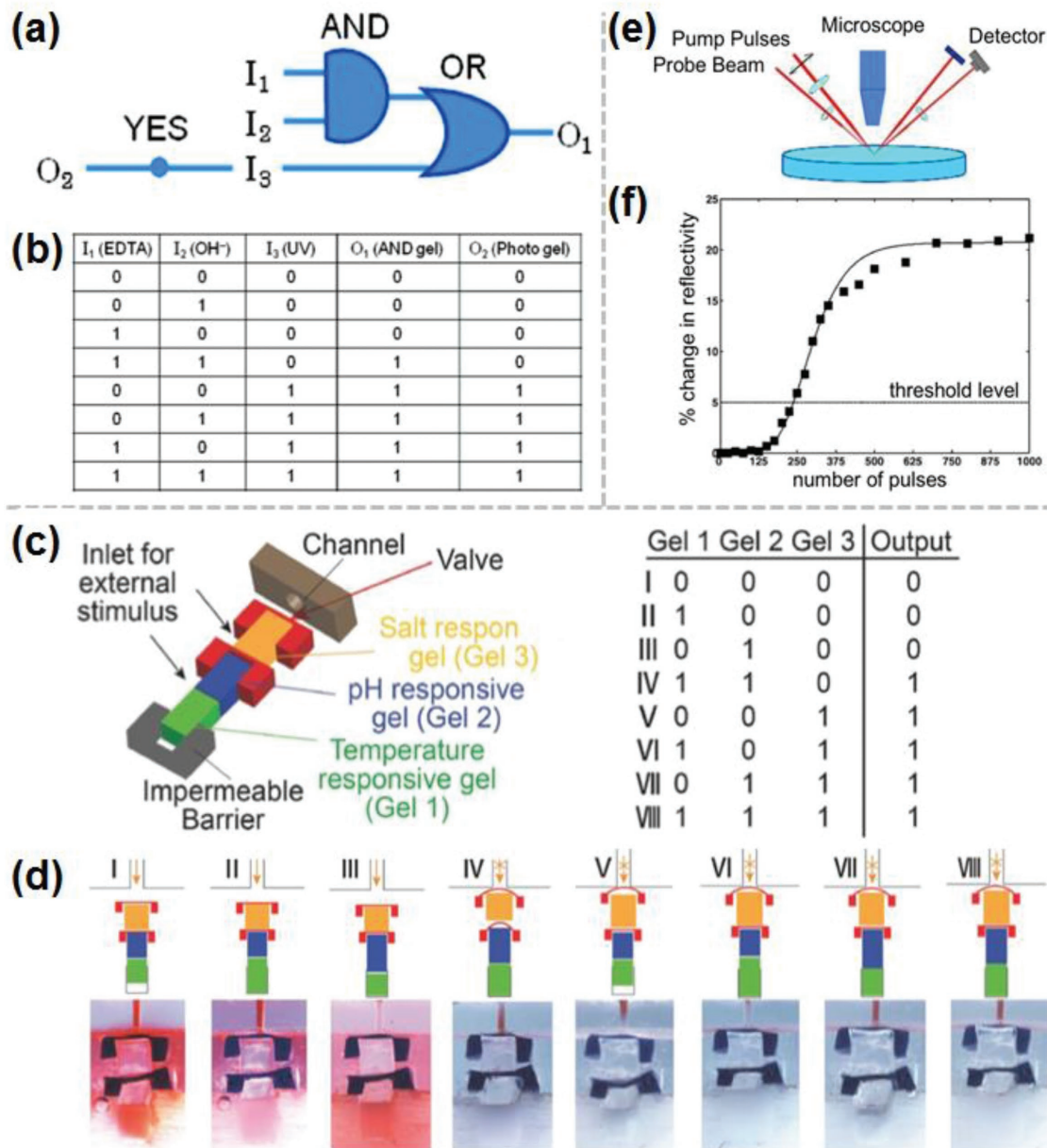


**Figure 20.** Computing via integrating multiple logic gates. a) Hydrogels that performed the task of an integrated logic circuit, which consisted of an AND gate, an OR gate, a YES gate, three inputs ( $I_1$ ,  $I_2$ , and  $I_3$ ), and two outputs ( $O_1$  and  $O_2$ ). b) Truth table for the integrated logic circuit shown in (a). a,b) Reproduced with permission.<sup>[351]</sup> Copyright 2009, American Chemical Society. c,d) Integrating different combinations of logic gates together by assembling stimuli-responsive hydrogels that responded to only one type of stimulus. c) Scheme illustrating the design for performing the function of an AND gate connected to an OR gate. d) The experimental images of the assembled hydrogels that performed as an AND gate connected to an OR gate. c,d) Reproduced with permission.<sup>[41]</sup> Copyright 2017, Wiley-VCH. e,f) Phase-change material that performed addition, subtraction, and division. e) Scheme of the experimental setup for performing the mathematical operations. f) Experimentally measured (squares) changes in optical reflectivity of the PCM (i.e., amorphous phase  $\text{Ge}_2\text{Sb}_2\text{Te}_5$ ) as a function of the number of pulses applied. e,f) Reproduced with permission.<sup>[360]</sup> Copyright 2011, Wiley-VCH.

combining these diverse types of stimuli-responsive hydrogels and arranging them in specific designs, different combinations of logic gates can be constructed. For example, we integrated an AND gate with an OR gate as illustrated in Figure 20c. The AND gate consisted of a pH-responsive and a temperature-responsive hydrogel constrained within an impermeable barrier (indicated as dark brown in Figure 20c) and a flexible polymeric

film (indicated in red above the pH-responsive hydrogel in Figure 20c). A space was left between the temperature-responsive hydrogel and the impermeable barrier as illustrated. When only one of the two hydrogels expanded under the influence of a stimulus, the expanded portion of the hydrogel filled into the space and did not push against the flexible polymeric film (i.e., output “0” from the AND gate). When both the hydrogel

expanded, the space was filled and the flexible polymeric film was pushed forward (i.e., output “1”). This AND gate was placed together with another salt-responsive hydrogel as illustrated in Figure 20c. In this configuration, whenever the output was “1” from the AND gate or when the salt-responsive hydrogel expanded, the polymeric flexible film (i.e., the red “valve”) was pushed forward; hence, the system gave an overall output “1” that demonstrated the function of an OR gate (Figure 20d). In this way, the integration of an AND gate and an OR gate was achieved. Changing the design of the system (i.e., the geometry of the valve and arrangement of the hydrogels) allowed the type of the logic gate to be changed (e.g., for achieving the NOR gate). Because the output involved pushing the flexible polymer outward, the output of the logical analysis can be used directly for different types of applications; for example, we demonstrated that the integrated logic gates controlled the release of a red dye based on the logical analysis of the stimuli. Conceptually, this approach can potentially be used to integrate a massive number of logic gates for performing complex analysis.

Arithmetic calculations were performed using the class of stimuli-responsive phase-change materials. PCMs (e.g., GeSbTe or AgInSbTe alloys) are gaining the interests of researchers because of their natural ability to accumulate the amount of stimulus applied. In particular, the light-responsive PCM (i.e.,  $\text{Ge}_2\text{Sb}_2\text{Te}_5$ ) was used to perform addition, subtraction, and division.<sup>[360]</sup> By applying light to this material, its reflectivity changed (as measured by the setup illustrated in Figure 20e). Importantly, this change was accumulative: the amount of change in reflectivity corresponded with the total duration of the light applied onto the PCM (Figure 20f). The accumulative change in reflectivity remained even in the absence of light (i.e., it also has the function of data storage as discussed previously). Addition (i.e.,  $x_1 + x_2$ ) was performed by shining two sequential pulses of light onto the PCM.  $t_1$  was the duration of the first pulse of light that was proportional to  $x_1$ , and  $t_2$  was the duration of the second pulse of light that was proportional to  $x_2$ . The accumulative change in reflectivity was measured after exposing the material to these two pulses of light (i.e.,  $t_1 + t_2$ ); thus, the result of this measurement represented the solution of the addition. To take into account results that were more than ten, a threshold of the duration of the light pulse,  $t_{\text{thres}}$ , that was proportional to ten was defined. Once this threshold was exceeded, the PCM was reset by a source of light of a higher energy. Hence, the final result was determined by measuring the remaining duration of the light pulse and knowing the number of times that the PCM was reset. Subtraction (i.e.,  $x_1 - x_2$ ) was performed by first defining a threshold,  $t_{\text{thres}}$ , as the number to be subtracted (i.e.,  $x_1$ ). After defining  $t_{\text{thres}}$ , the PCM was exposed to a pulse of light with the duration  $t_1$  that was proportional to  $x_2$ . To perform the subtraction, another pulse of light with duration  $t_2$  was applied until  $t_{\text{thres}}$  was reached. Because  $t_2 = t_{\text{thres}} - t_1$ ,  $t_2$  thus represented the solution of  $x_1 - x_2$ . Division (i.e.,  $x_1/x_2$ ) was performed by first defining the threshold,  $t_{\text{thres}}$ , as proportional to the divisor (i.e.,  $x_2$ ). The results involved two numbers: the quotient and the remainder. The material was exposed to a light pulse with duration  $t_1$  that was proportional to  $x_1$ . If  $x_1 < x_2$ ,  $t_1$  represented the remainder of the division. If  $x_1 > x_2$ ,  $t_1 > t_{\text{thres}}$ . Once the pulse of light applied on the material exceeded  $t_{\text{thres}}$ , the material was reset (i.e., by a

light of higher energy) to its original state. The remaining duration of the pulse of light was then continued to be directed onto the material. If the threshold was exceeded again, the material was reset. Eventually, the remaining duration of the pulse of light represented the remainder, and the number of times the material was reset represented the quotient.

#### 6.4. Biocomputing

Biocomputing uses biological materials for performing complex computational operations.<sup>[364–367]</sup> The most commonly used biomaterial is DNA due to a number of reasons. Most importantly, DNA can be synthesized with the exact sequence of nucleotides desired. The specifically designed sequence of nucleotides allows the strands of DNA to have very specific interactions between them as governed by the principle of Watson–Crick base pairing. In one study, the specificity of the interaction allowed strands of DNA to be used to solve a complex computational problem (i.e., the seven-city Hamilton path).<sup>[364]</sup> Another unique feature of DNA is that it is capable of forming many types of conformational designs, including circular,<sup>[368]</sup> hairpin,<sup>[365]</sup> G-quadruplex,<sup>[369]</sup> and seesaw.<sup>[365,366]</sup> For example, the construction of an interesting logic gate—the majority logic gate—was made possible by a circular DNA.<sup>[368]</sup> The majority logic gate gives an output “1” when the majority of the inputs are “1,” and output “0” when the majority of the inputs are “0.” One study used a circular DNA that was composed of three identical segments (except for the toehold segment) of double-stranded DNA that were joined together end to end. The input of the system was a strand of DNA (i.e., the “input DNA”) that had complementary sequences to the outer strand of each segment of the circular DNA. The system also contained fluorophore-functionalized double-stranded DNA. Because the circular DNA consisted of three segments, the system operated as a majority logic gate by giving a fluorescence signal (i.e., output “1”) only when two or more input DNA were present. Specifically, each input DNA was able to hybridize with the outer strand of each segment of the circular DNA, thus removing the outer strand from the circular DNA. Consequently, the base strand of the segment of the circular DNA was exposed. Due to the specific geometry of the circular DNA, the fluorophore-functionalized double-stranded DNA was able to interact with the circular DNA only when two or more base strands were exposed; this interaction then produced fluorescence. Therefore, fluorescence was observed only when two or more input DNA were present for exposing two or more base strands of the circular DNA. Hence, the function of the majority gate was achieved.

One more important feature of DNA is that when it is used for biocomputing, the analytical operations usually consist mainly of strands of DNA—including both the inputs and outputs. Therefore, a series of complex reactions can sequentially be performed by using these strands of DNA; thus, the logic gates constructed out of DNA can be combined easily into complex integrated circuits. Examples include the identification of numbers (e.g., odd, even,<sup>[370]</sup> or composite numbers<sup>[331]</sup>) and other mathematical operations (e.g., full adders,<sup>[371,372]</sup> full subtractors,<sup>[373]</sup> and binary square root<sup>[365]</sup>).

The ability to perform complex computational tasks by DNA has been used for smart bio-sensing,<sup>[374]</sup> therapy,<sup>[375]</sup> molecular keypad locks,<sup>[376]</sup> and automata for biomedical applications.<sup>[377]</sup> In the following paragraphs, we discuss three interesting types of analytical functions performed by DNA: flexibly changing the type of logic gates under the influence of a stimulus, calculating binary square root, and performing the function of a neural network.

In the previous section on logic gates, we discussed the ability of some types of stimuli-responsive materials to perform the function of specific types of logic gates. In an interesting study, a system of DNA was reported to have the ability to flexibly change the type of logic gate operated under the influence of a stimulus.<sup>[378]</sup> This system consisted of four main components as illustrated in the oval in the center of Figure 21: the input DNA strands, substrates (i.e., the “Library 1” substrates), Mg<sup>2+</sup> and UO<sub>2</sub><sup>2+</sup> ions, and fluorophore-functionalized substrates that served as the fluorescent output. The two DNA strands that were used as the inputs were referred to as I<sub>1</sub> and I<sub>2</sub>. When both these input DNA strands were not added, there was no fluorescent output. Otherwise, three types of inputs were possible: I<sub>1</sub> (without I<sub>2</sub>), I<sub>2</sub> (without I<sub>1</sub>), and both I<sub>1</sub> and I<sub>2</sub>. Based on these three inputs, three different types of assembled structures were obtained by allowing the input DNA strand(s) to bind with the substrates (in “Library 1”) as shown in Figure 21. Importantly, the system had three types of responses depending

on pH. At a low pH (e.g., pH 5.2), the interaction between the UO<sub>2</sub><sup>2+</sup> ion and one of the assembled structure (i.e., by the presence of both I<sub>1</sub> and I<sub>2</sub>) was activated. The Mg<sup>2+</sup> ions, however, did not interact with any assembled structures. At a high pH (e.g., pH 7.2), the interactions between the Mg<sup>2+</sup> ions and two of the assembled structures (i.e., by the presence of either I<sub>1</sub> or I<sub>2</sub>) were activated. The UO<sub>2</sub><sup>2+</sup> ions, however, did not interact with any assembled structures. At a moderate range of pH (i.e., pH 6–7.2), all the types of interactions between the Mg<sup>2+</sup> and UO<sub>2</sub><sup>2+</sup> ions and the assembled structures were activated. As long as the interaction was activated (i.e., for either the Mg<sup>2+</sup> or UO<sub>2</sub><sup>2+</sup> ions), the whole assembly acted as a DNAzyme that catalyzed the reaction of the fluorophore-functionalized substrates for producing the fluorescent signal (i.e., output “1”). Therefore, at pH 5.2, the system performed as an AND gate because the fluorescent output was produced only when both I<sub>1</sub> and I<sub>2</sub> were present due to the UO<sub>2</sub><sup>2+</sup>-activated DNAzymes. At pH 7.2, the system performed as an XOR gate because the fluorescent output was produced only when either I<sub>1</sub> or I<sub>2</sub> was present but not both at the same time due to the Mg<sup>2+</sup>-activated DNAzymes. For pH 6–7.2, all the ions were activated; hence, the system acted as an OR gate. Other libraries that consisted of different types of input DNA strands and substrates gave rise to different sets of possible logic gates. For example, it was demonstrated that a second library could achieve either the AND gate, Half Adder, or XOR gate depending on pH. A third library

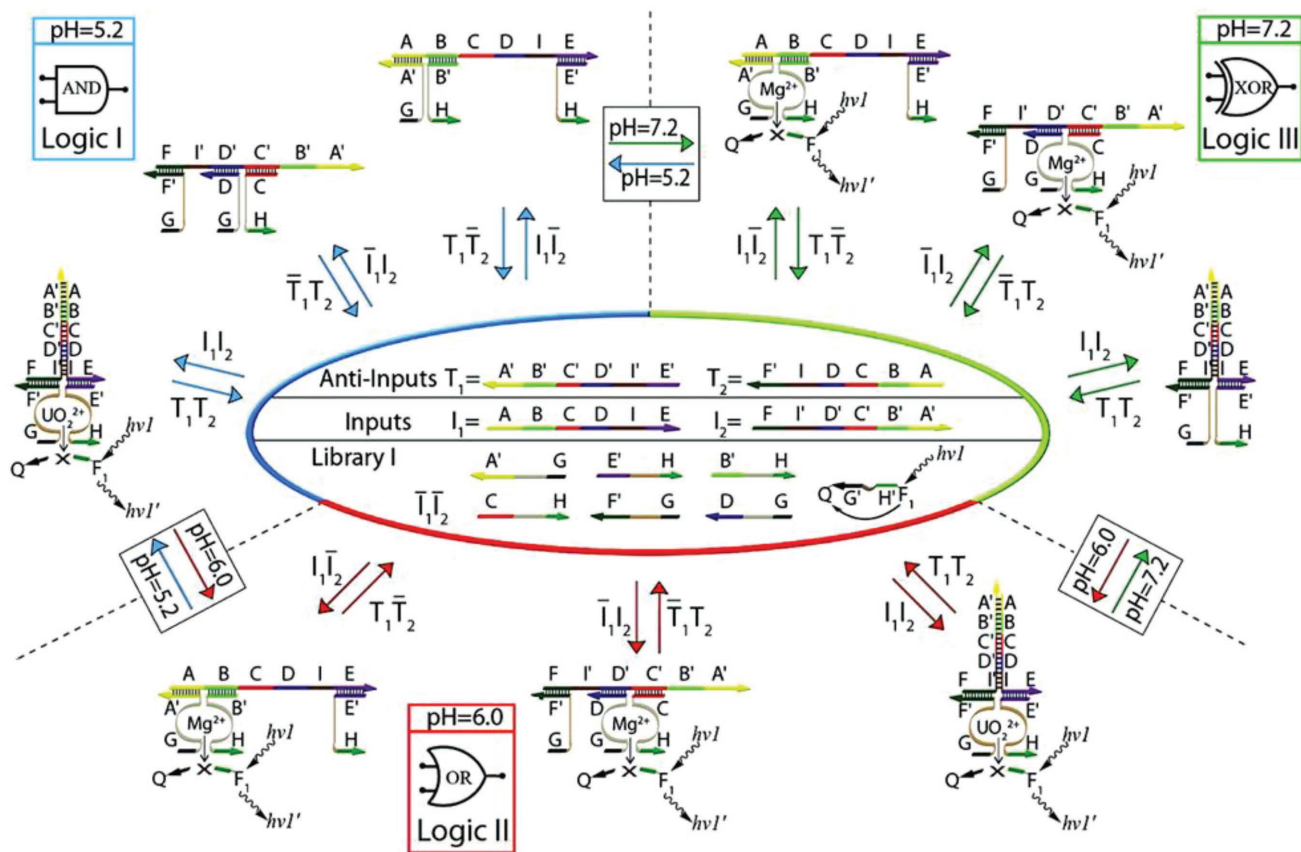


**Figure 21.** System of DNA that performed the task of either the AND, OR, or XOR gate depending on the pH. Reproduced with permission.<sup>[378]</sup> Copyright 2012, American Chemical Society.

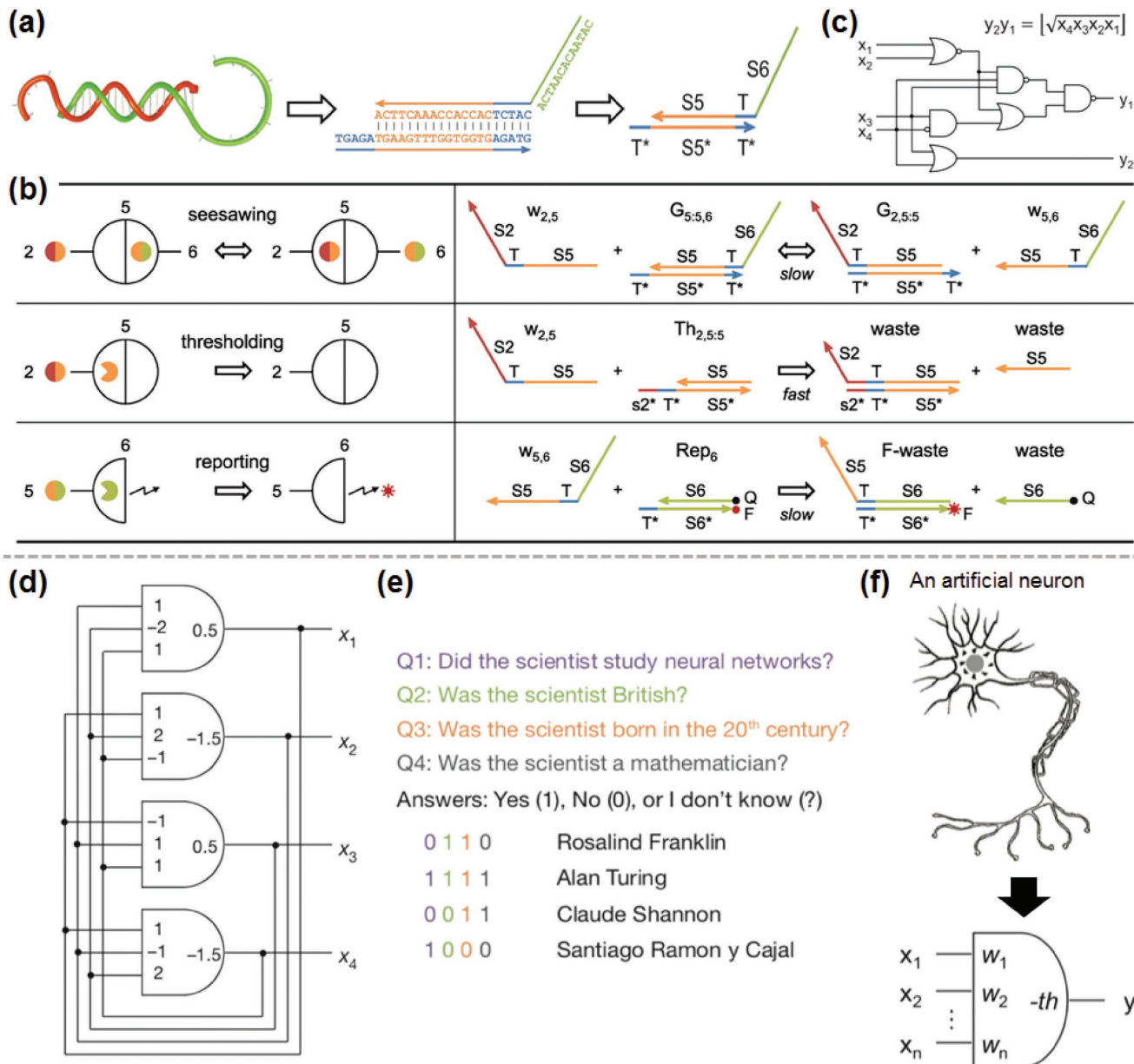


**Figure 22.** Biocomputing with DNA. a–c) Computing the square root of four-bit binary numbers. a) Schematic representation of the double-stranded DNA. b) Three fundamental reaction mechanisms involved in the mathematical operation: seesawing, thresholding, and reporting. c) The digital logic circuit that computes the floor of the square root of four-bit binary numbers. a–c) Reproduced with permission.<sup>[365]</sup> Copyright 2011, American Association for the Advancement of Science. d–f) The artificial neural network based on DNA. d) The four-neuron recurrent neural network. e) Playing the “read your mind” game by a human and the four-neuron recurrent neural network. f) An artificial neuron constructed from DNA. d–f) Reproduced with permission.<sup>[366]</sup> Copyright 2011, Springer Nature.

gave rise to either the half adder, XOR-YES( $I_1$ ), or half subtractor depending on pH.

The second example involves the calculation of the square root of binary numbers by using specifically sequenced strands of DNA (**Figure 22a**) for constructing a logical circuit.<sup>[365]</sup> The system contained a number of different types of DNA: the input DNA, gate DNA, threshold DNA, fuel DNA, and fluorophore-functionalized reporter DNA. The input DNA (i.e., the stimulus) was a single-stranded DNA that consisted of a recognition domain and a secondary segment (represented as

“ $W_{2,5}$ ” in Figure 22b). The gate DNA was a double-stranded DNA that consisted of a base strand and an output strand (“ $G_{5:5,6}$ ”). When the input DNA and the gate DNA interacted, the recognition domain of the input DNA formed complementary base pairs with the base strand of the gate DNA (or the process of “seesawing” as indicated in Figure 22b), thus releasing the output strand of the gate DNA (“ $W_{5,6}$ ”). This output strand was able to interact with the reporter DNA to produce a fluorescence signal (i.e., output “1,” or the process of “reporting”). On the other hand, the threshold DNA served as a “competitor”: the

input DNA interacted more favorably with the threshold DNA ("Th<sub>2,5,5</sub>") than the gate DNA (or the process of "thresholding"). Therefore, as long as the threshold DNA was present, the gate DNA remained intact and the output strand was not released; hence, there was no fluorescence signal (i.e., output "0").

These DNA strands were first used to perform the task of a single logic gate. The two inputs to the logic gate consisted of two types of input DNA strands that had the same recognition domain but two differently sequenced secondary segments. The logic gates were constructed based on the relative concentrations of the two input DNA and the threshold DNA. For the AND gate, the concentration of the threshold DNA was relatively high: the concentration of the input DNA could only be higher than that of the threshold DNA when both the input DNA strands were present. Once the interactions between the input DNA and the threshold DNA completely depleted the threshold DNA, any excess input DNA—even if the amount of excess was small—then underwent a catalytic reaction with the large amount of fuel DNA initially present in the solution to release a significant amount of output strand from the gate DNA (output "1"). For the OR gate, the concentration of the threshold DNA was relatively lower than that for the AND gate. Hence, the presence of either one of the two input DNA was sufficient to fully deplete the threshold DNA; hence, output "1" was produced.

Multiple logic gates need to be integrated for more complex analysis. For the calculation of the four-bit binary square root, the integrated circuit used in electronics is shown in Figure 22c. Logic gates constructed out of the system of DNA was combined by extending the concept discussed for a single logic gate. The many inputs and outputs of the logic gates consisted of many different types of DNA that were sequenced in a different but highly specific way. These specifically designed DNA strands allowed the input of one logic gate to be represented by the output of another logic gate according to the logic circuit required, while preventing other undesirable interactions among the DNA strands. In general, a complex system that was composed of different types of DNA was constructed for the calculation of the four-bit binary square root. For example, for the input 0100 (or the equivalent of the number 4), the resulting output calculated was 10 (or the number 2).

The third example involves a complex artificial neural network constructed out of a system of DNA for the purpose of achieving artificial intelligence.<sup>[366]</sup> The system is based on the Hopfield network: a recurrent artificial neural network that has the ability to recall associated memory based on incomplete information. A Hopfield network has multiple local minima that are stable. Any initial conditions that deviate from the local minima would converge to one of these local minima as a result of the recurring algorithm. Importantly, the local minima can be generated at the specifically desired states by varying the parameters of the Hopfield network; in other words, the network can be "trained" to produce the desired local minima. In this study, a four-neuron Hopfield associative memory was created (Figure 22d) by a network of DNA. Experimentally, the approach involved in building each of the artificial neurons (Figure 22f) in the neural network was based on the same mechanisms as discussed in the authors' earlier work on computing binary square root (i.e., the mechanisms illustrated in Figure 22b).

This recurrent neural network was used for playing the "read-your-mind" game. The "read-your-mind" game consisted of four questions for identifying a certain scientist as described in Figure 22e. Each question had a true or false response represented by 1 or 0, respectively. The four responses to these questions were used to identify the answer (or the scientist). Rosalind Franklin was based on the responses 0 1 1 0; Alan Turing was based on the responses 1 1 1 1; Claude Shannon was based on the responses 0 0 1 1; Santiago Ramon y Cajal was based on the responses 1 0 0 0. First, the authors "trained" the network of DNA to produce the four desired local minima that corresponded to the four different answers (or scientists). Once "trained," the network was able to solve for the answer based on a set of incomplete information (i.e., the case when not all four responses were given)—importantly, the network was also able to produce all the rest of the ungiven information based on the incomplete set of information given to the system. For example, when a human "told" the DNA network (i.e., by adding the input DNA strands into the system as the stimulus) that the scientist was a nonmathematician and born in the 20<sup>th</sup> century, without answering the other two questions (i.e.,  $x_1 = ?$ ,  $x_2 = ?$ ,  $x_3 = 1$ ,  $x_4 = 0$ ), the DNA network was able to give the fluorescence output corresponding to the full set of responses belonging to Rosalind Franklin ( $x_1 = 0$ ,  $x_2 = 1$ ,  $x_3 = 1$ ,  $x_4 = 0$ ). Therefore, the DNA network was able to produce the ungiven responses (i.e.,  $x_1$  and  $x_2$ ) based on the local minimum (0 1 1 0) established for this specific answer.

## 7. Complex Function

In order to achieve more advanced systems, multiple functions can be incorporated within a single material. In particular, multifunctional materials (or particles) are important in the field of theranostics. In many demonstrated examples, a single therapeutic agent can sense multiple stimuli at the same time for performing different functions, such as targeting (e.g., the detection of localized signals, such as a difference in pH, in the microenvironment<sup>[379–381]</sup> or the selective recognition of cancer cells by functionalizing the surface of the particles with a molecule specific to the cells<sup>[373,380,382]</sup>), tracking and imaging (e.g., incorporation of magnetic nanoparticles that are detectable by magnetic resonance imaging<sup>[379–381]</sup>), controlled release (e.g., the change from solid to liquid phase by near infrared radiation, NIR, for the release of drugs<sup>[379]</sup>), and multimodal therapeutic functions (e.g., photothermal, radiothermal, and photodynamic therapies). For example, a type of nanoparticles was fabricated in one study to have two therapeutic functions: photothermal therapy and the generation of free radicals by NIR.<sup>[379]</sup> In another study, a nanoparticle was able to generate heat by applying a certain radiofrequency (i.e., radiothermal therapy) and reactive oxygen species by laser irradiation (photodynamic therapy).<sup>[380]</sup>

In particular, a combination of many functions driven by different types of stimuli had been incorporated in a single nanowire.<sup>[383]</sup> The nanowire consisted of three metallic segments arranged in the order of Au–Ni–Au (~2 μm long and ~200 nm diameter), and an additional segment of polypyrrole–polystyrene sulfonate (PPy–PSS) as illustrated in Figure 23a. The surfaces

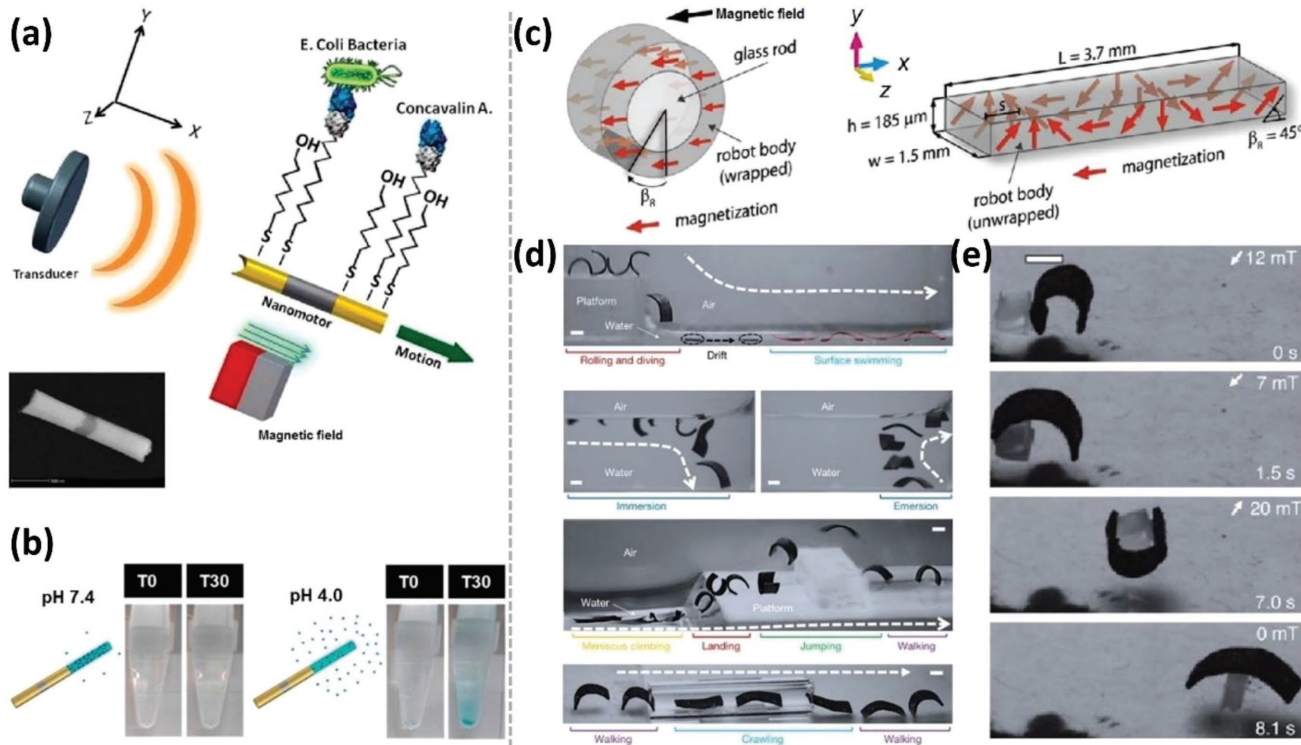


**Figure 23.** Complex functions. a,b) A multifunctional nanowire. a) Scheme of an ultrasound-propelled magnetically guided nanowire motor that could selectively capture and transport biological targets. b) pH-controlled release of brilliant green. “T0” and “T30” represent 0 and 30 min, respectively. a,b) Reproduced with permission.<sup>[383]</sup> Copyright 2013, American Chemical Society. c–e) A multifunctional soft magnetic robot. c) The process of magnetizing the soft robot rolled over a glass rod (scheme on the left) and the magnetization profile when straightened (scheme on the right). d) Multimodal locomotion. e) Time-lapse images of the soft robot capturing, transporting, and releasing a cargo. c–e) Reproduced with permission.<sup>[384]</sup> Copyright 2018, Springer Nature.

of Au were functionalized with bioreceptors (i.e., Concanavalin A, Con A). This nanowire was propelled to move by ultrasound waves produced by a piezoelectric transducer. The magnetic component of the nanowire (i.e., nickel) allowed an externally applied magnetic field to guide the nanowire along a desired trajectory. The Con A captured biological targets (i.e., bacteria such as *Escherichia coli* and *Staphylococcus aureus*) onto the surface of the nanowire. The PPy–PSS segment served as the carrier for controlled release of drug. In this study, brilliant green (BG) was used as a replacement of the drug. This positively charged BG attached onto the surface of the nanowire via electrostatic interactions with the negatively charged PPy–PSS polymeric backbone. When the nanowire moved into a region of low pH (e.g., pH 4), the PPy–PSS became protonated and no longer bound with the positively charged BG; hence, the BG released (Figure 23b). In general, this nanowire was controlled to move, navigate to a desired location, capture a target, and release drugs.

Besides incorporating multiple functions that operate independently based on multiple sources of stimuli into a single material, it is also possible to perform many types of functions by applying only a single type of stimulus onto a single piece of material. In one fascinating example, multiple types of motions were achieved by applying a magnetic field to a piece of magnetic material.<sup>[384]</sup> The material (or robot) was a simple flat slab (3.7 mm long, 1.5 mm wide, and 0.185 mm thick) of

soft and elastic silicone polymer doped with magnetic micro-particles (i.e., neodymium–iron–boron, NdFeB;  $\approx 5 \mu\text{m}$  diameter). This piece of soft magnetic material was magnetized in a specific way: the material was first deformed into a circular shape by rolling it over a glass rod and then a strong magnetic field (1.65 T) was applied in a specific direction onto the material (Figure 23c). This method of preparation caused the orientation of magnetization to be spatially different across the material. Specifically, the orientation varied  $360^\circ$  continuously through the length of the material (i.e., as illustrated in Figure 23c for the case when the material was straightened out). After preparing the magnetic material, this simple piece of material behaved as a soft robot. By applying a spatially uniform magnetic field with a specific magnitude and direction onto the material, each localized region of the material experienced a different amount and direction of the magnetic force due to the varying orientation of magnetization; hence, the robot deformed into a particular shape (e.g., “C,” “V,” sine, or cosine). When a time-varying magnetic field was applied, the robot moved. Many interesting types of motions were achieved, such as rotating, drifting on the surface of the water, swimming underwater, climbing liquid menisci, rolling, walking, jumping over obstacles, and crawling within narrow tunnels (Figure 23d). In addition, the robot was demonstrated to pick up an object, transport it to another location, and release it (Figure 23e).

## 8. Design Considerations for Pathway to Intelligence

The construction of an intelligent system requires each of the functions discussed in previous sections to be carefully designed and fabricated for achieving the desired purposes of the system. Fortunately, based on the large number of studies published previously, a wide range of materials can be used for creating the functions, including polymers, elastomers, hydrogels, inorganic and metallic particles, and biological materials (e.g., DNA). Table 1 lists a few examples of the materials used for creating each function as discussed here. This wide range of materials allows systems to be fabricated with a large amount of flexibility (e.g., for the purpose of specific applications or achieving a desired set of materials properties). In addition, a wide range of sizes of the materials was used as previously investigated. For each function, stimuli-responsive materials that range from nanoscale to macroscopic scale were fabricated for achieving their intended purposes—therefore, it seems that the functions are not limited to materials of any specific range of sizes.

Although size is not a limiting factor conceptually for realizing the functions, it is nevertheless an important factor to consider for the design and construction of the functions. When the size of the materials decreases, it is generally more technically challenging to fabricate them with the desired features (e.g., nanofabrication is usually more difficult to carry out than microfabrication). Another consideration is that certain phenomena only happen at a specific dimension.<sup>[385]</sup> For example, some material properties are only present at the nanoscale (e.g., fluorescence of semiconductor quantum dots<sup>[386]</sup> and superparamagnetism<sup>[387]</sup>). Some types of forces involved in the interactions (e.g., self-assembly) among the materials also depend on size.<sup>[388]</sup> Several types of forces are operative only at the molecular or nanometer scale (e.g., Van der Waals and steric forces), while some forces are macroscopic in range (e.g., capillary force). In addition, the type of stimulus used for driving the operations of the functions can influence the choice of the size of the materials. For example, the electric field produced by a charged material can generally have an influence over a distance,  $d$ , of macroscopic size (e.g., mm) that scales with  $\approx 1/d^2$ ; however, if the field is screened, its distance of influence can decrease dramatically (e.g., the Debye length of an electrolyte solution is typically only on the order of nanometers). For stimuli that involve the diffusion of molecules (e.g., ions, alcohol, glucose, and biomolecules), the size of the stimuli-responsive materials needs to be small in order for the response to be sufficiently fast. The reason is because the time of diffusion of molecules scales with  $d^2$ ; hence, a decrease in size of the stimuli-responsive material greatly reduces the time of response.

An additional consideration is the choice of an equilibrium or nonequilibrium process for the operation of the functions. Many of the stimuli-responsive processes described involve equilibrium states: the initial state of the system is transformed into another equilibrium state by the stimulus for various types of functions (e.g., size change, shape change, static self-assembly, and rupturing). A typical example involves the change in size of a piece of stimuli-responsive hydrogel from

an expanded state to a contracted state when the pH of the surrounding medium is changed. On the other hand, some processes are nonequilibrium: they operate continuously and require a constant influx of energy. These nonequilibrium processes may happen in two ways. First, some types of stimuli need to be applied continuously for the process to work. For example, when light was supplied continuously onto the azobenzene derivatives grafted within the pores of mesostructured silica nanoparticles, the molecules were able to undergo repeated cycles of *cis-trans* isomerization.<sup>[389]</sup> This oscillatory motion of the molecules allowed them to expel the other chemicals filled within the pores. In the absence of light, however, the azobenzene derivatives did not expel the chemicals from the pores. The second category involves functions that operate continuously by definition. Examples include self-oscillation, self-regulation, self-replication, dynamic self-assembly, and motion. Energy is constantly applied and dissipated; hence, these functions are nonequilibrium processes. In comparison, nonequilibrium processes always require a constant supply of energy whereas equilibrium processes do not require any more energy when the final state is attained; hence, nonequilibrium processes may not be energy efficient. On the other hand, it is certainly advantageous for complex systems (e.g., cells) to operate continuously for performing essential tasks (e.g., searching for resources). Therefore, an optimum design of the intelligent system may involve a balance of both equilibrium and nonequilibrium processes.

Table 1 lists a few illustrative examples of the roles of each functions for the construction of intelligent systems. For the pathway to intelligence, however, a system needs to have a combination of the practical, regulatory, and analytical functions as discussed in the previous sections for achieving the desired purposes of the system. Many basic tasks of complex systems that are required for survival require the combination and coordination of many functions operating together (e.g., the search for food, gathering of resources, or communication with other systems). Table 1 shows the functions that are closely related to each other for the purpose of performing specific tasks. There is a range of options by which these functions can be combined into a single system. On one hand, researchers are actively discovering and fabricating materials that perform a combination of complex functions by themselves. On the other hand, there may be a limit to the complexity that a single material can perform. A more plausible option is to combine different types of functions that have been demonstrated in separate studies into a single integrated complex system. This approach is similar to many types of biological systems. A cell, for example, contains many different organelles (or separate compartments); a specific function is carried out separately in each of these organelles. Importantly, because all the functions are stimuli-responsive, each function can, at least conceptually, be able to produce an output that can potentially be used as the input for another function. Therefore, although the stimuli-responsive functions operate separately, they can communicate with each other via the stimuli involved.

Figure 24 shows a general impression of a possible set of relationships between the functions. The functions that are placed closer to each other are proposed to be more closely related. First, the artificial intelligent system is driven by the

**Table 1.** Factors to consider when using stimuli-responsive functions for building intelligent systems.

Functions	Purpose for intelligence	Closely related functions	Materials used in (and size of) systems discussed <sup>a,b)</sup>	Ref.
Size change	Change dimension (e.g., for actuation)	– Shape change	• P(HEMA- <i>co</i> -AA), P(HEMA- <i>co</i> -DMAEMA) hydrogel ( <i>d</i> : 100 μm; <i>t</i> : 50 μm) • P(AAm) hydrogel containing ferrocene ( <i>d</i> : 8–30 mm)	[50,51]
	Produce mechanical force	– Capture and release – Rupture		
	Block by expansion or open by contraction	– Gating		
Self-assembly/ disassembly	Build higher ordered structures	– Self-organization – Self-replication	• Metallic NP ( <i>d</i> : ≈5 nm) self-assembled into crystals ( <i>l</i> : ≈1 μm) • Magnetite-doped polydimethylsiloxane ( <i>d</i> : 1 mm; <i>t</i> : ≈400 μm)	[66,71]
	Release individual components	– Self-organization – Amplification		
Targeting	Locate a specific position (e.g., for finding resources and favorable environments)	– Motion – Communication (e.g., via detecting external signals)	• Maghemite nanocrystals ( <i>d</i> : 5–10 nm) encapsulated in phospholipids vesicles ( <i>d</i> : ≈200 nm)	[83]
Gating	Control entry of substances	– Communication (e.g., via external signals) – To internal processes (e.g., regulatory functions and analytical processing functions) – Rectification	• Au nanocages ( <i>l</i> : 50 nm) functionalized with P(NIPAM) and P(NIPAM- <i>co</i> -AAm) • Porous silica NP ( <i>d</i> : 400 nm) functionalized with azobenzene derivatives and β-cyclodextrin	[87,89]
	Control release of substances	– From internal processes (e.g., regulatory functions and analytical processing functions) – Communication (e.g., via external signaling) – Rectification		
	Break structures for extracting contents	– To internal processes (e.g., regulatory functions and analytical processing functions) – Size change (e.g., the mechanical force used for gripping) – Shape change (e.g., for actuation)	• P(NIPAM) shell ( <i>d</i> : ≈300 μm) • Macroscopic P(NIPAM) hydrogel ( <i>d</i> : mm) and microscopic PNIPAM hydrogel particles ( <i>d</i> : 15 μm)	[90,46]
Capture and release	Transport material (e.g., for gathering resources or building)	– Targeting – Motion – Size change (e.g., the mechanical force used for gripping) – Shape change (e.g., for actuation)	• Silicon substrate functionalized with photo-switchable molecules ( <i>t</i> of molecular film: ≈2–4 nm) • Epoxy fins (≈10 μm) embedded in P(AAm- <i>co</i> -AA) hydrogel	[92,95]
Shape change	Produce actuation	– Capture and release – Size change	• Photoresponsive molecules modified P(AAm) hydrogel (≈10 mm) • Polypyrrole film ( <i>l</i> : 20 mm; <i>w</i> : 5 mm; <i>t</i> : 21 μm) • P(NIPAM- <i>co</i> -AA) film ( <i>t</i> : 7–17 μm) • PpMS/P(NIPAM)/PpMS trilayer film ( <i>t</i> : 1–8 μm) • Nanofibrillated cellulose-P(AAm) hydrogel composite fiber ( <i>d</i> : ≈100 μm–1 mm)	[107,108,112,128,130]
Pattern formation	Produce mechanical force (e.g., gripping)	– Capture and release – Size change		
	Display ordered features on surface	– Communication (e.g., for signaling or camouflage)	• PS/liquid crystal elastomer bilayer ( <i>t</i> of PS: 30 nm; <i>t</i> of LCE: 360 μm) • Silicon elastomer/polyimide bilayer ( <i>t</i> : ≈100 μm)	[146,155]
Motion	Search surrounding (e.g., for resources or favorable environments)	– Targeting	• Filament of DNA-linked superparamagnetic particles ( <i>d</i> : 1 μm; <i>l</i> : 12–34 μm) • Mg particles coated with TiO <sub>2</sub> , drug-containing PLGA and chitosan ( <i>d</i> : 20 μm) • Oil droplets ( <i>d</i> : ≈1 mm) • PEE-polypyrrole composite film ( <i>t</i> : 15–40 μm)	[172,160,164,173]

**Table 1.** Continued.

Functions	Purpose for intelligence	Closely related functions	Materials used in (and size of) systems discussed <sup>a,b)</sup>	Ref.
Communication	Avoid dangers (e.g., predators and unfavorable environments)	– Targeting (e.g., finding safe locations)		
	Transport materials (e.g., for building)	– Targeting – Capture and release		
	Connect processes	– All connections between functions	• Mesoporous silica NP capped with functional molecules ( $d$ : 100 nm) • Janus Au-mesoporous silica NP ( $d$ : 100 nm) • PS microspheres half-coated with Ni, Au, and Ag trilayer ( $d$ : 2 $\mu$ m), silica microspheres half-coated with Pt ( $d$ : 1.2 $\mu$ m)	[181–183]
Self-regulation	Coordinate with external systems (e.g., external signaling)	– Analytical processing functions		
	Maintain optimum condition of processes	– Analytical processing functions – Internal regulation functions	• Core-shell PVA microneedles ( $r$ of needle tip: 5 $\mu$ m) • Epoxy fins ( $\approx$ 10 $\mu$ m) embedded in P(AAm- <i>co</i> -AA) or PNIPAM hydrogel	[204,205]
Self-oscillation	Provide periodic response	– Analytical processing functions (e.g., providing timed analysis and response)	• Catalyst modified PNIPAM hydrogel ( $d$ : $\approx$ 600 $\mu$ m) • P(NIPAM- <i>co</i> -MEP) hydrogel ( $d$ : 300 $\mu$ m) • Liquid crystalline polymer film ( $l$ : 16 mm; $w$ : 1.5 mm; $t$ : 0.02 mm)	[212–214]
Rectification	Directional flow of substances	– Gating	• Asymmetric nanochannel in PET films functionalized with carboxylate group ( $t$ of film: 12 $\mu$ m; $d$ of base of pores: 500 nm) • Asymmetric nanochannel in PET films functionalized with photoresponsive molecules ( $t$ of film: 12 $\mu$ m; $d$ of base of pores: 350 nm)	[227,228]
Amplification	Multiply signals	– Boost ability of practical functions – Communication (i.e., increase signals between functions)	• Supramolecular allosteric catalyst ( $\approx$ nm) • DNA, prefluorophore molecules and nucleophilic molecules ( $\approx$ nm) • Diblock copolymer micelles ( $d$ : 80 nm) • Dendrimer molecules ( $\approx$ nm) • Polyamine particles with iron oxide cores ( $d$ : 1 $\mu$ m) and Au NP ( $d$ : 13–30 nm) functionalized with oligonucleotides • P(AA- <i>co</i> -HEMA) hydrogel ( $t$ : 1 mm) coated with superhydrophobic NP ( $t$ of NP layer: <5 $\mu$ m)	[252,250,239,247,248,267,231]
	Increase sensitivity of detection	– Analytical processing functions		
Self-organization	Dynamic rearrangement of components	– Self-assembly/disassembly	• Triblock copolymer multicompartiment micelles ( $r$ : $\approx$ 100–400 nm) • Diblock copolymer ( $r$ : 5–100 nm)	[270,271]
Self-replication	Multiply entities (e.g., for evolution)	– Self-assembly/disassembly	• Peptide ( $\approx$ nm) • PS microspheres ( $d$ : 1 $\mu$ m) and DNA molecules	[281,282]
	Amplify signal	– Amplification		
Memory/ data storage	Store information for logical operations	– Communication (e.g., external signals) – Logic gates – Computing	• Triblock copolymer membrane with P(AA) polymer brush grafted in its nanopores ( $d$ of pores: $\approx$ 20 nm) • Organohydrogel ( $\approx$ cm) • Carbon nanotubes and Fe <sub>3</sub> O <sub>4</sub> NP-doped epoxy strip ( $t$ : 1 mm) • Ionomer strip ( $l$ : 2–3.5 cm; $t$ : 0.08 mm) • Copolyester urethane network strip ( $l$ : 40 mm; $w$ : 4 mm; $t$ : 0.4 mm) • GeSbTe alloy ( $l$ , $w$ : 400 nm) • Au or Ag NP ( $d$ : $\approx$ 5 nm) embedded in organogel film ( $l$ , $w$ : 5 cm; $t$ : 150 $\mu$ m)	[292,297,310,313,317,324,328]

**Table 1.** Continued.

Functions	Purpose for intelligence	Closely related functions	Materials used in (and size of) systems discussed <sup>a,b)</sup>	Ref.
Logic gates	Analyze information and produce a logical response	– To all basic, practical, and regulatory functions – Memory/data storage – Computing	• Mesoporous silica NP ( $d: \approx 400$ nm) • P(HEMA- <i>co</i> -MMA) organogel ( $l: 30$ mm; $w: 10$ mm; $t: 1.2$ mm)	[349,350]
Computing/ biocomputing	Complex analysis and logical response	– To all basic, practical, and regulatory functions – Memory/data storage – Computing	• Glycolipid-type hydrogelator ( $\approx$ cm) • P(AA- <i>co</i> -HEMA), P(NIPAM), P(AMPS- <i>co</i> -HEMA) hydrogel ( $\approx 1$ mm) • GeSbTe alloy • DNA molecules ( $\approx$ nm)	[351,41,360,365,366,368,378]

<sup>a</sup>)NP: nanoparticles; HEMA: 2-hydroxyethyl methacrylate; AA: acrylic acid; DMAEMA: 2-(dimethylamino)ethyl methacrylate; AAm: acrylamide; NIPAM: *N*-isopropylacrylamide; PS: polystyrene; PVA: polyvinyl alcohol; PpMS: poly(*p*-methylstyrene); PEE: pentaerythritol ethoxylate; PLGA: poly(lactic-*co*-glycolic acid); PET: polyethylene terephthalate; MEP: 2-(methacryloyloxy)ethyl phosphate; MMA: methyl methacrylate; AMPS: 2-acrylamido-2-methylpropanesulfonic acid; <sup>b</sup>) $d$ : diameter;  $r$ : radius;  $h$ : height;  $t$ : thickness;  $l$ : length;  $w$ : width.

stimuli applied from external sources. With the supply of energy, the analytical processing functions operate by analyzing (i.e., computing) the information gathered (i.e., memory). The results of the analysis are then transmitted to the rest of the system via the function of communication. Amplification may be needed to enhance the signal of communication between functions. Subsequently, the signals communicated from the analytical processing functions direct a series of internal regulatory functions to be performed accordingly (e.g., self-regulation for maintaining conditions within the systems at the desired levels, or self-assembly/disassembly and self-organization for rearranging components within one system). Different types

of tasks can then be performed by a combination of practical functions. A few important examples include actuation, transport of materials, and the search for resources (e.g., food). The energy obtained from the resources may serve as the stimuli—importantly, acquiring the source of stimuli closes the loop for sustaining the operation of the complex system. In addition, interaction with the external environment (i.e., via the function of communication) allows the system to constantly gather data. This information is fed back to the analytical processing functions for storing data, learning from experience, and improving the logical decision made by the system. In general, the construction of this integrated complex system may involve

a combination of different types of stimuli-responsive materials, each of which operates via their well-studied mechanism separately (e.g., by the materials and mechanisms described in previous studies). This illustration thus shows an example of the complexity of the functions (e.g., functions such as communications that play different roles within the system), the relationships between the functions, and the necessity of the functions (i.e., practical, regulatory, and analytical) to work together for achieving “intelligence.”

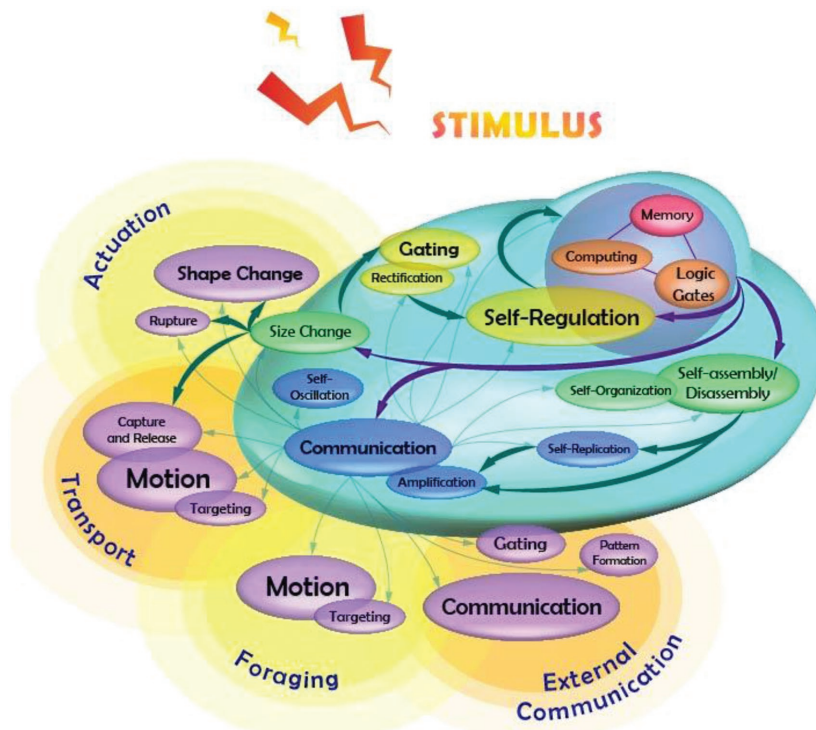


**Figure 24.** An artistic impression of an artificial intelligent system based on stimuli-responsive functions.

## 9. Conclusion

When stimuli-responsive materials were first developed more than a century ago,<sup>[368]</sup> the initial studies investigated only the basic functions of the stimuli-responsive materials (e.g., the change in size of stimuli-responsive hydrogels by applying an external stimulus). Ever since then, a vast amount of research has been performed based on using these stimuli-responsive materials for performing functions that are more advanced, complex, and smart. Currently, researchers are able to perform many types of practical functions, regulatory functions, and analytical

processing functions. These different types of functions were established based on different interesting types of materials and fundamental mechanisms. On the other hand, the pathway to fabricating truly intelligent materials or systems is certainly challenging. Many of the functions (e.g., self-replication) are still far from being established. Proper communication channels that integrate the various materials and functions together need to be developed. More complex functions that potentially can mimic cellular activities (e.g., cell growth and mitosis) also need to be created. Regardless of the challenges, judging by the increasing speed at which smart functions based on stimuli-responsive materials are actively being developed by researchers in recent years, the possibility of constructing truly intelligent systems may not be too far away.

## Acknowledgements

X.Z. and L.C. contributed equally to this work. This work was financially supported by the Ministry of Education, Singapore under Grant No. R-279-000-398-133.

## Conflict of Interest

The authors declare no conflict of interest.

## Keywords

artificial intelligence, complexity, functional materials, smart systems, stimuli-responsive materials

Received: July 16, 2018

Revised: October 9, 2018

Published online: January 9, 2019

- [1] R. B. Fletcher, J. Hattie, *Intelligence and Intelligence Testing*, Taylor and Francis, Abingdon, UK **2011**.
- [2] J. Schull, *Behav. Brain Sci.* **1990**, 13, 63.
- [3] L. C. van Loon, *Trends Plant Sci.* **2016**, 21, 286.
- [4] J. Bohm, S. Scherzer, E. Krol, I. Kreuzer, K. von Meyer, C. Lorey, T. D. Mueller, L. Shabala, I. Monte, R. Solano, K. A. S. Al-Rasheid, H. Rennenberg, S. Shabala, E. Neher, R. Hedrich, *Curr. Biol.* **2016**, 26, 286.
- [5] C. Cadart, E. Zlotek-Zlotkiewicz, M. Le Berre, M. Piel, H. K. Matthews, *Dev. Cell* **2014**, 29, 159.
- [6] A. C. Lloyd, *Cell* **2013**, 154, 1194.
- [7] D. A. Fletcher, D. Mullins, *Nature* **2010**, 463, 485.
- [8] T. D. Pollard, J. A. Cooper, *Science* **2009**, 326, 1208.
- [9] S. Soh, M. Byrska, K. Kandere-Grzybowska, B. A. Grzybowski, *Angew. Chem., Int. Ed.* **2010**, 49, 4170.
- [10] C. Hunte, E. Scrpanti, M. Venturi, A. Rimon, E. Padan, H. Michel, *Nature* **2005**, 435, 1197.
- [11] M. Méchali, *Nat. Rev. Mol. Cell Biol.* **2010**, 11, 728.
- [12] B. Görke, J. Stülke, *Nat. Rev. Microbiol.* **2008**, 6, 613.
- [13] I. Ferain, C. A. Colinge, J. P. Colinge, *Nature* **2011**, 479, 310.
- [14] J. Hwang, M. Pototschnig, R. Lettow, G. Zumofen, A. Renn, S. Gotzinger, V. Sandoghdar, *Nature* **2009**, 460, 76.
- [15] E. Lakdawalla, *The Design and Engineering of Curiosity*, Springer, New York **2018**.
- [16] Z. Shi, *Advanced Artificial intelligence*, World Scientific, Singapore **2011**.
- [17] D. Silver, J. Schrittwieser, K. Simonyan, I. Antonoglou, A. Huang, A. Guez, T. Hubert, L. Baker, M. Lai, A. Bolton, Y. T. Chen, T. Lillicrap, F. Hui, L. Sifre, G. van den Driessche, T. Graepel, D. Hassabis, *Nature* **2017**, 550, 354.
- [18] W. Fuß, C. Kosmidis, W. E. Schmid, S. A. Trushin, *Angew. Chem., Int. Ed.* **2004**, 43, 4178.
- [19] V. I. Minkin, *Chem. Rev.* **2004**, 104, 2751.
- [20] L. F. Chen, W. Q. Wang, B. Su, Y. Q. Wen, C. B. Li, Y. B. Zhou, M. Z. Li, X. D. Shi, H. W. Du, Y. L. Song, L. Jiang, *ACS Nano* **2014**, 8, 744.
- [21] G. Berkovic, V. Krongauz, V. Weiss, *Chem. Rev.* **2000**, 100, 1741.
- [22] H. M. D. Bandara, S. C. Burdette, *Chem. Soc. Rev.* **2012**, 41, 1809.
- [23] R. Klajn, *Pure Appl. Chem.* **2010**, 82, 2247.
- [24] H. G. Schild, *Prog. Polym. Sci.* **1992**, 17, 163.
- [25] W. Lu, X. X. Le, J. W. Zhang, Y. J. Huang, T. Chen, *Chem. Soc. Rev.* **2017**, 46, 1284.
- [26] E. Aznar, M. Oroval, L. Pascual, J. R. Murguia, R. Martinez-Manez, F. Sancenon, *Chem. Rev.* **2016**, 116, 561.
- [27] Y. W. Yang, Y. L. Sun, N. Song, *Acc. Chem. Res.* **2014**, 47, 1950.
- [28] H. Murakami, A. Kawabuchi, K. Kotoo, M. Kunitake, N. Nakashima, *J. Am. Chem. Soc.* **1997**, 119, 7605.
- [29] H. Murakami, A. Kawabuchi, R. Matsumoto, T. Ido, N. Nakashima, *J. Am. Chem. Soc.* **2005**, 127, 15891.
- [30] Y. Inoue, P. Kuad, Y. Okumura, Y. Takashima, H. Yamaguchi, A. Harada, *J. Am. Chem. Soc.* **2007**, 129, 6396.
- [31] C. V. Smith, D. P. Jones, T. M. Guenthner, L. H. Lash, B. H. Lauterburg, *Toxicol. Appl. Pharmacol.* **1996**, 140, 1.
- [32] J. F. Quinn, M. R. Whittaker, T. P. Davis, *Polym. Chem.* **2017**, 8, 97.
- [33] O. Sato, *Nat. Chem.* **2016**, 8, 644.
- [34] G. Isapour, M. Lattuada, *Adv. Mater.* **2018**, 30, 1707069.
- [35] X. W. Yu, H. H. Cheng, M. Zhang, Y. Zhao, L. T. Qu, G. Q. Shi, *Nat. Rev. Mater.* **2017**, 2, 17046.
- [36] M. A. C. Stuart, W. T. S. Huck, J. Genzer, M. Müller, C. Ober, M. Stamm, G. B. Sukhorukov, I. Szleifer, V. V. Tsukruk, M. Urban, F. Winnik, S. Zauscher, I. Luzinov, S. Minko, *Nat. Mater.* **2010**, 9, 101.
- [37] I. Cobo, M. Li, B. S. Sumerlin, S. Perrier, *Nat. Mater.* **2015**, 14, 143.
- [38] S. Guragain, B. P. Bastakoti, V. Malgras, K. Nakashima, Y. Yamauchi, *Chem. – Eur. J.* **2015**, 21, 13164.
- [39] D. Schmaljohann, *Adv. Drug Delivery Rev.* **2006**, 58, 1655.
- [40] M. Das, H. Zhang, E. Kumacheva, *Annu. Rev. Mater. Res.* **2006**, 36, 117.
- [41] X. Zhang, S. Soh, *Adv. Mater.* **2017**, 29, 1606483.
- [42] P. J. Glazer, J. Leuven, H. An, S. G. Lemay, E. Mendes, *Adv. Funct. Mater.* **2013**, 23, 2964.
- [43] D. Buenger, F. Topuz, J. Groll, *Prog. Polym. Sci.* **2012**, 37, 1678.
- [44] X. Huang, Y. Sun, S. Soh, *Adv. Mater.* **2015**, 27, 4062.
- [45] J. Shin, S. G. Han, W. Lee, *Sens. Actuators, B* **2012**, 168, 20.
- [46] Y. Fang, J. Tan, S. Lim, S. Soh, *NPG Asia Mater.* **2018**, 10, e465.
- [47] F. M. Winnik, *Macromolecules* **1990**, 23, 233.
- [48] B. Jeong, A. Gutowska, *Trends Biotechnol.* **2002**, 20, 305.
- [49] D. T. Eddington, D. J. Beebe, *Adv. Drug Delivery Rev.* **2004**, 56, 199.
- [50] D. J. Beebe, J. S. Moore, J. M. Bauer, Q. Yu, R. H. Liu, C. Devadoss, B.-H. Jo, *Nature* **2000**, 404, 588.
- [51] M. Ni, N. Zhang, W. Xia, X. Wu, C. Yao, X. Liu, X.-Y. Hu, C. Lin, L. Wang, *J. Am. Chem. Soc.* **2016**, 138, 6643.
- [52] R. G. Jones, C. K. Ober, P. Hodge, P. Kratochvil, G. Moad, M. Vert, *Pure Appl. Chem.* **2013**, 85, 463.
- [53] G. M. Whitesides, B. Grzybowski, *Science* **2002**, 295, 2418.
- [54] S. Whitelam, R. L. Jack, *Annu. Rev. Phys. Chem.* **2015**, 66, 143.

- [55] D. A. Brock, T. E. Douglas, D. C. Queller, J. E. Strassmann, *Nature* **2011**, *469*, 393.
- [56] Y. Lee, S. Fukushima, Y. Bae, S. Hiki, T. Ishii, K. Kataoka, *J. Am. Chem. Soc.* **2007**, *129*, 5362.
- [57] T. A. T. Lee, A. Cooper, R. P. Apkarian, V. P. Conticello, *Adv. Mater.* **2000**, *12*, 1105.
- [58] A. A. Shah, B. Schultz, W. J. Zhang, S. C. Glotzer, M. J. Solomon, *Nat. Mater.* **2015**, *14*, 117.
- [59] S. Das, P. Ranjan, P. S. Maiti, G. Singh, G. Leitus, R. Klajn, *Adv. Mater.* **2013**, *25*, 422.
- [60] T. Heuser, A. K. Steppert, C. M. Lopez, B. L. Zhu, A. Walther, *Nano Lett.* **2015**, *15*, 2213.
- [61] C. J. Brinker, Y. F. Lu, A. Sellinger, H. Y. Fan, *Adv. Mater.* **1999**, *11*, 579.
- [62] S. Maiti, I. Fortunati, C. Ferrante, P. Scrimin, L. J. Prins, *Nat. Chem.* **2016**, *8*, 725.
- [63] A. G. Dong, J. Chen, P. M. Vora, J. M. Kikkawa, C. B. Murray, *Nature* **2010**, *466*, 474.
- [64] C. A. Angulo-Pachon, J. F. Miravet, *Chem. Commun.* **2016**, *52*, 5398.
- [65] H. S. Liao, J. Lin, Y. Liu, P. Huang, A. Jin, X. Y. Chen, *Nanoscale* **2016**, *8*, 14814.
- [66] A. M. Kalsin, M. Fialkowski, M. Paszewski, S. K. Smoukov, K. J. M. Bishop, B. A. Grzybowski, *Science* **2006**, *312*, 420.
- [67] B. A. Grzybowski, K. Fitzner, J. Paczesny, S. Granick, *Chem. Soc. Rev.* **2017**, *46*, 5647.
- [68] J. A. Shapiro, *Annu. Rev. Microbiol.* **1998**, *52*, 81.
- [69] E. Bonabeau, M. Dorigo, G. Theraulaz, *Nature* **2000**, *406*, 39.
- [70] C. G. Pappas, I. R. Sasselli, R. V. Ulijn, *Angew. Chem., Int. Ed.* **2015**, *54*, 8119.
- [71] B. A. Grzybowski, H. A. Stone, G. M. Whitesides, *Nature* **2000**, *405*, 1033.
- [72] D. Trachootham, J. Alexandre, P. Huang, *Nat. Rev. Drug Discovery* **2009**, *8*, 579.
- [73] C. E. Ashley, E. C. Carnes, G. K. Phillips, D. Padilla, P. N. Durfee, P. A. Brown, T. N. Hanna, J. Liu, B. Phillips, M. B. Carter, N. J. Carroll, X. Jiang, D. R. Dunphy, C. L. Willman, D. N. Petsev, D. G. Evans, A. N. Parikh, B. Chackerman, W. Wharton, D. S. Peabody, C. J. Brinker, *Nat. Mater.* **2011**, *10*, 389.
- [74] C.-Y. Quan, J.-X. Chen, H.-Y. Wang, C. Li, C. Chang, X.-Z. Zhang, R.-X. Zhuo, *ACS Nano* **2010**, *4*, 4211.
- [75] A. E. Nel, L. Mädler, D. Velegol, T. Xia, E. M. V. Hoek, P. Somasundaran, F. Klaessig, V. Castranova, M. Thompson, *Nat. Mater.* **2009**, *8*, 543.
- [76] E. K. Rofstad, B. Mathiesen, K. Kindem, K. Galappathi, *Cancer Res.* **2006**, *66*, 6699.
- [77] M. Grabe, G. Oster, *J. Gen. Physiol.* **2001**, *117*, 329.
- [78] C. Stefanadis, C. Chrysochoou, D. Markou, K. Petraki, D. B. Panagiotakos, C. Fasoulakis, A. Kyriakidis, C. Papadimitriou, P. K. Toutouzas, *J. Clin. Oncol.* **2001**, *19*, 676.
- [79] L. Zhang, R. Guo, M. Yang, X. Jiang, B. Liu, *Adv. Mater.* **2007**, *19*, 2988.
- [80] F. H. Meng, Y. A. Zhong, R. Cheng, C. Deng, Z. Y. Zhong, *Nanomedicine* **2014**, *9*, 487.
- [81] F. Scherer, M. Anton, U. Schillinger, J. Henke, C. Bergemann, A. Krüger, B. Gänbsbacher, C. Plank, *Gene Ther.* **2002**, *9*, 102.
- [82] R. Sensenig, Y. Sapir, C. MacDonald, S. Cohen, B. Polyak, *Nanomedicine* **2012**, *7*, 1425.
- [83] H. Marie, L. Lemaire, F. Franconi, S. Lajnef, Y.-M. Frapart, V. Nicolas, G. Frébourg, M. Trichet, C. Ménager, S. Lesieur, *Adv. Funct. Mater.* **2015**, *25*, 1258.
- [84] Y. Jiang, A. Lee, J. Chen, M. Cadene, B. T. Chait, R. MacKinnon, *Nature* **2002**, *417*, 523.
- [85] S. Chaterji, I. K. Kwon, K. Park, *Prog. Polym. Sci.* **2007**, *32*, 1083.
- [86] Y. Guan, Y. J. Zhang, *Soft Matter* **2011**, *7*, 6375.
- [87] M. S. Yavuz, Y. Y. Cheng, J. Y. Chen, C. M. Cobley, Q. Zhang, M. Rycenga, J. W. Xie, C. Kim, K. H. Song, A. G. Schwartz, L. H. V. Wang, Y. N. Xia, *Nat. Mater.* **2009**, *8*, 935.
- [88] Z. Liu, W. Wang, R. Xie, X. J. Ju, L. Y. Chu, *Chem. Soc. Rev.* **2016**, *45*, 460.
- [89] D. P. Ferris, Y. L. Zhao, N. M. Khashab, H. A. Khatib, J. F. Stoddart, J. I. Zink, *J. Am. Chem. Soc.* **2009**, *131*, 1686.
- [90] L. Liu, W. Wang, X.-J. Ju, R. Xie, L.-Y. Chu, *Soft Matter* **2010**, *6*, 3759.
- [91] H. Mairbäurl, R. E. Weber, *Compr. Physiol.* **2012**, *2*, 1463.
- [92] G. Birlik Demirel, *ChemPhysChem* **2014**, *15*, 1693.
- [93] M. Hartlieb, D. Pretzel, C. Englert, M. Hentschel, K. Kempe, M. Gottschaldt, U. S. Schubert, *Biomacromolecules* **2014**, *15*, 1970.
- [94] S. Kumar, X. Tong, Y. L. Dory, M. Lepage, Y. Zhao, *Chem. Commun.* **2013**, *49*, 90.
- [95] A. Shastri, L. M. McGregor, Y. Liu, V. Harris, H. Nan, M. Mujica, Y. Vasquez, A. Bhattacharya, Y. Ma, M. Aizenberg, *Nat. Chem.* **2015**, *7*, 447.
- [96] T. Shiraki, A. Dawn, T. N. L. Le, Y. Tsuchiya, S.-i. Tamaru, S. Shinkai, *Chem. Commun.* **2011**, *47*, 7065.
- [97] Y. Xiao, M. Shen, X. Shi, *J. Mater. Chem. B* **2018**, *6*, 1420.
- [98] H. Liu, S. Wang, *Sci. China: Chem.* **2014**, *57*, 552.
- [99] Y. Hao, H. Cui, J. Meng, S. Wang, *J. Photochem. Photobiol., A* **2018**, *355*, 202.
- [100] C. Gong, M. W. Lam, H. Yu, *Adv. Funct. Mater.* **2006**, *16*, 1759.
- [101] K. Yoshimatsu, B. K. Lesel, Y. Yonamine, J. M. Beierle, Y. Hoshino, K. J. Shea, *Angew. Chem., Int. Ed.* **2012**, *51*, 2405.
- [102] S. Hou, H. Zhao, L. Zhao, Q. Shen, K. S. Wei, D. Y. Suh, A. Nakao, M. A. Garcia, M. Song, T. Lee, *Adv. Mater.* **2013**, *25*, 1547.
- [103] Y. Zhang, H.-F. Ji, G. M. Brown, T. Thundat, *Anal. Chem.* **2003**, *75*, 4773.
- [104] S. Peleshanko, M. D. Julian, M. Ornatska, M. E. McConney, M. C. LeMieux, N. Chen, C. Tucker, Y. Yang, C. Liu, J. A. Humphrey, *Adv. Mater.* **2007**, *19*, 2903.
- [105] L. Ionov, *Mater. Today* **2014**, *17*, 494.
- [106] C. M. Andres, J. Zhu, T. Shyu, C. Flynn, N. A. Kotov, *Langmuir* **2014**, *30*, 5378.
- [107] Y. Takashima, S. Hatanaka, M. Otsubo, M. Nakahata, T. Kakuta, A. Hashidzume, H. Yamaguchi, A. Harada, *Nat. Commun.* **2012**, *3*, 1270.
- [108] H. Okuzaki, T. Kuwabara, K. Funasaka, T. Saido, *Adv. Funct. Mater.* **2013**, *23*, 4400.
- [109] S.-J. Jeon, A. W. Hauser, R. C. Hayward, *Acc. Chem. Res.* **2017**, *50*, 161.
- [110] Y. Klein, E. Efrati, E. Sharon, *Science* **2007**, *315*, 1116.
- [111] M. Jamal, A. M. Zarafshar, D. H. Gracias, *Nat. Commun.* **2011**, *2*, 527.
- [112] J. Kim, J. A. Hanna, M. Byun, C. D. Santangelo, R. C. Hayward, *Science* **2012**, *335*, 1201.
- [113] M. Byun, C. D. Santangelo, R. C. Hayward, *Soft Matter* **2013**, *9*, 8264.
- [114] R. Luo, J. Wu, N. D. Dinh, C. H. Chen, *Adv. Funct. Mater.* **2015**, *25*, 7272.
- [115] T. Asoh, M. Matsusaki, T. Kaneko, M. Akashi, *Adv. Mater.* **2008**, *20*, 2080.
- [116] Z. Hu, X. Zhang, Y. Li, *Science* **1995**, *269*, 525.
- [117] T. S. Shim, S. H. Kim, C. J. Heo, H. C. Jeon, S. M. Yang, *Angew. Chem., Int. Ed.* **2012**, *51*, 1420.
- [118] J. Duan, X. Liang, K. Zhu, J. Guo, L. Zhang, *Soft Matter* **2017**, *13*, 345.
- [119] E. Zhang, T. Wang, W. Hong, W. Sun, X. Liu, Z. Tong, *J. Mater. Chem. A* **2014**, *2*, 15633.
- [120] X. Zhang, C. L. Pint, M. H. Lee, B. E. Schubert, A. Jamshidi, K. Takei, H. Ko, A. Gillies, R. Bardhan, J. J. Urban, *Nano Lett.* **2011**, *11*, 3239.

- [121] B. Shin, J. Ha, M. Lee, K. Park, G. H. Park, T. H. Choi, K.-J. Cho, H.-Y. Kim, *Sci. Rob.* **2018**, 3, eaar2629.
- [122] M. Dai, O. T. Picot, J. M. Verjans, L. T. de Haan, A. P. Schenning, T. Peijs, C. W. Bastiaansen, *ACS Appl. Mater. Interfaces* **2013**, 5, 4945.
- [123] E. Palneau, D. Morales, M. D. Dickey, O. D. Velev, *Nat. Commun.* **2013**, 4, 2257.
- [124] D. Wang, Y. Hu, P. Liu, D. Luo, *Acc. Chem. Res.* **2017**, 50, 733.
- [125] E. Wang, M. S. Desai, S. W. Lee, *Nano Lett.* **2013**, 13, 2826.
- [126] J. Kim, J. A. Hanna, R. C. Hayward, C. D. Santangelo, *Soft Matter* **2012**, 8, 2375.
- [127] J. Guan, H. He, D. J. Hansford, L. J. Lee, *J. Phys. Chem. B* **2005**, 109, 23134.
- [128] J. H. Na, A. A. Evans, J. Bae, M. C. Chiappelli, C. D. Santangelo, R. J. Lang, T. C. Hull, R. C. Hayward, *Adv. Mater.* **2015**, 27, 79.
- [129] Y. Mao, K. Yu, M. S. Isakov, J. Wu, M. L. Dunn, H. Jerry Qi, *Sci. Rep.* **2015**, 5, 13616.
- [130] A. S. Gladman, E. A. Matsumoto, R. G. Nuzzo, L. Mahadevan, J. A. Lewis, *Nat. Mater.* **2016**, 15, 413.
- [131] J. Zi, X. Yu, Y. Li, X. Hu, C. Xu, X. Wang, X. Liu, R. Fu, *Proc. Natl. Acad. Sci. USA* **2003**, 100, 12576.
- [132] O. Sato, S. Kubo, Z.-Z. Gu, *Acc. Chem. Res.* **2009**, 42, 1.
- [133] L. Feng, S. Li, Y. Li, H. Li, L. Zhang, J. Zhai, Y. Song, B. Liu, L. Jiang, D. Zhu, *Adv. Mater.* **2002**, 14, 1857.
- [134] E. Kreit, L. M. Mäthger, R. T. Hanlon, P. B. Dennis, R. R. Naik, E. Forsythe, J. Heikenfeld, *J. R. Soc., Interface* **2013**, 10.
- [135] L. M. Mäthger, E. J. Denton, N. J. Marshall, R. T. Hanlon, *J. R. Soc., Interface* **2009**, 6, S149.
- [136] Q. Wang, G. R. Gossweiler, S. L. Craig, X. Zhao, *Nat. Commun.* **2014**, 5, 4899.
- [137] C. Rianna, L. Rossano, R. H. Kollarigowda, F. Formiggini, S. Cavalli, M. Ventre, P. A. Netti, *Adv. Funct. Mater.* **2016**, 26, 7572.
- [138] G. Koçer, J. ter Schiphorst, M. Hendrikx, H. G. Kassa, P. Leclère, A. P. H. J. Schenning, P. Jonkheijm, *Adv. Mater.* **2017**, 29, 1606407.
- [139] J.-B. Chang, H. K. Choi, A. F. Hannon, A. Alexander-Katz, C. A. Ross, K. K. Berggren, *Nat. Commun.* **2014**, 5, 3305.
- [140] T. J. White, D. J. Broer, *Nat. Mater.* **2015**, 14, 1087.
- [141] F.-R. Fan, L. Lin, G. Zhu, W. Wu, R. Zhang, Z. L. Wang, *Nano Lett.* **2012**, 12, 3109.
- [142] F. Li, H. Hou, J. Yin, X. Jiang, *Sci. Adv.* **2018**, 4, eaar5762.
- [143] D. Liu, D. J. Broer, *Angew. Chem., Int. Ed.* **2014**, 53, 4542.
- [144] M. Camacho-Lopez, H. Finkelmann, P. Palfy-Muhoray, M. Shelley, *Nat. Mater.* **2004**, 3, 307.
- [145] O. Christian, B. Martin, Z. Rudolf, *Adv. Mater.* **2010**, 22, 3366.
- [146] A. Agrawal, P. Luchette, P. Palfy-Muhoray, S. L. Biswal, W. G. Chapman, R. Verduzco, *Soft Matter* **2012**, 8, 7138.
- [147] Y. Sawa, K. Urayama, T. Takigawa, A. DeSimone, L. Teresi, *Macromolecules* **2010**, 43, 4362.
- [148] M. D. Kempe, N. R. Scruggs, R. Verduzco, J. Lal, J. A. Kornfield, *Nat. Mater.* **2004**, 3, 177.
- [149] A. Fukunaga, K. Urayama, T. Takigawa, A. DeSimone, L. Teresi, *Macromolecules* **2008**, 41, 9389.
- [150] J. Y. Chung, A. J. Nolte, C. M. Stafford, *Adv. Mater.* **2011**, 23, 349.
- [151] Q. Wang, L. Zhang, X. Zhao, *Phys. Rev. Lett.* **2011**, 106, 118301.
- [152] X. Zhao, Z. Suo, *Appl. Phys. Lett.* **2007**, 91, 061921.
- [153] X. Zhao, W. Hong, Z. Suo, *Phys. Rev. B* **2007**, 76, 134113.
- [154] C. Keplinger, M. Kaltenbrunner, N. Arnold, S. Bauer, *Proc. Natl. Acad. Sci. USA* **2010**, 107, 4505.
- [155] Q. Wang, M. Tahir, J. Zang, X. Zhao, *Adv. Mater.* **2012**, 24, 1947.
- [156] T. L. Xu, F. Soto, W. Gao, V. Garcia-Gradilla, J. X. Li, X. J. Zhang, J. Wang, *J. Am. Chem. Soc.* **2014**, 136, 8552.
- [157] S. Balasubramanian, D. Kagan, C. M. J. Hu, S. Campuzano, M. J. Lobo-Castanon, N. Lim, D. Y. Kang, M. Zimmerman, L. F. Zhang, J. Wang, *Angew. Chem., Int. Ed.* **2011**, 50, 4161.
- [158] D. Kagan, R. Laocharoenruk, M. Zimmerman, C. Clawson, S. Balasubramanian, D. Kong, D. Bishop, S. Sattayasamitsathit, L. F. Zhang, J. Wang, *Small* **2010**, 6, 2741.
- [159] D. Pantarotto, W. R. Browne, B. L. Feringa, *Chem. Commun.* **2008**, 1533.
- [160] B. Esteban-Fernandez de Avila, P. Angsantikul, J. X. Li, M. A. Lopez-Ramirez, D. E. Ramirez-Herrera, S. Thamphiwatana, C. R. Chen, J. Delezuk, R. Samakapiruk, V. Ramez, L. F. Zhang, J. Wang, *Nat. Commun.* **2017**, 8, 272.
- [161] N. Mano, A. Heller, *J. Am. Chem. Soc.* **2005**, 127, 11574.
- [162] M. Ibele, T. E. Mallouk, A. Sen, *Angew. Chem., Int. Ed.* **2009**, 48, 3308.
- [163] J. Berná, D. A. Leigh, M. Lubomska, S. M. Mendoza, E. M. Pérez, P. Rudolf, G. Teobaldi, F. Zerbetto, *Nat. Mater.* **2005**, 4, 704.
- [164] I. Lagzi, S. Soh, P. J. Wesson, K. P. Browne, B. A. Grzybowski, *J. Am. Chem. Soc.* **2010**, 132, 1198.
- [165] T. L. Xu, W. Gao, L. P. Xu, X. J. Zhang, S. T. Wang, *Adv. Mater.* **2017**, 29, 1603250.
- [166] J. Katuri, X. Ma, M. M. Stanton, S. Sanchez, *Acc. Chem. Res.* **2017**, 50, 2.
- [167] W. Gao, J. Wang, *ACS Nano* **2014**, 8, 3170.
- [168] M. Guix, C. C. Mayorga-Martinez, A. Merkoçi, *Chem. Rev.* **2014**, 114, 6285.
- [169] W. Wang, W. Duan, S. Ahmed, T. E. Mallouk, A. Sen, *Nano Today* **2013**, 8, 531.
- [170] S. Sengupta, M. E. Ibele, A. Sen, *Angew. Chem., Int. Ed.* **2012**, 51, 8434.
- [171] R. S. M. Rikken, R. J. M. Nolte, J. C. Maan, J. C. M. van Hest, D. A. Wilson, P. C. M. Christianen, *Soft Matter* **2014**, 10, 1295.
- [172] R. Dreyfus, J. Baudry, M. L. Roper, M. Fermigier, H. A. Stone, J. Bibette, *Nature* **2005**, 437, 862.
- [173] M. M. Ma, L. Guo, D. G. Anderson, R. Langer, *Science* **2013**, 339, 186.
- [174] A. Sbarbati, F. Osculati, *Cells Tissues Organs* **2006**, 183, 206.
- [175] G. Robinson, E. Z. Y. Huang, *Apidologie* **1998**, 29, 159.
- [176] R. Wayne, *Bot. Rev.* **1994**, 60, 265.
- [177] C. M. Waters, B. L. Bassler, *Annu. Rev. Cell Dev. Biol.* **2005**, 21, 319.
- [178] T. M. Jessell, E. R. Kandel, *Cell* **1993**, 72, 1.
- [179] J. S. Dickschat, *Nat. Prod. Rep.* **2010**, 27, 343.
- [180] C. Zipfel, G. E. D. Oldroyd, *Nature* **2017**, 543, 328.
- [181] C. Giménez, E. Climent, E. Aznar, R. Martínez-Máñez, F. Sancenón, M. D. Marcos, P. Amorós, K. Rurack, *Angew. Chem., Int. Ed.* **2014**, 53, 12629.
- [182] A. Llopis-Lorente, P. Díez, A. Sánchez, M. D. Marcos, F. Sancenón, P. Martínez-Ruiz, R. Villalonga, R. Martínez-Máñez, *Nat. Commun.* **2017**, 8, 15511.
- [183] C. Chen, X. Chang, H. Teymourian, D. E. Ramírez-Herrera, B. Esteban-Fernández de Ávila, X. Lu, J. Li, S. He, C. Fang, Y. Liang, F. Mou, J. Guan, J. Wang, *Angew. Chem.* **2018**, 130, 247.
- [184] D. He, S. Garg, T. D. Waite, *Langmuir* **2012**, 28, 10266.
- [185] M. T. Schaaf, A. C. Pickerell, C. T. Williams, J. R. Monnier, *J. Catal.* **2008**, 254, 131.
- [186] J. X. Wang, N. S. Marinković, R. R. Adžić, B. M. Ocko, *Surf. Sci.* **1998**, 398, L291.
- [187] W. Yu, M. D. Porosoff, J. G. Chen, *Chem. Rev.* **2012**, 112, 5780.
- [188] M. A. Hasnat, M. M. Rahman, S. M. Borhanuddin, A. Siddiqua, N. M. Bahadur, M. R. Karim, *Catal. Commun.* **2010**, 12, 286.
- [189] K. Nakamura, *Am. J. Physiol.: Regul. Integr. Comp. Physiol.* **2011**, 301, R1207.
- [190] M. H. Xiong, Y. Bao, X. Z. Yang, Y. C. Wang, B. Sun, J. Wang, *J. Am. Chem. Soc.* **2012**, 134, 4355.
- [191] Y. L. Chen, S. Zhu, L. Zhang, P. J. Feng, X. K. Yao, C. G. Qian, C. Zhang, X. Q. Jiang, Q. D. Shen, *Nanoscale* **2016**, 8, 3368.
- [192] M. F. Maitz, U. Freudenberg, M. V. Tsurkan, M. Fischer, T. Beyrich, C. Werner, *Nat. Commun.* **2013**, 4, 2168.

- [193] K. Y. Lin, J. H. Lo, N. Consul, G. A. Kwong, S. N. Bhatia, *ACS Nano* **2014**, *8*, 8776.
- [194] K. Ishihara, K. Matsui, *J. Polym. Sci., Part C: Polym. Lett.* **1986**, *24*, 413.
- [195] K. Ishihara, M. Kobayashi, N. Ishimaru, I. Shinohara, *Polym. J.* **1984**, *16*, 625.
- [196] Y. Ito, M. Casolaro, K. Kono, Y. Imanishi, *J. Controlled Release* **1989**, *10*, 195.
- [197] Z. Gu, T. T. Dang, M. Ma, B. C. Tang, H. Cheng, S. Jiang, Y. Dong, Y. Zhang, D. G. Anderson, *ACS Nano* **2013**, *7*, 6758.
- [198] V. Lapeyre, C. Ancla, B. Catarsi, V. Ravaine, *J. Colloid Interface Sci.* **2008**, *327*, 316.
- [199] B. G. De Geest, A. M. Jonas, J. Demeester, S. C. De Smedt, *Langmuir* **2006**, *22*, 5070.
- [200] A. Guiseppi-Elie, S. I. Brahim, D. Narinesingh, *Adv. Mater.* **2002**, *14*, 743.
- [201] K. Makino, E. J. Mack, T. Okano, S. W. Kim, *J. Controlled Release* **1990**, *12*, 235.
- [202] W. Tai, R. Mo, J. Di, V. Subramanian, X. Gu, J. B. Buse, Z. Gu, *Biomacromolecules* **2014**, *15*, 3495.
- [203] R. Ma, L. Shi, *Polym. Chem.* **2014**, *5*, 1503.
- [204] J. Wang, Y. Ye, J. Yu, A. R. Kahkoska, X. Zhang, C. Wang, W. Sun, R. D. Corder, Z. Chen, S. A. Khan, J. B. Buse, Z. Gu, *ACS Nano* **2018**, *12*, 2466.
- [205] X. He, M. Aizenberg, O. Kuksenok, L. D. Zarzar, A. Shastri, A. C. Balazs, J. Aizenberg, *Nature* **2012**, *487*, 214.
- [206] Y. S. Kirn, R. Tammate, A. M. Akimoto, R. Yoshida, *Mater. Horiz.* **2017**, *4*, 38.
- [207] S. Maeda, Y. Hara, T. Sakai, R. Yoshida, S. Hashimoto, *Adv. Mater.* **2007**, *19*, 3480.
- [208] S. Nakata, M. Yoshii, S. Suzuki, R. Yoshida, *Langmuir* **2014**, *30*, 517.
- [209] Y. Shiraki, R. Yoshida, *Angew. Chem., Int. Ed.* **2012**, *51*, 6112.
- [210] R. Yoshida, Y. Murase, *Colloids Surf., B* **2012**, *99*, 60.
- [211] Y. Murase, R. Takeshima, R. Yoshida, *Macromol. Biosci.* **2011**, *11*, 1713.
- [212] I. C. Chen, O. Kuksenok, V. V. Yashin, A. C. Balazs, K. J. Van Vliet, *Adv. Funct. Mater.* **2012**, *22*, 2535.
- [213] R. Yoshida, Y. Uesusuki, *Biomacromolecules* **2005**, *6*, 2923.
- [214] K. Kumar, C. Knie, D. Bleger, M. A. Peletier, H. Friedrich, S. Hecht, D. J. Broer, M. G. Debije, A. Schenning, *Nat. Commun.* **2016**, *7*, 11975.
- [215] D. Oliver, T. Baukrowitz, B. Fakler, *Eur. J. Biochem.* **2000**, *267*, 5824.
- [216] E. Gouaux, R. MacKinnon, *Science* **2005**, *310*, 1461.
- [217] T. Dudev, C. Lim, *Acc. Chem. Res.* **2014**, *47*, 3580.
- [218] G. Pérez-Mitta, A. S. Peinetti, M. L. Cortez, M. E. Toimil-Molares, C. Trautmann, O. Azzaroni, *Nano Lett.* **2018**, *18*, 3303.
- [219] I. Vlassioul, P. Y. Apel, S. N. Dmitriev, K. Healy, Z. S. Siwy, *Proc. Natl. Acad. Sci. USA* **2009**, *106*, 21039.
- [220] E. N. Savariar, K. Krishnamoorthy, S. Thayumanavan, *Nat. Nanotechnol.* **2008**, *3*, 112.
- [221] L. Wen, X. Hou, Y. Tian, J. Zhai, L. Jiang, *Adv. Funct. Mater.* **2010**, *20*, 2636.
- [222] H. Daiguiji, P. Yang, A. Majumdar, *Nano Lett.* **2004**, *4*, 137.
- [223] Z. Siwy, E. Heins, C. C. Harrell, P. Kohli, C. R. Martin, *J. Am. Chem. Soc.* **2004**, *126*, 10850.
- [224] X. Hou, W. Guo, L. Jiang, *Chem. Soc. Rev.* **2011**, *40*, 2385.
- [225] Z. S. Siwy, *Adv. Funct. Mater.* **2006**, *16*, 735.
- [226] A. Alcaraz, P. Ramírez, E. García-Giménez, M. L. López, A. Andrio, V. M. Aguilella, *J. Phys. Chem. B* **2006**, *110*, 21205.
- [227] Z. Siwy, P. Apel, D. Baur, D. D. Dobrev, Y. E. Korchev, R. Neumann, R. Spohr, C. Trautmann, K.-O. Voss, *Surf. Sci.* **2003**, *532–535*, 1061.
- [228] M. Zhang, X. Hou, J. Wang, Y. Tian, X. Fan, J. Zhai, L. Jiang, *Adv. Mater.* **2012**, *24*, 2424.
- [229] P. Scrimin, L. J. Prins, *Chem. Soc. Rev.* **2011**, *40*, 4488.
- [230] J. P. Lei, H. X. Ju, *Chem. Soc. Rev.* **2012**, *41*, 2122.
- [231] X. Zhang, S. Soh, *Adv. Mater. Technol.* **2018**, *3*, 1800042.
- [232] H. Takeuchi, T. Kurahashi, *J. Neurosci.* **2005**, *25*, 11084.
- [233] J. Reisert, J. Lai, K. W. Yau, J. Bradley, *Neuron* **2005**, *45*, 553.
- [234] T. Hengl, H. Kaneko, K. Dauner, K. Vocke, S. Frings, F. Mohrlen, *Proc. Natl. Acad. Sci. USA* **2010**, *107*, 6052.
- [235] C. Janetopoulos, L. Ma, P. N. Devreotes, P. A. Iglesias, *Proc. Natl. Acad. Sci. USA* **2004**, *101*, 8951.
- [236] H. J. Avens, C. N. Bowman, *Acta Biomater.* **2010**, *6*, 83.
- [237] F. L. Zhou, B. X. Li, *Anal. Chem.* **2015**, *87*, 7156.
- [238] H. D. Sikes, R. R. Hansen, L. M. Johnson, R. Jenison, J. W. Birks, K. L. Rowlen, C. N. Bowman, *Nat. Mater.* **2008**, *7*, 52.
- [239] W. J. Zhao, S. Yang, J. F. Yang, J. S. Li, J. Zheng, Z. H. Qing, R. H. Yang, *Anal. Chem.* **2016**, *88*, 10728.
- [240] R. R. Hansen, H. D. Sikes, C. N. Bowman, *Biomacromolecules* **2008**, *9*, 355.
- [241] M. S. Baker, S. T. Phillips, *J. Am. Chem. Soc.* **2011**, *133*, 5170.
- [242] A. J. Lan, K. H. Li, H. H. Wu, D. H. Olson, T. J. Emge, W. Ki, M. C. Hong, J. Li, *Angew. Chem., Int. Ed.* **2009**, *48*, 2334.
- [243] S. Pramanik, C. Zheng, X. Zhang, T. J. Emge, J. Li, *J. Am. Chem. Soc.* **2011**, *133*, 4153.
- [244] J. Z. Liu, Y. C. Zhong, P. Lu, Y. N. Hong, J. W. Y. Lam, M. Faisal, Y. Yu, K. S. Wong, B. Z. Tang, *Polym. Chem.* **2010**, *1*, 426.
- [245] K. Haba, M. Popkov, M. Shamis, R. A. Lerner, C. F. Barbas, D. Shabat, *Angew. Chem., Int. Ed.* **2005**, *44*, 716.
- [246] T. Yoshii, S. Onogi, H. Shigemitsu, I. Hamachi, *J. Am. Chem. Soc.* **2015**, *137*, 3360.
- [247] E. Sella, D. Shabat, *J. Am. Chem. Soc.* **2009**, *131*, 9934.
- [248] E. Sella, A. Lubelski, J. Klafter, D. Shabat, *J. Am. Chem. Soc.* **2010**, *132*, 3945.
- [249] B. C. Yin, Y. Q. Liu, B. C. Ye, *J. Am. Chem. Soc.* **2012**, *134*, 5064.
- [250] A. Shibata, T. Uzawa, Y. Nakashima, M. Ito, Y. Nakano, S. Shuto, Y. Ito, H. Abe, *J. Am. Chem. Soc.* **2013**, *135*, 14172.
- [251] T. Porstmann, S. T. Kiessig, *J. Immunol. Methods* **1992**, *150*, 5.
- [252] N. C. Gianneschi, S. T. Nguyen, C. A. Mirkin, *J. Am. Chem. Soc.* **2005**, *127*, 1644.
- [253] P. Hornbeck, S. E. Winston, S. A. Fuller, *Curr. Protoc. Mol. Biol.* **1991**, *15*, 11.2.1.
- [254] G. A. D. Metcalf, A. Shibakawa, H. Patel, A. Sita-Lumsden, A. Zivi, N. Rama, C. L. Bevan, S. Ladame, *Anal. Chem.* **2016**, *88*, 8091.
- [255] C. Percivalle, J. F. Bartolo, S. Ladame, *Org. Biomol. Chem.* **2013**, *11*, 16.
- [256] Y. Choi, G. Metcalf, M. H. Sleiman, D. Vair-Turnbull, S. Ladame, *Bioorg. Med. Chem.* **2014**, *22*, 4395.
- [257] K. Gorska, N. Winssinger, *Angew. Chem., Int. Ed.* **2013**, *52*, 6820.
- [258] D. Al Sulaiman, J. Y. H. Chang, S. Ladame, *Angew. Chem., Int. Ed.* **2017**, *56*, 5247.
- [259] B. J. Berron, A. M. May, Z. Zheng, V. Balasubramanian, C. N. Bowman, *Lab Chip* **2012**, *12*, 708.
- [260] B. J. Berron, L. M. Johnson, X. Ba, J. D. McCall, N. J. Alvey, K. S. Anseth, C. N. Bowman, *Biotechnol. Bioeng.* **2011**, *108*, 1521.
- [261] H. Qian, L. He, *Anal. Chem.* **2009**, *81*, 4536.
- [262] E. Sella, D. Shabat, *Chem. Commun.* **2008**, 5701.
- [263] E. Sella, R. Weinstain, R. Erez, N. Z. Burns, P. S. Baran, D. Shabat, *Chem. Commun.* **2010**, *46*, 6575.
- [264] M. A. Swiderska, J. L. Reymond, *Nat. Chem.* **2009**, *1*, 527.
- [265] J. M. Nam, S. I. Stoeva, C. A. Mirkin, *J. Am. Chem. Soc.* **2004**, *126*, 5932.
- [266] B. K. Oh, J. M. Nam, S. W. Lee, C. A. Mirkin, *Small* **2006**, *2*, 103.
- [267] J. M. Nam, C. S. Thaxton, C. A. Mirkin, *Science* **2003**, *301*, 1884.
- [268] D. G. Georganopoulou, L. Chang, J. M. Nam, C. S. Thaxton, E. J. Mufson, W. L. Klein, C. A. Mirkin, *Proc. Natl. Acad. Sci. USA* **2005**, *102*, 2273.
- [269] E. Bonabeau, G. Theraulaz, J. L. Deneubourg, S. Aron, S. Camazine, *Trends Ecol. Evol.* **1997**, *12*, 188.

- [270] H. B. Liu, Y. Zhao, C. A. Dreiss, Y. J. Feng, *Soft Matter* **2014**, *10*, 6387.
- [271] A. A. Steinschulte, A. Scotti, K. Rahimi, O. Neveskyi, A. Oppermann, S. Schneider, S. Bochenek, M. F. Schulte, K. Geisel, F. Jansen, A. Jung, S. Mallmann, R. Winter, W. Richtering, D. Woll, R. Schweins, N. J. Warren, F. A. Plamper, *Adv. Mater.* **2017**, *29*, 1703495.
- [272] A. Robertson, A. J. Sinclair, D. Philp, *Chem. Soc. Rev.* **2000**, *29*, 141.
- [273] A. Pross, *Origins Life Evol. Biospheres* **2004**, *34*, 307.
- [274] E. Szathmáry, J. Maynard Smith, *J. Theor. Biol.* **1997**, *187*, 555.
- [275] G. Clixby, L. Twyman, *Org. Biomol. Chem.* **2016**, *14*, 4170.
- [276] G. von Kiedrowski, *Angew. Chem., Int. Ed. Engl.* **1986**, *25*, 932.
- [277] N. Paul, G. F. Joyce, *Proc. Natl. Acad. Sci. USA* **2002**, *99*, 12733.
- [278] T. A. Lincoln, G. F. Joyce, *Science* **2009**, *323*, 1229.
- [279] R. Issac, J. Chmielewski, *J. Am. Chem. Soc.* **2002**, *124*, 6808.
- [280] A. Vidonne, D. Philp, *Eur. J. Org. Chem.* **2009**, *2009*, 593.
- [281] Z. Dadon, M. Samiappan, E. Y. Safranchik, G. Ashkenasy, *Chem. – Eur. J.* **2010**, *16*, 12096.
- [282] M. E. Leunissen, R. Dreyfus, R. Sha, T. Wang, N. C. Seeman, D. J. Pine, P. M. Chaikin, *Soft Matter* **2009**, *5*, 2422.
- [283] O. Gia, S. Marciani Magno, A. Garbesi, F. P. Colonna, M. Palumbo, *Biochemistry* **1992**, *31*, 11818.
- [284] F. Ikhouane, J. Rodellar, *Systems with Hysteresis: Analysis, Identification and Control Using the Bouc–Wen Model*, John Wiley & Sons, Chichester, UK **2007**.
- [285] J. Ma, J. Hu, Z. Li, C. W. Nan, *Adv. Mater.* **2011**, *23*, 1062.
- [286] C. Chappert, A. Fert, F. N. Van Dau, *Nat. Mater.* **2007**, *6*, 813.
- [287] T. Mori, S. Beppu, M. R. Berber, H. Mori, T. Makimura, A. Tsukamoto, K. Minagawa, T. Hirano, M. Tanaka, T. Niidome, Y. Katayama, T. Hirano, Y. Maeda, *Langmuir* **2010**, *26*, 9224.
- [288] K. Zhang, X. Feng, C. Ye, M. A. Hempenius, G. J. Vancso, *J. Am. Chem. Soc.* **2017**, *139*, 10029.
- [289] L. Sambe, V. R. de La Rosa, K. Belal, F. Stoffelbach, J. Lyskawa, F. Delattre, M. Bria, G. Cooke, R. Hoogenboom, P. Woisel, *Angew. Chem.* **2014**, *126*, 5144.
- [290] V. R. de la Rosa, R. Hoogenboom, *Chem. – Eur. J.* **2015**, *21*, 1302.
- [291] E. Kim, C. Kang, H. Baek, K. Hwang, D. Kwak, E. Lee, Y. Kang, E. L. Thomas, *Adv. Funct. Mater.* **2010**, *20*, 1728.
- [292] J. L. Weidman, R. A. Mulvenna, B. W. Boudouris, W. A. Phillip, *J. Am. Chem. Soc.* **2016**, *138*, 7030.
- [293] K. E. Secrist, A. J. Nolte, *Macromolecules* **2011**, *44*, 2859.
- [294] D. Kim, H. Kim, E. Lee, K. S. Jin, J. Yoon, *Chem. Mater.* **2016**, *28*, 8807.
- [295] K. Hwang, D. Kwak, C. Kang, D. Kim, Y. Ahn, Y. Kang, *Angew. Chem., Int. Ed.* **2011**, *50*, 6311.
- [296] M. D. Hager, S. Bode, C. Weber, U. S. Schubert, *Prog. Polym. Sci.* **2015**, *49–50*, 3.
- [297] Z. Zhao, K. Zhang, Y. Liu, J. Zhou, M. Liu, *Adv. Mater.* **2017**, *29*, 1701695.
- [298] Z. Cheng, D. Zhang, T. Lv, H. Lai, E. Zhang, H. Kang, Y. Wang, P. Liu, Y. Liu, Y. Du, *Adv. Funct. Mater.* **2018**, *28*, 1705002.
- [299] E. M. Lee, K. Smith, K. Gall, B. D. Boyan, Z. Schwartz, *Biomaterials* **2016**, *110*, 34.
- [300] Y. Zhang, H. Gao, H. Wang, Z. Xu, X. Chen, B. Liu, Y. Shi, Y. Lu, L. Wen, Y. Li, *Adv. Funct. Mater.* **2018**, *28*, 1705962.
- [301] E. L. Kirkby, J. D. Rule, V. J. Michaud, N. R. Sottos, S. R. White, J. A. E. Manson, *Adv. Funct. Mater.* **2008**, *18*, 2253.
- [302] J. H. Lee, R. Hincheet, S. K. Kim, S. Kim, S.-W. Kim, *Energy Environ. Sci.* **2015**, *8*, 3605.
- [303] X. Hu, D. Zhang, S. S. Sheiko, *Adv. Mater.* **2018**, *30*, 1707461.
- [304] Y. Zhang, J. Liao, T. Wang, W. Sun, Z. Tong, *Adv. Funct. Mater.* **2018**, *28*, 1707245.
- [305] H. Yang, W. R. Leow, T. Wang, J. Wang, J. Yu, K. He, D. Qi, C. Wan, X. Chen, *Adv. Mater.* **2017**, *29*, 1701627.
- [306] A. Lendlein, H. Jiang, O. Jünger, R. Langer, *Nature* **2005**, *434*, 879.
- [307] S. Singh, B. Dutta, S. W. D'Souza, M. Zavareh, P. Devi, A. Gibbs, T. Hickel, S. Chadov, C. Felser, D. Pandey, *Nat. Commun.* **2017**, *8*, 1006.
- [308] V. Sessini, J.-M. Raquez, G. Lo Re, R. Mincheva, J. M. Kenny, P. Dubois, L. Peponi, *ACS Appl. Mater. Interfaces* **2016**, *8*, 19197.
- [309] D. Quitmann, N. Gushterov, G. Sadowski, F. Katzenberg, J. C. Tiller, *ACS Appl. Mater. Interfaces* **2013**, *5*, 3504.
- [310] Z. He, N. Satarkar, T. Xie, Y. T. Cheng, J. Z. Hilt, *Adv. Mater.* **2011**, *23*, 3192.
- [311] J. R. Kumpfer, S. J. Rowan, *J. Am. Chem. Soc.* **2011**, *133*, 12866.
- [312] X. Luo, P. T. Mather, *Adv. Funct. Mater.* **2010**, *20*, 2649.
- [313] T. Xie, *Nature* **2010**, *464*, 267.
- [314] T. Xie, K. A. Page, S. A. Eastman, *Adv. Funct. Mater.* **2011**, *21*, 2057.
- [315] H. Meng, G. Li, *Polymer* **2013**, *54*, 2199.
- [316] M. Frensemeier, J. S. Kaiser, C. P. Frick, A. S. Schneider, E. Arzt, R. S. Fertig, E. Kroner, *Adv. Funct. Mater.* **2015**, *25*, 3013.
- [317] M. Behl, K. Kratz, J. Zotzmann, U. Nöchel, A. Lendlein, *Adv. Mater.* **2013**, *25*, 4466.
- [318] M. Wuttig, H. Bhaskaran, T. Taubner, *Nat. Photonics* **2017**, *11*, 465.
- [319] H. Seungbum, A. Orlando, W. Dirk, *Emerging Non-Volatile Memories*, Springer, New York **2014**.
- [320] S. Raoux, *Annu. Rev. Mater. Res.* **2009**, *39*, 25.
- [321] A. V. Kolobov, P. Fons, A. I. Frenkel, A. L. Ankudinov, J. Tominaga, T. Uruga, *Nat. Mater.* **2004**, *3*, 703.
- [322] A. Redaelli, A. Pirovano, F. Pellizzer, A. L. Lacaita, D. Ielmini, R. Bez, *IEEE Electron Device Lett.* **2004**, *25*, 684.
- [323] M. Wuttig, N. Yamada, *Nat. Mater.* **2007**, *6*, 824.
- [324] C. Ríos, M. Stegmaier, P. Hosseini, D. Wang, T. Scherer, C. D. Wright, H. Bhaskaran, W. H. Pernice, *Nat. Photonics* **2015**, *9*, 725.
- [325] M. I. Khazi, W. Jeong, J.-M. Kim, *Adv. Mater.* **2018**, *30*, 1705310.
- [326] T. Horiguchi, Y. Koshiba, Y. Ueda, C. Origuchi, K. Tsutsui, *Thin Solid Films* **2008**, *516*, 2591.
- [327] W. Jeong, M. I. Khazi, D. H. Park, Y. S. Jung, J. M. Kim, *Adv. Funct. Mater.* **2016**, *26*, 5230.
- [328] R. Klajn, P. J. Wesson, K. J. Bishop, B. A. Grzybowski, *Angew. Chem.* **2009**, *121*, 7169.
- [329] H. Nishi, T. Namari, S. Kobatake, *J. Mater. Chem.* **2011**, *21*, 17249.
- [330] L. Sheng, M. Li, S. Zhu, H. Li, G. Xi, Y.-G. Li, Y. Wang, Q. Li, S. Liang, K. Zhong, *Nat. Commun.* **2014**, *5*, 3044.
- [331] J. Zhu, L. Zhang, S. Dong, E. Wang, *ACS Nano* **2013**, *7*, 10211.
- [332] Z. Wang, Z. Ma, Y. Wang, Z. Xu, Y. Luo, Y. Wei, X. Jia, *Adv. Mater.* **2015**, *27*, 6469.
- [333] R. Thirumalai, R. D. Mukhopadhyay, V. K. Praveen, A. Ajayaghosh, *Sci. Rep.* **2015**, *5*, 9842.
- [334] S. Yamamoto, H. Furuya, K. Tsutsui, S. Ueno, K. Sato, *Cryst. Growth Des.* **2008**, *8*, 2256.
- [335] I. Kawashima, H. Takahashi, S. Hirano, R. Matsushima, *J. Soc. Inf. Disp.* **2004**, *12*, 81.
- [336] B. Garai, A. Mallick, R. Banerjee, *Chem. Sci.* **2016**, *7*, 2195.
- [337] V. Nagy, I. Suleimanov, G. Molnár, L. Salmon, A. Bousseksou, L. Csóka, *J. Mater. Chem. B* **2015**, *3*, 7897.
- [338] H. Wu, Y. Chen, Y. Liu, *Adv. Mater.* **2017**, *29*, 1605271.
- [339] Y. Matsunaga, J. S. Yang, *Angew. Chem., Int. Ed.* **2015**, *54*, 7985.
- [340] J. Sun, J. Han, Y. Liu, Y. Duan, T. Han, J. Yuan, *J. Mater. Chem. B* **2016**, *4*, 8276.
- [341] G. Zhang, J. Lu, M. Sabat, C. L. Fraser, *J. Am. Chem. Soc.* **2010**, *132*, 2160.
- [342] Y. Jiang, D. Gindre, M. Allain, P. Liu, C. Cabanatos, J. Roncali, *Adv. Mater.* **2015**, *27*, 4285.
- [343] K. C. Naeem, A. Subhakumari, S. Varughese, V. C. Nair, *J. Mater. Chem. A* **2015**, *3*, 10225.

- [344] A. Kishimura, T. Yamashita, K. Yamaguchi, T. Aida, *Nat. Mater.* **2005**, *4*, 546.
- [345] Y. Ma, P. She, K. Y. Zhang, H. Yang, Y. Qin, Z. Xu, S. Liu, Q. Zhao, W. Huang, *Nat. Commun.* **2018**, *9*, 3.
- [346] H. Sun, S. Liu, W. Lin, K. Y. Zhang, W. Lv, X. Huang, F. Huo, H. Yang, G. Jenkins, Q. Zhao, W. Huang, *Nat. Commun.* **2014**, *5*, 3601.
- [347] A. P. De Silva, H. Q. N. Gunaratne, C. P. McCoy, *Nature* **1993**, *364*, 42.
- [348] J. Andréasson, S. D. Straight, S. Bandyopadhyay, R. H. Mitchell, T. A. Moore, A. L. Moore, D. Gust, *Angew. Chem., Int. Ed.* **2007**, *46*, 958.
- [349] S. Angelos, Y. W. Yang, N. M. Khashab, J. F. Stoddart, J. I. Zink, *J. Am. Chem. Soc.* **2009**, *131*, 11344.
- [350] S. J. Bradberry, J. P. Byrne, C. P. McCoy, T. Gunnlaugsson, *Chem. Commun.* **2015**, *51*, 16565.
- [351] H. Komatsu, S. Matsumoto, S. Tamaru, K. Kaneko, M. Ikeda, I. Hamachi, *J. Am. Chem. Soc.* **2009**, *131*, 5580.
- [352] D. A. Leigh, M. A. F. Morales, E. M. Perez, J. K. Y. Wong, C. G. Saiz, A. M. Z. Slawin, A. J. Carmichael, D. M. Haddleton, A. M. Brouwer, W. J. Buma, G. W. H. Wurpel, S. Leon, F. Zerbetto, *Angew. Chem., Int. Ed.* **2005**, *44*, 3062.
- [353] J. Matsui, M. Mitsuishi, A. Aoki, T. Miyashita, *Angew. Chem., Int. Ed.* **2003**, *42*, 2272.
- [354] E. Perez-Inestrosa, J. M. Montenegro, D. Collado, R. Suau, *Chem. Commun.* **2008**, 1085.
- [355] Z. Qi, C. A. Schalley, *Acc. Chem. Res.* **2014**, *47*, 2222.
- [356] S. Giordani, F. M. Raymo, *Org. Lett.* **2003**, *5*, 3559.
- [357] M. Zhou, N. D. Zhou, F. Kuralay, J. R. Windmiller, S. Parkhomovsky, G. Valdes-Ramirez, E. Katz, J. Wang, *Angew. Chem., Int. Ed.* **2012**, *51*, 2686.
- [358] X. J. Jiang, D. K. P. Ng, *Angew. Chem., Int. Ed.* **2014**, *53*, 10481.
- [359] D. Margulies, G. Melman, A. Shanzer, *Nat. Mater.* **2005**, *4*, 768.
- [360] C. D. Wright, Y. W. Liu, K. I. Kohary, M. M. Aziz, R. J. Hicken, *Adv. Mater.* **2011**, *23*, 3408.
- [361] A. Prasanna de Silva, N. D. McClenaghan, *J. Am. Chem. Soc.* **2000**, *122*, 3965.
- [362] D. H. Qu, Q. C. Wang, H. Tian, *Angew. Chem., Int. Ed.* **2005**, *44*, 5296.
- [363] J. Andréasson, G. Kodis, Y. Terazono, P. A. Liddell, S. Bandyopadhyay, R. H. Mitchell, T. A. Moore, A. L. Moore, D. Gust, *J. Am. Chem. Soc.* **2004**, *126*, 15926.
- [364] L. M. Adleman, *Science* **1994**, *266*, 1021.
- [365] L. Qian, E. Winfree, *Science* **2011**, *332*, 1196.
- [366] L. Qian, E. Winfree, J. Bruck, *Nature* **2011**, *475*, 368.
- [367] R. Orbach, B. Willner, I. Willner, *Chem. Commun.* **2015**, *51*, 4144.
- [368] W. Li, Y. Yang, H. Yan, Y. Liu, *Nano Lett.* **2013**, *13*, 2980.
- [369] J. Zhu, L. Zhang, T. Li, S. Dong, E. Wang, *Adv. Mater.* **2013**, *25*, 2440.
- [370] S. Zhang, K. Wang, K.-B. Li, F. Chen, W. Shi, W.-P. Jia, J. Zhang, D.-M. Han, *Nanoscale* **2017**, *9*, 11912.
- [371] H. Lederman, J. Macdonald, D. Stefanovic, M. N. Stojanovic, *Biochemistry* **2006**, *45*, 1194.
- [372] S. Ogasawara, Y. Kyoi, K. Fujimoto, *ChemBioChem* **2007**, *8*, 1520.
- [373] H.-Y. Lin, J.-Z. Chen, H.-Y. Li, C.-N. Yang, *Sci. Rep.* **2015**, *5*, 10686.
- [374] M. Zhang, B.-C. Ye, *Chem. Commun.* **2012**, *48*, 3647.
- [375] M. You, L. Peng, N. Shao, L. Zhang, L. Qiu, C. Cui, W. Tan, *J. Am. Chem. Soc.* **2014**, *136*, 1256.
- [376] Z. Huang, Y. Tao, F. Pu, J. Ren, X. Qu, *Chem. – Eur. J.* **2012**, *18*, 6663.
- [377] Z.-G. Wang, J. Elbaz, F. Remacle, R. Levine, I. Willner, *Proc. Natl. Acad. Sci. USA* **2010**, *107*, 21996.
- [378] J. Elbaz, F. Wang, F. Remacle, I. Willner, *Nano Lett.* **2012**, *12*, 6049.
- [379] L. Feng, S. Gai, Y. Dai, F. He, C. Sun, P. Yang, R. Lv, N. Niu, G. An, J. Lin, *Chem. Mater.* **2018**, *30*, 526.
- [380] J. Shi, L. Wang, J. Gao, Y. Liu, J. Zhang, R. Ma, R. Liu, Z. Zhang, *Biomaterials* **2014**, *35*, 5771.
- [381] C.-H. Fan, Y.-H. Cheng, C.-Y. Ting, Y.-J. Ho, P.-H. Hsu, H.-L. Liu, C.-K. Yeh, *Theranostics* **2016**, *6*, 1542.
- [382] F. Gao, L. Li, C. Fu, L. Nie, D. Chen, F. Tang, *Adv. Mater.* **2013**, *25*, 5508.
- [383] V. Garcia-Gradilla, J. Orozco, S. Sattayasamitsathit, F. Soto, F. Kuralay, A. Pourazary, A. Katzenberg, W. Gao, Y. Shen, J. Wang, *ACS Nano* **2013**, *7*, 9232.
- [384] W. Hu, G. Z. Lum, M. Mastrangeli, M. Sitti, *Nature* **2018**, *554*, 81.
- [385] H. Hahn, A. Sidorenko, I. Tigrinyanu, *Nanoscale Phenomena: Fundamentals and Applications*, Springer Science & Business Media, Berlin, Germany **2009**.
- [386] K. Sapsford, T. Pons, I. Medintz, H. Mattoussi, *Sensors* **2006**, *6*, 925.
- [387] S. I. Woods, J. R. Kirtley, S. Sun, R. H. Koch, *Phys. Rev. Lett.* **2001**, *87*, 137205.
- [388] K. J. M. Bishop, C. E. Wilmer, S. Soh, B. A. Grzybowski, *Small* **2009**, *5*, 1600.
- [389] S. Angelos, E. Choi, F. Vögtle, L. De Cola, J. I. Zink, *J. Phys. Chem. C* **2007**, *111*, 6589.